THE UNIVERSITY OF CHICAGO

cHOClate: A DNA-BASED FLUORESCENT PROBE TO QUANTITATIVELY MAP SUBCELLULAR HOCl

A DISSERTATION SUBMITTED TO

THE FACULTY OF THE DIVISION OF THE PHYSICAL SCIENCES

IN CANDIDACY FOR THE DEGREE OF

DOCTOR OF PHILOSOPHY

DEPARTMENT OF CHEMISTRY

BY

SHAREEFA THEKKAN

CHICAGO, ILLINOIS

MARCH 2019

List of Contents

List of Tables

List of Figures

Acknowledgements

I wish to take this opportunity to extend my gratitude to all the people who have generously helped me during my PhD work. I would like to express my sincere gratitude to my thesis supervisor Prof. Yamuna Krishnan for her enthusiasm, encouragement and continued support during my research. I was lucky to work with her as she gave me the intellectual freedom to choose the project of my interest and cherish that choice. I thank my collaborator as well as my thesis committee member Prof. Lev Becker for his critical and helpful insights into my work. Many interesting details of this work have emerged from discussion with him. I thank my thesis committee member Prof. Bryan Dickinson for critical comments about my work as well as extending his generosity for mass spectral characterization of chemical compounds. I am thankful to Prof. Deborah Nelson and Dr. Christine A. Petersen, University of Iowa for generously providing the mouse macrophage cell lines. I would like to thank Prof. Srinivasan Chandrasekaran from organic chemistry department, IISc Bangalore, India and Dr. Srinivas Oruganti from Institute of Life science, Hyderabad University, India for generously allowing me to use their chemical synthesis facility to carry out my work during the early years of my PhD.

I would like to thank Maulik for his scientific inputs in these studies and experimental help in immunostaining experiments. I would like to thank Krishna Dan and Aneesh T Veetil for their help and suggestions with chemical synthesis in critical times. I thank Chang Cui, Alex Hoffmann, Guolin Zou, and Kelly Schoenfelt from Prof. Lev Becker's lab for isolating innate immune cells from human blood and mice for my studies. I would like to thank my donors Maulik, Alex, Nagarjun and Chang for generously donating blood for my studies. I thank Kristen M. Becker for her priceless help with drawing blood for my studies.

I would like to thank Sonali and Suruchi for welcoming me in the lab and giving me scientific support during early days of my PhD. I thank Sunaina, Saheli, Shabana, and Saikat for being such helpful seniors who invested their time in my intellectual growth. I express my love and gratitude to Kasturi, Ved and Bhavya for the scientific and nonscientific fun we had in the lab and outside the lab. I would like to thank Anand, Junyi, Matt, Ka Ho and Muthu for stimulating scientific discussions in the lab. I am grateful to Matt, Maulik and Aneesh for critically reading my thesis. I specially thank Maulik and Aneesh for stimulating scientific discussions about various topics in the tea time, which helped me to approach any topics from a scientific perspective. I am glad that I got an opportunity to work in a scientifically rich and diverse environment which was filled with both enthusiasm and fun at the same time.

I am thankful to Rahul, Jason, Rebecca, Vladimir and Aida for various reagents during the studies. I thank members of Dickinson lab for being great neighbors whom we could run in to for any sort of help. I thank Becker group who were generous to provide me any experimental or reagent help during my studies. I thank my friends Ambili, Anwesha, Suhail and Remya for always available for me. I thank Neethu, Justyna, Maria, Kiran, Victor, Kimberly, Aga, Leon for making my stay in Chicago lively.

I especially thank the lab support teams in NCBS and University of Chicago. I thank my friends in Bangalore specially Yadu, Prathibha, Jithesh, Binnu, Ajoy, Balaji, Divya and Vibha for giving me different scientific as well as non-scientific help. I am grateful to my mom Ayisha and father Abdurahiman for believing in me and taught me to be optimistic. I thank my in-laws Meharunnisa and Abdul Rahiman for their sincere support and for being my well-wishers. I am grateful to my siblings for their generous support and

encouragement during this period. I am grateful to my husband Nijam, for being patient and a constant source of encouragement for my PhD journey from starting to end.

Abbreviations

HOCl	Hypochlorous acid
MPO	Myeloperoxidase
ANCA	Antineutrophil cytoplasmic antibodies
H_2O_2	Hydrogen peroxide
NO	Nitric oxide
TBHP	Tert- Butyl hydrogen peroxide
ABAH	4- Aminobenzoic acid hydrazide
DPI	Diphenylene iodonium
1400 W	N-(3-(Aminomethyl)benzyl) acetamidine
NPPB	5-nitro-2-(3-phenylpropyl-amino) benzoic acid
LPS	Lipopolysaccharide
M-CSF	Macrophage colony stimulating factor
R6G	Rhodamine 6G
ETosis	Extracellular trap cell death
iNOS	Inducible Nitric oxide synthase
cHOClate	Conjugatable HOCl sensor

Synopsis

Chapter 1: Introduction

HOCl derived from enzyme myeloperoxidase (MPO) has various pathophysiological roles ranging from pathogen clearance to inflammatory diseases. Innate immune cells use various defence mechanisms such as phagocytosis, degranulation and extracellular trap cell death (ETosis) to fight the incoming microbes (Faurschou and Borregaard, 2003; Guimarães-Costa et al., 2012; Hampton et al., 1998). Among this phagocytosis is the most common mechanism, where the professional phagocytes engulf the microbes and dead cells in the body. The degradation of cargo in the phagosome is brought about by the combined action of proteolytic enzymes, redox enzymes and ion homeostasis etc. (Kinchen and Ravichandran, 2008; Nüsse, 2011; Winterbourn et al., 2016). The redox enzymes like NOX, MPO are important in generating reactive oxygen species (ROS) which can attack and decompose the pathogens non-specifically (Winterbourn et al., 2006).

Defects in ROS generations are implicated in impaired clearance of pathogens and hence infection in host. HOCl is one of the most destructive ROS in the phagosome, which is generated by the enzyme myeloperoxidase (MPO) delivered by phagosome-lysosome fusion (Huynh et al., 2007; Nordenfelt and Tapper, 2011). Mutations in MPO leads to impaired clearance of microbes like *Candida albicans, Staphylococcus aureus, Klebsiella pneumoniae* as studied in cell lines and mice (Aratani et al., 1999; Hirche et al., 2005). The resistant bacteria like *Anaplasma phagocytophilum*, *Streptococcus pyogenes* in healthy neutrophils and Mycobacterium *tuberculosis* in healthy macrophages survive in the phagosomes by preventing fusion with azurophilic granules or lysosomes respectively

(Corleis et al., 2012; Huynh and Grinstein, 2007; Urban et al., 2006). Since MPO is delivered to phagosomes by fusion with these vesicles, the possible way of survival could be by protecting from MPO derived HOCl.

Further the catalytic activity of MPO is crucial for ETosis, an alternative pathogen clearance pathway where microbes are trapped on a web like structure formed by the decondensed chromatin and antimicrobial enzymes (Guimarães-Costa et al., 2012; Metzler et al., 2011; Papayannopoulos et al., 2010). Here chromatin decondensation is initiated by the relocalisation of MPO from azurophilic granules to nucleus and studies showed a possible role for MPO derived HOCl in this process (Akong-Moore et al., 2012; Papayannopoulos et al., 2010).

HOCl and MPO are clinically relevant since MPO derived products are observed in atherosclerotic lesions (Hazen and Heinecke, 1997). Inflammatory diseases like multiple sclerosis and renal ischemia reperfusion leads to organ failure and are characterised by deposition of chlorinated species (Gray et al., 2008; Matthijsen et al., 2007). Here the activity of MPO is attributed from the extracellularly secreted MPO where pH is 7.2. Further, systemic lupus vasculitis, Inflammatory bowel diseases are characterised by the presence high levels of anti MPO antibodies (ANCA) or MPO levels respectively (Jennette and Falk, 2015). The origin of these process or enzymatic activity of MPO in these cases is not yet studied probably due to unavailability of a subcellular targetable sensor.

Since HOCl generation by MPO in various cellular locations is resulted in various pathophysiological conditions sensing HOCl with subcellular resolution will be helpful to unravel the mechanism behind this. Subcellular pH is a well-accepted functional marker

for various locations in the cell. In my PhD work I developed a quantitative sensor which detects HOCl and pH simultaneously in subcellular locations in the live cells.

Chapter 2: DNA based sensor for simultaneous measurement of pH and HOCl

I have developed a DNA based HOCl sensor which measure HOCl and pH independently and simultaneously. In chapter 2, I describe the design and in vitro characterization of the sensor. The sensor called *cHOClate* is designed based on a DNA scaffold which is covalently attached to three fluorophores; an HOCl sensitive fluorophore 1 which is a Cy 5 dye derivative (Oushiki et al., 2010; Panchuk-Voloshina et al., 1999); a pH sensitive fluorophore, Rhodmine-6G amide (Rhod 6G) (Tian et al., 2012) and an HOCl and pH insensitive fluorophore, Atto-488. This involves identification of an HOCl sensitive fluorophore 1, using mass spectrometric and photophysical characterization. The pH and HOCl sensing properties of *cHOClate* was characterized by fluorescence measurements. Since *cHOClate* is a DNA duplex-based design and ROS can also react with base pairs in DNA, I also showed that integrity of DNA is unaffected by ROS in the studied conditions.

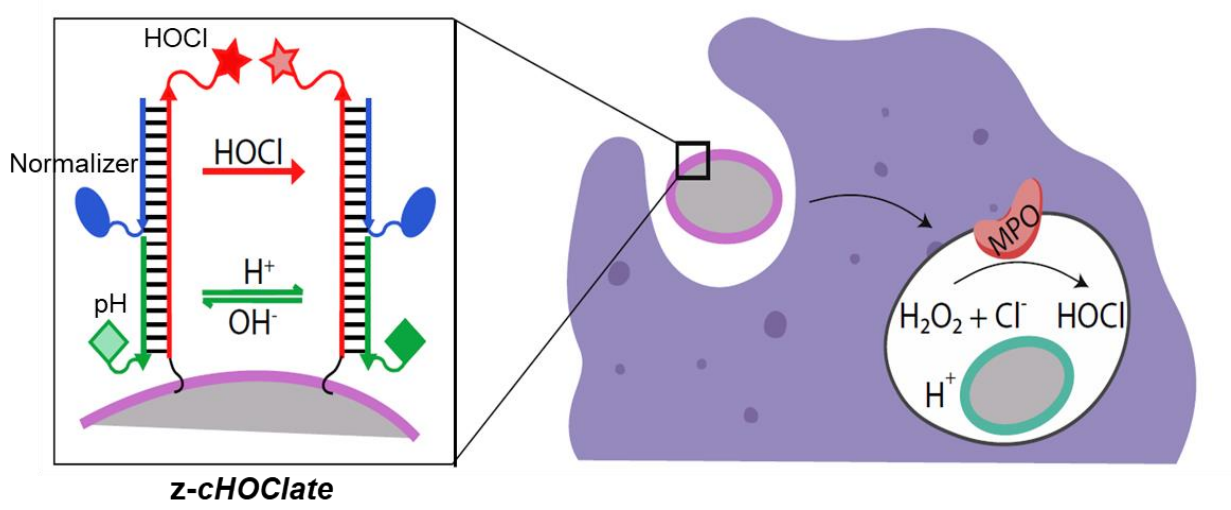

Figure S1: Graphical abstract. *cHOClate* contains three fluorophores: an HOCl sensitive fluorophore (red star) which undergoes turn off fluorescence with HOCl; a pH sensitive fluorophore (green diamond) which undergoes turn on fluorescence at acidic pH and a normalizer (blue oval) which is insensitive to both pH and HOCl. Ratio of Red/Blue (R/B) serve as a measure of HOCl while ratio of Green/Blue (G/B) serve as the measure of pH. Z-*cHOClate* (zymosan particles surface labeled with *cHOClate*) targets *cHOClate* to phagosome for HOCl and pH measurements. In the extracellular medium pH is neutral and HOCl is low, so the Z-cHOClate will show high R/B and low G/B- represented as purple in colour. In the mature phagosome of macrophages pH is acidic and HOCl is high, so Z-*cHOClate* will have high low R/B and high G/B- represented in cyan.

Chapter 3: Detection of phagosomal HOCl in live macrophages

Chapter 3 describes use of *cHOClate* for sensing HOCl in the maturing phagosomes of live macrophage cell lines. To target to phagosome, I covalently conjugated *cHOClate* to well accepted phagocytic cargo, zymosan particle using click chemistry and the resultant particles are called Z-*cHOClate* (Ohno et al., 1999; Underhill, 2003). The pH and HOCl

sensing properties of *Z-cHOClate* was characterized by fluorescence measurements. Use of pharmacological inhibitors for MPO confirmed the specificity of Z-*cHOClate* in detecting intraphagosomal HOCl. Using Z-*cHOClate*, I showed that chloride channels blocking in turn affects the HOCl production in the phagosomes of macrophages. Z-*cHOClate* revealed that, HOCl production in macrophage phagosomes happens in a burst of 3 minutes after phagosome maturation is achieved. Generalizability of the sensor in detecting phagosomal HOCl is proved using variety of mouse macrophage cell lines. Immunostaining and western blot proved that there is an upregulation of MPO in the mouse macrophage cell lines upon phagocytosis of Z-cHOClate.

Chapter 4: *Z-cHOClate* detects differential MPO levels in innate immune cells

In Chapter 4, I describe use of Z-*cHOClate* for differentiating active levels of myeloperoxidase in primary innate immune cells and in the immune stimulated primary macrophages from mouse and human. Z-*cHOClate* could detect dynamics of pH and HOCl in the neutrophil phagosomes. In contrast with macrophage phagosomes, neutrophil phagosomes stay near neutral while HOCl production happens within 5-10 minutes. This is in accordance with earlier reports where neutrophil phagosome is not acidifying (Nordenfelt and Tapper, 2011). Further we used Z-*cHOClate* to compare the pH and HOCl levels in primary innate immune cells derived from the same donor. Z-*cHOClate* revealed that MPO activity follows in the order macrophages< monocytes< neutrophils which is in concordance with the reported levels of MPO in these cells (King et al., 1997; Klebanoff et al., 2013).

Z-*cHOClate* detects an increased production of HOCl in the phagosomes of human macrophages stimulated with LPS. Using immunostaining I confirmed that there is an

upregulation of MPO expression in LPS treated cells, which is further increased upon phagocytosis of zymosan. Similarly, Z-*cHOClate* confirm the presence of active myeloperoxidase in primary mouse macrophages, which was not detected before (Brennan et al., 2001; McMillen et al., 2005).

In summery my work has showed use of DNA scaffold for sensing HOCl and pH simultaneously and independently in a quantitative regime, which mapped HOCl production in the maturing phagosomes of innate immune cells from mice and human. This platform can be extended to simultaneous sensing of other ROS, small molecules and ions during phagosome maturation and impact of each of these species in pathogen clearance. Further *cHOClate* can be used to reveal the activity of MPO in other subcellular locations.

References

Akong-Moore, K., Chow, O.A., von KöckritZ-Blickwede, M., and Nizet, V. (2012). Influences of chloride and hypochlorite on neutrophil extracellular trap formation. PLoS One *7*, e42984.

Aratani, Y., Koyama, H., Nyui, S., Suzuki, K., Kura, F., and Maeda, N. (1999). Severe impairment in early host defense against Candida albicans in mice deficient in myeloperoxidase. Infect. Immun. *67*, 1828–1836.

Brennan, M.L., Anderson, M.M., Shih, D.M., Qu, X.D., Wang, X., Mehta, A.C., Lim, L.L., Shi, W., Hazen, S.L., Jacob, J.S., et al. (2001). Increased atherosclerosis in myeloperoxidase-deficient mice. J. Clin. Invest. *107*, 419–430.

Corleis, B., Korbel, D., Wilson, R., Bylund, J., Chee, R., and Schaible, U.E. (2012). Escape of Mycobacterium tuberculosis from oxidative killing by neutrophils. Cell Microbiol. *14*, 1109–1121.

Faurschou, M., and Borregaard, N. (2003). Neutrophil granules and secretory vesicles in inflammation. Microbes Infect. *5*, 1317–1327.

Gray, E., Thomas, T.L., Betmouni, S., Scolding, N., and Love, S. (2008). Elevated activity and microglial expression of myeloperoxidase in demyelinated cerebral cortex in multiple sclerosis. Brain Pathol. *18*, 86–95.

Guimarães-Costa, A.B., Nascimento, M.T.C., Wardini, A.B., Pinto-da-Silva, L.H., and Saraiva, E.M. (2012). ETosis: A Microbicidal Mechanism beyond Cell Death. J Parasitol Res *2012*, 929743.

Hampton, M.B., Kettle, A.J., and Winterbourn, C.C. (1998). Inside the neutrophil phagosome: oxidants, myeloperoxidase, and bacterial killing. Blood *92*, 3007–3017.

Hazen, S.L., and Heinecke, J.W. (1997). 3-Chlorotyrosine, a specific marker of myeloperoxidase-catalyzed oxidation, is markedly elevated in low density lipoprotein isolated from human atherosclerotic intima. J. Clin. Invest. *99*, 2075–2081.

Hirche, T.O., Gaut, J.P., Heinecke, J.W., and Belaaouaj, A. (2005). Myeloperoxidase plays critical roles in killing Klebsiella pneumoniae and inactivating neutrophil elastase: effects on host defense. J. Immunol. *174*, 1557–1565.

Huynh, K.K., and Grinstein, S. (2007). Regulation of vacuolar pH and its modulation by some microbial species. Microbiol. Mol. Biol. Rev. *71*, 452–462.

Huynh, K.K., Eskelinen, E.-L., Scott, C.C., Malevanets, A., Saftig, P., and Grinstein, S. (2007). LAMP proteins are required for fusion of lysosomes with phagosomes. EMBO J. *26*, 313–324.

Jennette, J.C., and Falk, R.J. (2015). ANCAs are also antimonocyte cytoplasmic autoantibodies. Clin. J. Am. Soc. Nephrol. *10*, 4–6.

Kinchen, J.M., and Ravichandran, K.S. (2008). Phagosome maturation: going through the acid test. Nat. Rev. Mol. Cell Biol. *9*, 781–795.

King, C.C., Jefferson, M.M., and Thomas, E.L. (1997). Secretion and inactivation of myeloperoxidase by isolated neutrophils. J. Leukoc. Biol. *61*, 293–302.

Klebanoff, S.J., Kettle, A.J., Rosen, H., Winterbourn, C.C., and Nauseef, W.M. (2013). Myeloperoxidase: a front-line defender against phagocytosed microorganisms. J. Leukoc. Biol. *93*, 185–198.

Matthijsen, R.A., Huugen, D., Hoebers, N.T., de Vries, B., PeutZ-Kootstra, C.J., Aratani, Y., Daha, M.R., Tervaert, J.W.C., Buurman, W.A., and Heeringa, P. (2007). Myeloperoxidase is critically involved in the induction of organ damage after renal ischemia reperfusion. Am. J. Pathol. *171*, 1743–1752.

McMillen, T.S., Heinecke, J.W., and LeBoeuf, R.C. (2005). Expression of human myeloperoxidase by macrophages promotes atherosclerosis in mice. Circulation *111*, 2798–2804.

Metzler, K.D., Fuchs, T.A., Nauseef, W.M., Reumaux, D., Roesler, J., Schulze, I., Wahn, V., Papayannopoulos, V., and Zychlinsky, A. (2011). Myeloperoxidase is required for neutrophil extracellular trap formation: implications for innate immunity. Blood *117*, 953–959.

Nordenfelt, P., and Tapper, H. (2011). Phagosome dynamics during phagocytosis by neutrophils. J. Leukoc. Biol. *90*, 271–284.

Nüsse, O. (2011). Biochemistry of the phagosome: the challenge to study a transient organelle. ScientificWorldJournal *11*, 2364–2381.

Ohno, N., Miura, T., Miura, N.N., Chiba, N., Uchiyama, M., Adachi, Y., and Yadomae, T. (1999). Inflammatory and immunopharmacological activities of meta-periodate oxidized zymosan. Zentralbl. Bakteriol. *289*, 63–77.

Oushiki, D., Kojima, H., Terai, T., Arita, M., Hanaoka, K., Urano, Y., and Nagano, T. (2010). Development and application of a near-infrared fluorescence probe for oxidative stress based on differential reactivity of linked cyanine dyes. J. Am. Chem. Soc. *132*, 2795–2801.

Panchuk-Voloshina, N., Haugland, R.P., Bishop-Stewart, J., Bhalgat, M.K., Millard, P.J., Mao, F., Leung, W.Y., and Haugland, R.P. (1999). Alexa Dyes, a Series of New Fluorescent Dyes that Yield Exceptionally Bright, Photostable Conjugates. Journal of Histochemistry & Cytochemistry *47*, 1179–1188.

Papayannopoulos, V., Metzler, K.D., Hakkim, A., and Zychlinsky, A. (2010). Neutrophil elastase and myeloperoxidase regulate the formation of neutrophil extracellular traps. J. Cell Biol. *191*, 677–691.

Tian, M., Peng, X., Fan, J., Wang, J., and Sun, S. (2012). A fluorescent sensor for pH based on rhodamine fluorophore. Dyes and Pigments *95*, 112–115.

Underhill, D.M. (2003). Macrophage recognition of zymosan particles. J Endotoxin Res *9*, 176–180.

Urban, C.F., Lourido, S., and Zychlinsky, A. (2006). How do microbes evade neutrophil killing? Cell Microbiol. *8*, 1687–1696.

Winterbourn, C.C., Hampton, M.B., Livesey, J.H., and Kettle, A.J. (2006). Modeling the reactions of superoxide and myeloperoxidase in the neutrophil phagosome: implications for microbial killing. J. Biol. Chem. *281*, 39860–39869.

Winterbourn, C.C., Kettle, A.J., and Hampton, M.B. (2016). Reactive oxygen species and neutrophil function. Annu. Rev. Biochem. *85*, 765–792.

List of Publications

Thekkan, S., Jani, M. S., Cui, C., Dan, K., Zhou, G., Becker, L.* and Krishnan, Y.*(2018) A DNA-based fluorescent reporter maps HOCl production in the maturing phagosome. *Nature Chemical Biology* (Article in press).

Chapter 1

Introduction

1.A: Pathogen defence and role of reactive oxygen species

The host body fights pathogen attack by the combined action of innate and adaptive immune system. While innate immune system is the first line of defence which is non-specific and fights a diverse number of pathogens; adaptive immune system is activated after many hours of pathogen invasion and it is very specific and efficient against the pathogens (2016). The innate immune system consists of circulating neutrophils, monocytes and antigen presenting cells (APC) such as macrophages and dendritic cells (Charles A Janeway et al., 2001a). These circulating cells and APCs constantly patrol the body to detect and eliminate foreign materials and pathogens. APCs display pathogen specific antigens on their surface to act as signals for inducing adaptive immune response (Charles A Janeway et al., 2001a).

The innate immune cells use various pathogen clearing mechanisms like phagocytosis, degranulation, extracellular trap cell death (ETosis) etc (Faurschou and Borregaard, 2003; Guimarães-Costa et al., 2012). Phagocytosis is the process of engulfing the pathogen, foreign particle or dead cells by immune cells and degrading them in specified compartments called phagosomes. Neutrophils, monocytes, macrophages, dendritic cells and mast cells are called professional phagocytes because they display pattern recognition receptors (PRRs) which can detect microbes like bacteria, fungus etc. to engulf them efficiently (Akira et al., 2006). Apart from phagocytosis immune cells also undergoes degranulation where the immune cells release cytotoxic antimicrobial peptides and other antimicrobial molecules from their secretary vesicles called granules

(Faurschou and Borregaard, 2003). Granulocytes, NK cells or lymphocytes are reported to show degranulation and releases diverse antimicrobial molecules in a cell specific manner. A third mechanism called ETosis, where condensed chromatin gets recoiled and releases extracellularly to trap and immobilize pathogens has been discovered recently (Guimarães-Costa et al., 2012). Though ETosis is predominant in the case of circulating neutrophils (NETosis), recent studies also uncovered the formation of ETs (extra cellular traps) by other innate immune cells such as macrophages, basophils etc. While the exact reasons on the choice of pathogen clearance mechanism used by immune cells is still not clear phagocytosis is the most studied and major way of pathogen clearance (Branzk and Papayannopoulos, 2013).

1.A.1: Phagocytosis and molecular players

Host body uses phagocytosis for clearing pathogens as well clearing the dead cells in the body. The molecular players involved in the phagocytosis of pathogen and dead cells are different, the former involves recognition of foreign pathogen associated molecular patterns (PAMPs) while the latter involves molecular markers called “eat me signals” on the surface of dead cells (Mogensen, 2009; Ravichandran, 2010). The process of phagocytosis occurs in 5 steps described below.

(1) Phagocyte activation- Resting phagocytes are activated by inflammatory mediators such as bacterial products (bacterial proteins, capsules, LPS, peptidoglycan, teichoic acids, etc.), complement proteins, inflammatory cytokines, and prostaglandins. As a result, they enhance the pattern-recognition receptors (PRRs) that recognize and bind to pathogen-associated molecular patterns (PAMPs) which are signature molecules of

microbes that are absent in human cells. Upon activation phagocytes exhibits increased metabolic and microbicidal activity by increasing the production of ATPs, lysosomal enzymes, lethal oxidants, etc.

(2) Chemotaxis of phagocyte- Chemotaxis is the movement of phagocytes toward an increasing concentration of a chemical attractant such as bacterial factors (bacterial proteins, capsules, LPS, peptidoglycan, teichoic acids, etc.), complement proteins (C5a), chemokines (chemotactic cytokines such as interleukin-8 secreted by various cells), fibrin split products, kinins, and phospholipids released by injured host cells. (3) Attachment of phagocyte to the microbes or dead cell- Attachment is the innate recognition of pathogen-associated molecular patterns or PAMPs by means of pattern-recognition receptors, such as scavenger receptors and mannose receptors, on the surface of the phagocyte.

(4) Ingestion of the pathogen- Polymerization and then depolymerization of actin filaments send pseudopods out to engulf the microbe and place it in a vesicle called a phagosome.

(5) Destruction of microbes- The ingested microbes are destroyed in the phagosome with the help of digestive enzymes, microbicidal chemicals, and reactive chemical species. Though the average time of phagocytosis varies depending on the cargo and host cells it takes ~30 minutes in most of the cases (Paul et al., 2013).

Defects in any of the phagocytosis steps leads to impaired clearance of bacteria or fungi can cause infectious diseases. For example, leukocytosis is the disease of impaired pathogen clearance by neutrophils, caused by loss of adhesive proteins on the neutrophil surface and thereby not able to exit circulation(Lekstrom-Himes and Gallin, 2000). Apart

from these, resistant microbes evade the immune system of healthy host by manipulating the phagocytic machinery. Pathogenic bacteria like *Mycobacterium Tuberculosis* and *Streptococcus Pneumonia* express virulent lipids or surface polysaccharides that efficiently mask their PAMPs from immune recognition (Charles A Janeway et al., 2001b).

1.A.2: ROS and HOCl in phagocytosis

The cargo inside the phagosomes are degraded by the combined action of reactive oxygen species or reactive nitrogen species (ROS/ RNS) generated by redox enzymes, antibacterial peptides and other proteolytic enzymes (Pauwels et al., 2017). Formation of this enclosed compartment is therefore crucial for the host cells because the radical species being generated will be high in concentration and effective in killing the microbes (Dupré-Crochet et al., 2013). Generation of reactive species or delivery of the proteolytic enzymes in the phagosomes is coupled with changes in ionic environment in the phagosome lumen, such as acidification, [Ca^{2+}] changes etc (Dupré-Crochet et al., 2013). These processes are assisted by phagosome-lysosome fusion to form phagolysosome, since lysosome is at acidic pH (~4.5) and contains proteolytic enzymes. The ionic environment in the phagosome changes depending on the type of host cell and pathogen, for e.g., macrophage phagosomes usually undergoes acidification while neutrophil phagosomes remains near neutral (Canton et al., 2014; Nordenfelt and Tapper, 2011).

The primary ROS generated in the phagosome is superoxide ($O_2^{\cdot -}$). Superoxide is formed by the assembly NADPH oxidase subunits on the phagosomal membrane. The enzyme oxidizes NADPH to $NADP^+$ in the cytosolic side, while reducing molecular oxygen(O_2) in the phagosome to $O_2^{\cdot -}$ by one electron reduction (DeLeo et al., 1999). This primary ROS

can give rise to a number of secondary ROS/ RNS species. Superoxide generated can be dismutated to hydrogen peroxide in the phagosome either with the help of superoxide dismutase (SOD) or spontaneous dismutation (Dupré-Crochet et al., 2013). H_2O_2 is converted to HOCl in presence of chloride ion (Cl^-) by the enzyme myeloperoxidase (MPO) which is delivered to the phagosome during phagosome maturation(Aiken et al., 2012; Robinson, 2008). H_2O_2 can further form hydroxyl radicals in presence Fe^{2+} present in the phagosomes. Phagocytes contains inducible Nitric oxide synthase (iNOS) which is recruited to phagosome and can generate nitric oxide ($^{\cdot}NO$) in phagosomes, which can further generate peroxynitrite ($ONOO^-$) by reaction with superoxide(Förstermann and Sessa, 2012).

ROS and RNS are chemically unstable and are highly reactive in nature. Species like H_2O_2 and HOCl can have longer life time compared to short lived ROS like superoxide, hydroxy radical, and peroxynitrite which has nano seconds life time. The reduction potential and life time of the ROS/RNS is reflected in its high reactivity towards biological molecules. The most important cellular target of ROS is DNA, where base oxidation, particularly guanine and blocking lesions or strand breaks may be lethal unless they are repaired (Fang, 2011). Among proteins, iron-sulfur (Fe-S) cluster-containing proteins from microbes are also vulnerable to ROS damage and may substantially restrict metabolic pathways (Fang, 2011). Bactericidal activities of HOCl and its toxicity for surrounding tissues occur because of its potential to modify lipids, DNA, amines and tyrosine forming halohydrins, 5-chlorouracil, chloramines and 3-chlorotyrosine, respectively. The usual consequence of MPO-mediated macromolecule modification is their fragmentation, through chloramine formations (Davies, 2011). Mutations in ROS generating proteins can

lead to impaired clearance of pathogens. This was reflected in chronic granulomatous disease (CGD) patients where an inherited deficiency in NOX2 components results in chronic infection (Fang, 2011). Deficiencies in iNOS can also cause impaired clearance of bacteria, fungi and viruses due to the lack of peroxynitrite formation (Akaike and Maeda, 2000).

HOCl has strong microbicidal properties, and the prevailing view is that chloride is the physiological halide for the MPO-mediated antimicrobial system. Though absence of life-threatening infections in MPO deficient humans challenge the bactericidal properties of HOCl, candidiasis in MPO deficient diabetic mellites patients are highly prevalent (Klebanoff et al., 2013). Further, MPO mutations has led to impaired clearance of microbes like *Staphylococcus aureus, Klebsiella pneumoniae, plasmodium yeolii* etc. in isolated human neutrophils and mice models (Aratani et al., 1999; Hampton et al., 1996; Humphreys et al., 1989; Theeß et al., 2017).

Despite the high amount of myeloperoxidase present in neutrophils (5% of total protein) many bacterial and fungal species escape the killing mechanism in phagosomes and even use neutrophils for their survival in the host body. *Anaplasma phagocytophilum*, like other Ehrlichia species use neutrophils as a host cell and evolved fascinating strategies to survive within this hostile environment(Borjesson et al., 2005; Carlyon and Fikrig, 2003). Streptococcus pyogenes, a gram-positive bacterium is one of the most common human pathogens causing pharyngitis, impetigo, scarlet fever and also severe systemic disease. During infections S. pyogenes seem to use neutrophils to hide from immune responses by inhibiting phagosome fusion with azurophilic granules (Urban et al., 2006).

The bacterium forms large capsules after incubation with host phagocytic cells resulting in increased virulence and resistance against phagocytic killing (Urban et al., 2006). Further, *Mycobacterium tuberculosis* and Group *A Streptococcus* affect acidification of phagosome by preventing phagosome-lysosome fusion and survive in the macrophages (Queval et al., 2017). Since the microbes survives by preventing fusion with MPO containing vesicles, HOCl might be the major ROS which could defend these species.

Hence, detection of HOCl in phagosomal compartments would provide insight about immune evasion mechanisms utilized by different pathogenic species. There seems to have a direct correlation between ROS generation and the maturation stage of a phagosome. Hence information about the temporal resolution of phagosomal maturation and MPO activity will give insights in to the mechanistic details of pathogen evasion.

1.A.3: ROS and HOCl in ETosis

Apart from well-studied roles in of pathogen degradation in phagosomes, ROS is also crucial for extracellular trap cell death (ETosis) (Fuchs et al., 2007). The formations extracellular traps (ETs) by innate immune cells can be stimulated using bacterial derived species like LPS, PMA or by the pathogens like bacteria and fungi (Branzk et al., 2014; Yu and Su, 2013). Though the exact reason behind ET formation is not clear, studies by Branzk N., et al. suggest a strong dependence on size of the pathogen, as small yeast particles of *Candida albicans* followed phagocytosis while hyphae structure showed ET formation (Branzk et al., 2014).

Most of the studies on extracellular trap formation is with neutrophils, neutrophil extracellular taps (NETs). NETs contain the decondensed chromatin along with

cytoplasmic granular proteins like neutrophil elastase (NE), Proteinase3 (PR3) and MPO (Brinkmann et al., 2004; Fuchs et al., 2007; Papayannopoulos et al., 2010). A signalling role for ROS is well established for the formation of NETs since alterations in H_2O_2 levels affects NETs (Fuchs et al., 2007). Pathogens stimulate H_2O_2 production in the cytosol, signalling by H_2O_2 leads to dissociation of azurophilic granule components and decondensation of chromatin. MPO delocalisation is shown to be important for the NET formation and this is affected by the availability of chloride ions (Akong-Moore et al., 2012; Metzler et al., 2014). So, either MPO or its enzymatic activity has a role in extracellular trap formation which is an alternative way of pathogen clearance.

1.B: HOCl in pathophysiology and expression of MPO in innate immune cells

1.B.1: MPO activity in inflammation

MPO can damage host tissue through the generation of reactive halogenating and nitrating agents. Indeed, decreased levels of 3-chlorotyrosine, 3-bromotyrosine, 3-nitrotyrosine, and protein carbamylation are seen at the inflammation sites of MPO-KO mice compared to WT mice (Gaut et al., 2001, 2002). Thus, based on the assumption that MPO has a detrimental effect during chronic inflammation, it can be expected that inflammation would be reduced under MPO-deficient conditions. Indeed, this has been observed in many acute and chronic inflammatory diseases (Aratani, 2018).

MPO derived chlorinated and nitrated lipoproteins are noticed in inflammatory vascular disease like cardiovascular atheroma and myocardial infarction (Hazell et al., 1996; Hazen and Heinecke, 1997; Lau and Baldus, 2006; Nicholls and Hazen, 2005). Studies from MPO deficient humans showed a decreased occurrence cardiovascular disease which place MPO as a risk factor cardiac arrest (Anatoliotakis et al., 2013; Nicholls and

Hazen, 2005). Further, researchers showed a prominent role for MPO in stroke where MPO modifies high density lipoproteins (HDLs) (Breckwoldt et al., 2008). Also, recent studies characterized multiple sclerotic lesions in the human brain by a high abundance of MPO derived products (Gray et al., 2008). Further, studies using MPO deficient mice showed that MPO derived products are critically involved in induction of organ damage after renal ischemia reperfusion, compared to the wild type controls (Matthijsen et al., 2007). Source of active MPO in these cases are thought to be the secreted MPO from neutrophils, since they are rich in MPO (van Leeuwen et al., 2008).

Inflammatory diseases are characterized with an increased recruitment of macrophages in the infected area (Bain and Mowat, 2014; Duffield, 2010). These clinical evidences suggest a possible role of macrophage derived myeloperoxidase in inflammatory diseases. Even though the abundance of MPO in macrophages will be scarce the accumulation of macrophages in the inflamed area may be the reason.

1.B.2: MPO in autoimmunity and inflammatory bowel disease (IBD)

Autoimmune disorders like ANCA- associated systemic vasculitis is enriched with antibodies against MPO which is seen to be periplasmic(Jennette and Falk, 2015; Thieblemont et al., 2016). Though one of the clinical tests for detecting systemic vasculitis is detecting anti-MPO antibodies, the enzymatic activity of MPO in these disorders is not yet clear.

Also, Inflammatory bowel disease (IBD) like Cron’s disease and colitis is characterized with high abundance of MPO in the stool samples (Masoodi et al., 2011). Recent studies also showed an increase in antifungal antibodies in the blood of Crohn’s disease patients (Mitsuyama et al., 2016; Standaert-Vitse et al., 2009). The emerging role of mycobiome

in the colon health suggests that, opportunistic fungi like *C. albicans* (in humans) or *C. tropicalis* (mice) are involved in the development of inflammatory bowel disease in mice and humans (Huffnagle and Noverr, 2013; Iliev et al., 2012; Leonardi et al., 2018; Sokol et al., 2017). The enzymatic activity of MPO in these cases re not yet considered, but the antifungal activity of MPO in pathogen clearance might have a role in controlling IBD development.

1.C: Expression, processing and activity of MPO in innate immune cells

MPO is mainly expressed in neutrophils, which contains ~ 5% of MPO as their protein dry weight, and is stored in azurophil granules (Odobasic et al., 2016). Monocytes express MPO which is 1% of their total protein and stored in lysosomes. Monocytes gradually lose their MPO during their differentiation to macrophages, though some of the tissue macrophages in humans express low levels of MPO (Odobasic et al., 2016). MPO in macrophages is thought to be the acquired from neutrophil engulfing or endocytosis of MPO.

MPO is synthesized as an inactive proprotein in ER and send to Golgi for post translational modifications. The mature enzyme is a 140-kDa heme-containing homodimer, with each monomer consisting of a heavy (55 – 64 kDa, 466 amino acids) and a light (10 – 15 kDa, 108 amino acids) subunit (Klebanoff, 2005). Incorporation of the covalently bound heme complex precedes the maturation process, implying enzymatic activity of the precursor (Klebanoff, 2005). Active MPO is stored in lysosomes, in neutrophils MPO is contained in specialized lysosomes called azurophilic granules. Host cells can also secrete MPO to the extracellular stimuli like PMA, antibody coated zymosan etc. (King et al., 1997).

Myeloperoxidase (MPO) generate HOCl from H_2O_2 and chloride anion (Klebanoff, 2005). MPO can also generate HSCN, HOBr, HOI by the oxidation of respective anions SCN-, Br- and I- using H_2O_2. In vitro experiments showed that MPO is most effective in oxidizing thiocyanate> Iodate> bromide> chloride with their rate constants following the same order (Furtmüller et al., 1998). But physiological chloride concentration is in millimolar compared to micromolar concentrations of other anions, and hence HOCl is the major species generated by MPO.

MPO is active at both neutral pH (~7.4) and acidic pH (~5). MPO has both peroxidase activity as well as chlorinating activity, a pH dependence for these both functions was shown by in vitro experiments. At acidic pH MPO showed more chlorinating activity since HOCl is the predominant species, while at neutral pH the peroxidase properties of MPO persists since it has more affinity to the peroxidase substrate guaiacol (Vlasova et al., 2006). Hence in macrophage phagosome the predominating activity will be chlorinating activity while in the neutrophil phagosomes the peroxidase activity predominates. This will still leave the question on the origin of chlorinated products in inflammatory diseases since extracellular pH is neutral. A probe which can sense HOCl or MPO activity with spatiotemporal precision in various locations in the cell would give the insight to the mechanistic details behind MPO regulation in pathophysiology.

1.D: Current probes for detecting HOCl

Methods to detect the MPO activity gains much attention since enzymatic activity of MPO is resulted in various pathophysiological conditions ranging from pathogen clearance to inflammatory diseases. Fluorescence based imaging techniques are widely used for detecting any analyte in biological samples with spatiotemporal resolution.

Immunostaining for 3-chlorotyrosins (which is the indirect measure of MPO activity) or antibody staining for MPO serve as a detection method in inflammatory diseases (Chen et al., 2008; Gray et al., 2008; Robaszkiewicz et al., 2011). Still this is from an ensemble activity where subcellular location is debatable and hence the underlined mechanism of enzyme dysregulation. Though immunostaining offers a sensitive technique to image MPO derived products, it is limited to fixed samples which limits early onset of this activity. Fluorescent small molecules or proteins for HOCl would offer a live method of MPO activity detection with spatiotemporal resolution. There are no fluorescent proteins for HOCl detection reported till date. Fluorescent small molecules ranging from green – NIR wavelength regions which are very bright (Brightness= extinction coefficient * fluorescent quantum yield) are used as a sensing strategy for HOCl. Figure 1.1 lists couple of highly used fluorophores for HOCl detection with their fluorescent properties (Kenmoku et al., 2007; Koide et al., 2011; Setsukinai et al., 2003). Targeting to a specific subcellular location and reliably quantitating HOCl using these fluorophores are limited since small molecules can leak from the compartment.

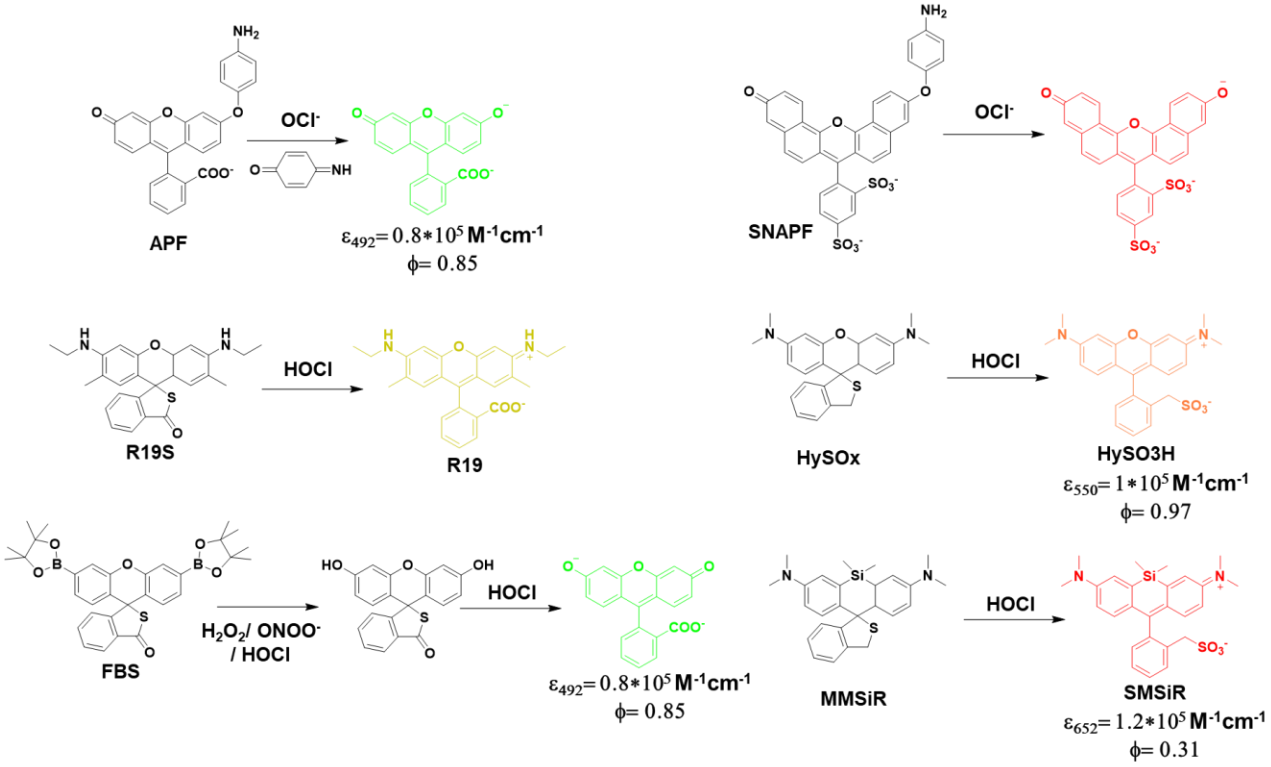

Figure 1.1: Small molecule fluorophores for HOCl/OCl$^-$

Reliable detection of any ROS demand fast responsive molecules since the life time of ROS is very short owing to their high reactivity, especially in the of biological environment (Schmitt et al., 2014). Further, the probe should be targetable to various subcellular locations and quantitative so that the measurements are not affected by the availability of sensor. Since MPO activity is noted intracellularly and extracellularly, sensing pH along with HOCl will report the functional implications of pH in MPO activity in pathophysiology.

1.E: DNA based ratiometric sensors for small molecules and ions in biological systems

One of the limitations of small molecule-based sensing of any analyte is that the relative signals would be a function of sensor availability(Jiang et al., 2018). Ratiometric sensing offers the advantage of a loading control where an insensitive fluorophore or internal wavelength will normalize the amount of available sensor (Lou et al., 2013; Zhang et al., 2014). Using of an internal wavelength from the fluorophore which is not sensitive to analyte is limited to very few numbers of fluorophores-analyte pairs. As a much generalisable approach use of two dye system is developed, where the fluorescence of one dye changes as a function of analyte while the other one remains unaffected. These methods use the quantitative analysis methods like FRET (Donor intensity/ acceptor FRET) or ratio of intensities of sensitive/ insensitive fluorophores (R/G) etc. Since developing a FRET pairs for each analyte is non-trivial, R/G based approach is much more adaptable to develop quantitative sensors.

While R/G based is approach is more generalizable, care should be taken to keep the sensitive and insensitive fluorophores beyond their FRETing distance as a rule of thumb, so that measurements made is reflective of the analyte concentration. This can be achieved by using rigid spacers, which at the same time keep the fluorophores beyond their FRETing distance as well biocompatible for the subsequent purpose. DNA duplex act as rigid rod below 200-base pairs (bp) which can be used as a spacer owing to its easy functionalisation, modularity, ability to accommodate fixed ratio between fluorophores and biocompatibility (Modi et al., 2009; Saha et al., 2015).

DNA based sensors have laid platform for ratiometric sensing of ions and small molecules like H^+, Cl^-, cAMP(cyclic AMP), Ca^{2+} etc. in intracellular compartments of live cells and organisms (Chakraborty et al., 2017; Modi et al., 2009; Saha et al., 2015; Sharma et al., 2014; Surana et al., 2011). These sensors use the simplistic design, where single strands of DNA (usually 24 - 100 bases long) containing fluorophores are hybridised through Watson crick base paring which in turn results in a fixed ratio of fluorophores. The ease of functionalisation of DNA gives the advantage that the position of fluorophores can be kept beyond the FRETing distance, and there by any fluorogenic sensor can be converted to a ratiometric sensor provided there is an insensitive fluorophore for the analyte. The prolonged stability for these devises in biological can be further improved by using the more stable versions of DNA like L-DNA, LNA or PNA which will still provide the advantage of 1:1 stoichiometry (Surana et al., 2015). I chose DNA duplex based ratiometric sensing for developing HOCl sensor.

Additionally, modularity of DNA nanostructures can accommodate multiple functionalities which can be used for quantitative sensing of multiple analytes as well as targeting the sensors to specific location in the cell. Considering these advantages, I have developed a DNA based sensor called *cHOClate* which can sense pH and HOCl quantitatively and simultaneously. *cHOClate* leverages modularity of DNA duplex further to accommodate a targeting module so that they can be used in various locations in the cells. I have demonstrated the use of *cHOClate* to simultaneously map pH and HOCl in the phagosomes of various innate immune cells from mice and human.

1F: References

Aiken, M.L., Painter, R.G., Zhou, Y., and Wang, G. (2012). Chloride transport in functionally active phagosomes isolated from Human neutrophils. Free Radic. Biol. Med. *53*, 2308–2317.

Akaike, T., and Maeda, H. (2000). Nitric oxide and virus infection. Immunology *101*, 300–308.

Akira, S., Uematsu, S., and Takeuchi, O. (2006). Pathogen recognition and innate immunity. Cell *124*, 783–801.

Akong-Moore, K., Chow, O.A., von KöckritZ-Blickwede, M., and Nizet, V. (2012). Influences of chloride and hypochlorite on neutrophil extracellular trap formation. PLoS One *7*, e42984.

Anatoliotakis, N., Deftereos, S., Bouras, G., Giannopoulos, G., Tsounis, D., Angelidis, C., Kaoukis, A., and Stefanadis, C. (2013). Myeloperoxidase: expressing inflammation and oxidative stress in cardiovascular disease. Curr. Top. Med. Chem. *13*, 115–138.

Aratani, Y. (2018). Myeloperoxidase: Its role for host defense, inflammation, and neutrophil function. Arch. Biochem. Biophys. *640*, 47–52.

Aratani, Y., Koyama, H., Nyui, S., Suzuki, K., Kura, F., and Maeda, N. (1999). Severe impairment in early host defense against Candida albicans in mice deficient in myeloperoxidase. Infect. Immun. *67*, 1828–1836.

Bain, C.C., and Mowat, A.M. (2014). Macrophages in intestinal homeostasis and inflammation. Immunol. Rev. *260*, 102–117.

Borjesson, D.L., Kobayashi, S.D., Whitney, A.R., Voyich, J.M., Argue, C.M., and Deleo, F.R. (2005). Insights into pathogen immune evasion mechanisms: Anaplasma phagocytophilum fails to induce an apoptosis differentiation program in human neutrophils. J. Immunol. *174*, 6364–6372.

Branzk, N., and Papayannopoulos, V. (2013). Molecular mechanisms regulating NETosis in infection and disease. Semin Immunopathol *35*, 513–530.

Branzk, N., Lubojemska, A., Hardison, S.E., Wang, Q., Gutierrez, M.G., Brown, G.D., and Papayannopoulos, V. (2014). Neutrophils sense microbe size and selectively release neutrophil extracellular traps in response to large pathogens. Nat. Immunol. *15*, 1017–1025.

Breckwoldt, M.O., Chen, J.W., Stangenberg, L., Aikawa, E., Rodriguez, E., Qiu, S., Moskowitz, M.A., and Weissleder, R. (2008). Tracking the inflammatory response in stroke in vivo by sensing the enzyme myeloperoxidase. Proc. Natl. Acad. Sci. USA *105*, 18584–18589.

Brinkmann, V., Reichard, U., Goosmann, C., Fauler, B., Uhlemann, Y., Weiss, D.S., Weinrauch, Y., and Zychlinsky, A. (2004). Neutrophil extracellular traps kill bacteria. Science (80-.). *303*, 1532–1535.

Canton, J., Khezri, R., Glogauer, M., and Grinstein, S. (2014). Contrasting phagosome pH regulation and maturation in human M1 and M2 macrophages. Mol. Biol. Cell *25*, 3330–3341.

Carlyon, J.A., and Fikrig, E. (2003). Invasion and survival strategies of*Anaplasma phagocytophilum*. Cell Microbiol. *5*, 743–754.

Chakraborty, K., Leung, K., and Krishnan, Y. (2017). High lumenal chloride in the lysosome is critical for lysosome function. Elife *6*, e28862.

Charles A Janeway, J., Travers, P., Walport, M., and Shlomchik, M.J. (2001a). Immunobiology.

Charles A Janeway, J., Travers, P., Walport, M., and Shlomchik, M.J. (2001b). Pathogens have evolved various means of evading or subverting normal host defenses.

Chen, J.W., Breckwoldt, M.O., Aikawa, E., Chiang, G., and Weissleder, R. (2008). Myeloperoxidase-targeted imaging of active inflammatory lesions in murine experimental autoimmune encephalomyelitis. Brain *131*, 1123–1133.

Davies, M.J. (2011). Myeloperoxidase-derived oxidation: mechanisms of biological damage and its prevention. J Clin Biochem Nutr *48*, 8–19.

DeLeo, F.R., Allen, L.A., Apicella, M., and Nauseef, W.M. (1999). NADPH oxidase activation and assembly during phagocytosis. J. Immunol. *163*, 6732–6740.

Duffield, J.S. (2010). Macrophages and immunologic inflammation of the kidney. Semin Nephrol *30*, 234–254.

Dupré-Crochet, S., Erard, M., and Nüβe, O. (2013). ROS production in phagocytes: why, when, and where? J. Leukoc. Biol. *94*, 657–670.

Fang, F.C. (2011). Antimicrobial actions of reactive oxygen species. MBio *2*.

Faurschou, M., and Borregaard, N. (2003). Neutrophil granules and secretory vesicles in inflammation. Microbes Infect. *5*, 1317–1327.

Förstermann, U., and Sessa, W.C. (2012). Nitric oxide synthases: regulation and function. Eur. Heart J. *33*, 829–37, 837a.

Fuchs, T.A., Abed, U., Goosmann, C., Hurwitz, R., Schulze, I., Wahn, V., Weinrauch, Y., Brinkmann, V., and Zychlinsky, A. (2007). Novel cell death program leads to neutrophil extracellular traps. J. Cell Biol. *176*, 231–241.

Furtmüller, P.G., Burner, U., and Obinger, C. (1998). Reaction of myeloperoxidase compound I with chloride, bromide, iodide, and thiocyanate. Biochemistry *37*, 17923–17930.

Gaut, J.P., Yeh, G.C., Tran, H.D., Byun, J., Henderson, J.P., Richter, G.M., Brennan, M.L., Lusis, A.J., Belaaouaj, A., Hotchkiss, R.S., et al. (2001). Neutrophils employ the myeloperoxidase system to generate antimicrobial brominating and chlorinating oxidants during sepsis. Proc. Natl. Acad. Sci. USA *98*, 11961–11966.

Gaut, J.P., Byun, J., Tran, H.D., Lauber, W.M., Carroll, J.A., Hotchkiss, R.S., Belaaouaj, A., and Heinecke, J.W. (2002). Myeloperoxidase produces nitrating oxidants in vivo. J. Clin. Invest. *109*, 1311–1319.

Gray, E., Thomas, T.L., Betmouni, S., Scolding, N., and Love, S. (2008). Elevated activity and microglial expression of myeloperoxidase in demyelinated cerebral cortex in multiple sclerosis. Brain Pathol. *18*, 86–95.

Guimarães-Costa, A.B., Nascimento, M.T.C., Wardini, A.B., Pinto-da-Silva, L.H., and Saraiva, E.M. (2012). ETosis: A Microbicidal Mechanism beyond Cell Death. J Parasitol Res *2012*, 929743.

Hampton, M.B., Kettle, A.J., and Winterbourn, C.C. (1996). Involvement of superoxide and myeloperoxidase in oxygen-dependent killing of Staphylococcus aureus by neutrophils. Infect. Immun. *64*, 3512–3517.

Hazell, L.J., Arnold, L., Flowers, D., Waeg, G., Malle, E., and Stocker, R. (1996). Presence of hypochlorite-modified proteins in human atherosclerotic lesions. J. Clin. Invest. *97*, 1535–1544.

Hazen, S.L., and Heinecke, J.W. (1997). 3-Chlorotyrosine, a specific marker of myeloperoxidase-catalyzed oxidation, is markedly elevated in low density lipoprotein isolated from human atherosclerotic intima. J. Clin. Invest. *99*, 2075–2081.

Huffnagle, G.B., and Noverr, M.C. (2013). The emerging world of the fungal microbiome. Trends Microbiol. *21*, 334–341.

Humphreys, J.M., Davies, B., Hart, C.A., and Edwards, S.W. (1989). Role of myeloperoxidase in the killing of Staphylococcus aureus by human neutrophils: studies with the myeloperoxidase inhibitor salicylhydroxamic acid. J. Gen. Microbiol. *135*, 1187–1193.

Iliev, I.D., Funari, V.A., Taylor, K.D., Nguyen, Q., Reyes, C.N., Strom, S.P., Brown, J., Becker, C.A., Fleshner, P.R., Dubinsky, M., et al. (2012). Interactions between commensal fungi and the C-type lectin receptor Dectin-1 influence colitis. Science (80-.). *336*, 1314–1317.

Jennette, J.C., and Falk, R.J. (2015). ANCAs are also antimonocyte cytoplasmic autoantibodies. Clin. J. Am. Soc. Nephrol. *10*, 4–6.

Jiang, X., Wang, L., Carroll, S.L., Chen, J., Wang, M.C., and Wang, J. (2018). Challenges and Opportunities for Small-Molecule Fluorescent Probes in Redox Biology Applications. Antioxid. Redox Signal.

Kenmoku, S., Urano, Y., Kojima, H., and Nagano, T. (2007). Development of a highly specific rhodamine-based fluorescence probe for hypochlorous acid and its application to real-time imaging of phagocytosis. J. Am. Chem. Soc. *129*, 7313–7318.

King, C.C., Jefferson, M.M., and Thomas, E.L. (1997). Secretion and inactivation of myeloperoxidase by isolated neutrophils. J. Leukoc. Biol. *61*, 293–302.

Klebanoff, S.J. (2005). Myeloperoxidase: friend and foe. J. Leukoc. Biol. *77*, 598–625.

Klebanoff, S.J., Kettle, A.J., Rosen, H., Winterbourn, C.C., and Nauseef, W.M. (2013). Myeloperoxidase: a front-line defender against phagocytosed microorganisms. J. Leukoc. Biol. *93*, 185–198.

Koide, Y., Urano, Y., Hanaoka, K., Terai, T., and Nagano, T. (2011). Development of an Si-rhodamine-based far-red to near-infrared fluorescence probe selective for hypochlorous acid and its applications for biological imaging. J. Am. Chem. Soc. *133*, 5680–5682.

Lau, D., and Baldus, S. (2006). Myeloperoxidase and its contributory role in inflammatory vascular disease. Pharmacol. Ther. *111*, 16–26.

Van Leeuwen, M., Gijbels, M.J.J., Duijvestijn, A., Smook, M., van de Gaar, M.J., Heeringa, P., de Winther, M.P.J., and Tervaert, J.W.C. (2008). Accumulation of myeloperoxidase-positive neutrophils in atherosclerotic lesions in LDLR-/- mice. Arterioscler. Thromb. Vasc. Biol. *28*, 84–89.

Lekstrom-Himes, J.A., and Gallin, J.I. (2000). Immunodeficiency diseases caused by defects in phagocytes. N. Engl. J. Med. *343*, 1703–1714.

Leonardi, I., Li, X., Semon, A., Li, D., Doron, I., Putzel, G., Bar, A., Prieto, D., Rescigno, M., McGovern, D.P.B., et al. (2018). CX3CR1+ mononuclear phagocytes control immunity to intestinal fungi. Science (80-.). *359*, 232–236.

Lou, Z., Li, P., Song, P., and Han, K. (2013). Ratiometric fluorescence imaging of cellular hypochlorous acid based on heptamethine cyanine dyes. Analyst *138*, 6291–6295.

Masoodi, I., Tijjani, B.M., Wani, H., Hassan, N.S., Khan, A.B., and Hussain, S. (2011). Biomarkers in the management of ulcerative colitis: a brief review. Ger. Med. Sci. *9*, Doc03.

Matthijsen, R.A., Huugen, D., Hoebers, N.T., de Vries, B., PeutZ-Kootstra, C.J., Aratani, Y., Daha, M.R., Tervaert, J.W.C., Buurman, W.A., and Heeringa, P. (2007). Myeloperoxidase is critically involved in the induction of organ damage after renal ischemia reperfusion. Am. J. Pathol. *171*, 1743–1752.

Metzler, K.D., Goosmann, C., Lubojemska, A., Zychlinsky, A., and Papayannopoulos, V. (2014). A myeloperoxidase-containing complex regulates neutrophil elastase release and actin dynamics during NETosis. Cell Rep. *8*, 883–896.

Mitsuyama, K., Niwa, M., Takedatsu, H., Yamasaki, H., Kuwaki, K., Yoshioka, S., Yamauchi, R., Fukunaga, S., and Torimura, T. (2016). Antibody markers in the diagnosis of inflammatory bowel disease. World J. Gastroenterol. *22*, 1304–1310.

Modi, S., M G, S., Goswami, D., Gupta, G.D., Mayor, S., and Krishnan, Y. (2009). A DNA nanomachine that maps spatial and temporal pH changes inside living cells. Nat. Nanotechnol. *4*, 325–330.

Mogensen, T.H. (2009). Pathogen recognition and inflammatory signaling in innate immune defenses. Clin. Microbiol. Rev. *22*, 240–73, Table of Contents.

Nicholls, S.J., and Hazen, S.L. (2005). Myeloperoxidase and cardiovascular disease. Arterioscler. Thromb. Vasc. Biol. *25*, 1102–1111.

Nordenfelt, P., and Tapper, H. (2011). Phagosome dynamics during phagocytosis by neutrophils. J. Leukoc. Biol. *90*, 271–284.

Odobasic, D., Kitching, A.R., and Holdsworth, S.R. (2016). Neutrophil-Mediated Regulation of Innate and Adaptive Immunity: The Role of Myeloperoxidase. J. Immunol. Res. *2016*, 2349817.

Papayannopoulos, V., Metzler, K.D., Hakkim, A., and Zychlinsky, A. (2010). Neutrophil elastase and myeloperoxidase regulate the formation of neutrophil extracellular traps. J. Cell Biol. *191*, 677–691.

Paul, D., Achouri, S., Yoon, Y.-Z., Herre, J., Bryant, C.E., and Cicuta, P. (2013). Phagocytosis dynamics depends on target shape. Biophys. J. *105*, 1143–1150.

Pauwels, A.-M., Trost, M., Beyaert, R., and Hoffmann, E. (2017). Patterns, receptors, and signals: regulation of phagosome maturation. Trends Immunol. *38*, 407–422.

Queval, C.J., Song, O.-R., Carralot, J.-P., Saliou, J.-M., Bongiovanni, A., Deloison, G., Deboosère, N., Jouny, S., Iantomasi, R., Delorme, V., et al. (2017). Mycobacterium tuberculosis Controls Phagosomal Acidification by Targeting CISH-Mediated Signaling. Cell Rep. *20*, 3188–3198.

Ravichandran, K.S. (2010). Find-me and eat-me signals in apoptotic cell clearance: progress and conundrums. J. Exp. Med. *207*, 1807–1817.

Robaszkiewicz, A., Bartosz, G., and Soszynski, M. (2011). Detection of 3-chlorinated tyrosine residues in human cells by flow cytometry. J. Immunol. Methods *369*, 141–145.

Robinson, J.M. (2008). Reactive oxygen species in phagocytic leukocytes. Histochem. Cell Biol. *130*, 281–297.

Saha, S., Prakash, V., Halder, S., Chakraborty, K., and Krishnan, Y. (2015). A pH-independent DNA nanodevice for quantifying chloride transport in organelles of living cells. Nat. Nanotechnol. *10*, 645–651.

Schmitt, F.-J., Renger, G., Friedrich, T., Kreslavski, V.D., Zharmukhamedov, S.K., Los, D.A., Kuznetsov, V.V., and Allakhverdiev, S.I. (2014). Reactive oxygen species: re-evaluation of generation, monitoring and role in stress-signaling in phototrophic organisms. Biochim. Biophys. Acta *1837*, 835–848.

Setsukinai, K., Urano, Y., Kakinuma, K., Majima, H.J., and Nagano, T. (2003). Development of novel fluorescence probes that can reliably detect reactive oxygen species and distinguish specific species. J. Biol. Chem. *278*, 3170–3175.

Sharma, S., Zaveri, A., Visweswariah, S.S., and Krishnan, Y. (2014). A fluorescent nucleic acid nanodevice quantitatively images elevated cyclic adenosine monophosphate in membrane-bound compartments. Small *10*, 4276–4280.

Sokol, H., Leducq, V., Aschard, H., Pham, H.-P., Jegou, S., Landman, C., Cohen, D., Liguori, G., Bourrier, A., Nion-Larmurier, I., et al. (2017). Fungal microbiota dysbiosis in IBD. Gut *66*, 1039–1048.

Standaert-Vitse, A., Sendid, B., Joossens, M., François, N., Vandewalle-El Khoury, P., Branche, J., Van Kruiningen, H., Jouault, T., Rutgeerts, P., Gower-Rousseau, C., et al. (2009). Candida albicans colonization and ASCA in familial Crohn's disease. Am. J. Gastroenterol. *104*, 1745–1753.

Surana, S., Bhat, J.M., Koushika, S.P., and Krishnan, Y. (2011). An autonomous DNA nanomachine maps spatiotemporal pH changes in a multicellular living organism. Nat Commun *2*, 340.

Surana, S., Shenoy, A.R., and Krishnan, Y. (2015). Designing DNA nanodevices for compatibility with the immune system of higher organisms. Nat. Nanotechnol. *10*, 741–747.

Theeß, W., Sellau, J., Steeg, C., Klinke, A., Baldus, S., Cramer, J.P., and Jacobs, T. (2017). Myeloperoxidase Attenuates Pathogen Clearance during Plasmodium yoelii Nonlethal Infection. Infect. Immun. *85*.

Thieblemont, N., Wright, H.L., Edwards, S.W., and Witko-Sarsat, V. (2016). Human neutrophils in auto-immunity. Semin. Immunol. *28*, 159–173.

Urban, C.F., Lourido, S., and Zychlinsky, A. (2006). How do microbes evade neutrophil killing? Cell Microbiol. *8*, 1687–1696.

Vlasova, I.I., Arnhold, J., Osipov, A.N., and Panasenko, O.M. (2006). pH-dependent regulation of myeloperoxidase activity. Biochemistry Moscow *71*, 667–677.

Yu, Y., and Su, K. (2013). Neutrophil Extracellular Traps and Systemic Lupus Erythematosus. J Clin Cell Immunol *4*.

Zhang, Y.-R., Chen, X.-P., Jing-Shao, Zhang, J.-Y., Yuan, Q., Miao, J.-Y., and Zhao, B.-X. (2014). A ratiometric fluorescent probe for sensing HOCl based on a coumarin-rhodamine dyad. Chem. Commun. (Camb) *50*, 14241–14244.

(2016). The innate and adaptive immune systems.

11.3E: Phagocytosis - Biology LibreTexts.

Group A Streptococcus Prevents the Acidification of Phagolysosomes in Macrophages | The FASEB Journal. FASEB J.

Chapter 2

DNA based sensor for simultaneous measurement of pH and HOCl

2.A: Introduction

Various detection methods like chemiluminescence, colorimetry, fluorescence, electrochemistry and chromatography have been used to sense hypochlorous acid (HOCl) (Gaut et al., 2002; Robaszkiewicz et al., 2011). Fluorescence-based techniques attract copious attention since they can report spatiotemporal HOCl production and thereby the activity of the only known HOCl producer, myeloperoxidase (MPO), in biological systems (Chen et al., 2016; Pulli et al., 2013; Shepherd et al., 2007; Xu et al., 2013). Immunostaining for MPO-derived chlorinated substances such as 3-chlorotyrosine is a method of choice to assess steady state MPO activity in fixed samples (Hazell et al., 1996; Hazen and Heinecke, 1997). There are no genetically encodable sensors of HOCl yet. Therefore, small molecule fluorophores which undergo a change in their photophysical properties upon reaction with HOCl are used to quantify HOCl production and MPO activity in the cytoplasm and in phagosomes of live cells (Chen et al., 2016; Shepherd et al., 2007; Sun et al., 2014).

Reliable detection of any reactive oxygen species (ROS) demands fast sensor kinetics due to their short lifetime, especially in the cellular environment (Schmitt et al., 2014). Cyanine dyes, having a delocalized pi electron cloud with a higher oxidation potential, undergo oxidative cleavage with HOCl, thereby losing their fluorescence (Sun et al., 2014). These fast-responsive dyes are therefore suitable for developing an HOCl sensor. Since HOCl production during phagocytosis has implications in pathogen killing detecting

HOCl in the phagosome would offer insight into how resistant pathogens by-pass phagosomal killing (Corleis et al., 2012). The destructive environment inside phagosomes is a result of changes in its chemical milieu, with acidification being one correlate of phagosome maturation, especially in macrophages. Hence, simultaneously sensing phagosomal pH and HOCl, will report HOCl production with temporal resolution through phagosome maturation. We therefore incorporate a rhodamine 6G amide derivative, which senses pH through acid-mediated lactam ring opening.

One limitation of small molecule-based sensing is that relative signals are affected by sensor availability (Jiang et al., 2018). Ratiometric sensing mitigates this issue by normalizing the amount of available sensor with a fluorophore insensitive to the target analyte (Lou et al., 2013; Zhang et al., 2014). DNA based sensors offer a platform for ratiometric sensing of ions and small molecules in intracellular compartments of live cells and organisms (Chakraborty et al., 2017; Modi et al., 2009; Saha et al., 2015; Sharma et al., 2014; Surana et al., 2011).The modularity of DNA nanostructures enables multiple functionalities to be used to append multiple small molecule fluorophores and targeting moieties in specific ratios (Modi et al., 2009; Saha et al., 2015). Considering these advantages, we have developed a DNA based sensor called *cHOClate* which can sense pH and HOCl quantitatively and simultaneously. *cHOClate* leverages modularity of DNA duplex further to accommodate a targeting module so that it can be used in various locations in cells. Chapter 2 describes the design, development and in vitro characterization of *cHOClate*.

2.B: Materials and methods

2.B.1: Reaction between Cy5 dyes and HOCl

The nature of the reaction between 1 and HOCl was verified using a carboxylic acid derivative of 1. Briefly 50 μM 1 was treated with 1 mM HOCl and stirred for 15 minutes at room temperature (RT). The resulting mixture was subjected to LC MS on an Advion Expression-L mass spectrometer (Ithaca, NY). Mass spectrometry revealed the oxidized products of 1 on reaction with HOCl (Figure 2.7)

2.B.2: Oligonucleotides

All oligonucleotides (Table 2.1) were purchased from IDT (USA). D1, D2 and D4 were purchased from IDT with required modifications. D3 and D5 were functionalized following the procedures described in section 2.B.3 (Figure 2.2 and 2.4). HPLC purified DNA oligonucleotides were used without further purification, whereas fluorescently modified oligonucleotides were ethanol precipitated prior to further use. Oligos were quantified using UV-Vis spectrophotometry by their absorbance at 260 nm, dissolved in Milli-Q water to prepare a 200 μM stock, aliquoted and stored at -20ºC.

Name	Sequence	Modifications
D1	5' -DBCO-TEG -TATATATAGCGATCTCGCTGCGTGTATGCTGTCTGGTGTGCAGTGTTGAT-**1**- 3'	5'-DBCO; 3'-**1**
D2	5' -ATCAACACTGCACACCAGACAGCA-ATTO-488- 3'	3'-Atto 488
D3	5' -TACACGCAGCGAGATCGCTATATATA-R6G- 3'	3'-R6G
D4	5' -**1**-TATATATAGGATCTTGCTGTCTGGTGTGC AGTGTTGAT- 3'	5'-**1**
D5	5' -EtBr-ATCAACACTGCACACCAGACAGCAAGATCCTATATATA- 3'	5'-EtBr

Table 2.1: Sequences used for *cHOClate* and *pcHOClate*. Sequences are color coded to indicate the complimentary regions. D1, D2 and D3 are assembled to form *cHOClate*; D4 and D5 are assembled to form *pcHOClate*.

2.B.3: Functionalization of oligonucleotides with fluorophores

Oligonucleotides D3 and D5 were purchased from IDT with 3'-N3 and D5 with 5'-DBCO modifications, respectively. They were functionalized with the indicated fluorophores using strain promoted azide- alkyne click chemistry and characterized by gel mobility shift assay using denaturing PAGE as described below.

2.B.3.a: Functionalization of D3 with R6G

2.B.3.a.i: Synthesis of DNA conjugatable R6G derivative

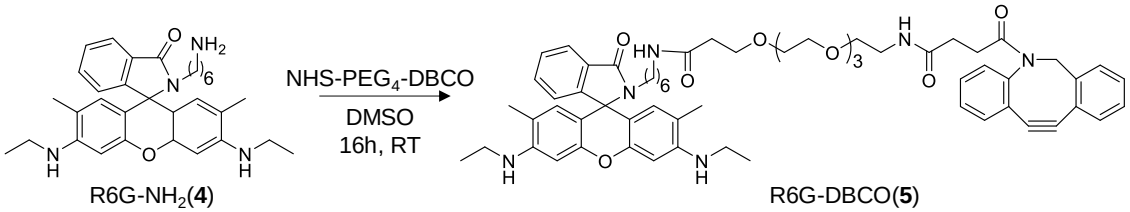

Figure 2.1: Synthesis of R6G-DBCO (5)

N-(6-Aminohexyl) rhodamine 6G-amide bis(trifluoroacetate) (4) (1.3 μmol) was dissolved in dry THF and added to DBCO- PEG_4-NHS (0.8 μmol) dissolved in dry THF under N_2. The solution was flushed with nitrogen, stirred for 16h at RT, and the product was purified on a silica (230-400 mesh) flash column using methanol/dichloromethane solvent composition to obtain R6G-DBCO (5) in 60% yield. ^{1}H NMR (500MHz, DMSO-d6) δ (ppm): 7.97 (s, 1H), 7.91 (bs, 1H), 7.79 (t, 1H), 7.73 (m, 1H), 7.62 (m, 1H), 7.53 (t, 2H), 7.35 (m, 2H), 7.24 (m, 2H), 7.16 (d, 1H), 7.02 (m, 2H), 6.29 (s, 2H), 6.08 (s, 2H), 5.09 (m, 3H), 3.45 (m, 4H), 3.28 (m, 16H), 3.16(m, 4H), 2.96 (m, 4H), 2.21 (t, 4H), 1.88 (s, 6H), 1.23 (t, 8H), 0.89 (t, 6H). ^{13}C NMR (125 MHz, DMSO-d6) δ (ppm): 176.58, 174.63, 170.09, 169.86, 156.2,156.1,155.3,155.1,153.23, 149.0, 148.92, 148.8, 143.5, 143.4, 132.71, 130.7,130.43, 128.52, 128.18, 123.80, 122.93, 108.27, 76.58, 62.62, 55.33, 50.42, 48.21,

44.64, 44.38, 42.31, 37.49, 33.67, 31.30, 24.50, 22.10, 17.01, 14.15, 13.92, 12.58. ESI-MS: m/z calculated for [$C_{62}H_{76}N_6O_9$ +H^+] = 1049.5 Da, found = 1049.2 Da.

2.B.3.a.ii: Functionalization of D3 with R6G

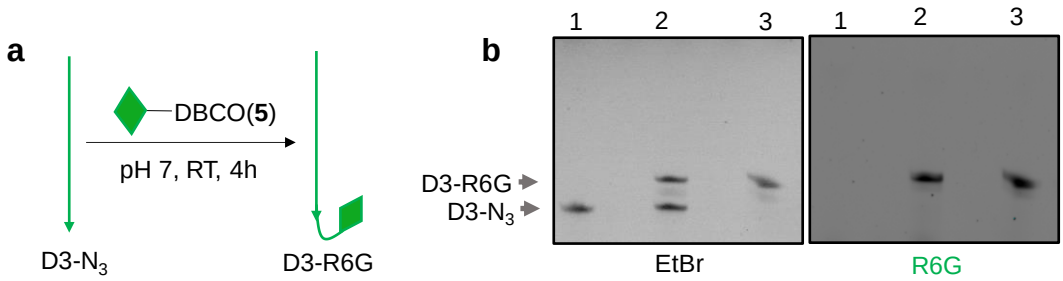

Figure 2.2: Functionalization of D3 with R6G. a) D3-N_3 is functionalized with R6G-DBCO using strain promoted click chemistry. b) Characterization of R6G functionalized D3 using denaturing PAGE (18% Acrylamide, 8M urea, 1X TBE) in both EtBr(left) and R6G(right) channels; lane 1: D3-N_3, lane 2: mixture of D3-N_3 and D3-R6G reaction mixture, lane 3: D3-R6G reaction mixture.

D3-N_3 (2.5 nmol) was added to a solution of 5 (10 nmol) in potassium phosphate buffer (50 mM, pH 7) and stirred for 4h at RT (Figure. 2.1.a). The product was precipitated with ethanol and characterized by denaturing polyacrylamide gel electrophoresis (PAGE, 18% Acrylamide, 8M urea, 1X TBE) visualized in EtBr (λ_{ex}= 302 nm) and R6G (λ_{ex}= 545 nm) channels (Figure. 2.2.b).

2.B.3.b: Functionalization of D5 with EtBr

2.B.3.b.i: Synthesis of DNA conjugatable EtBr derivative

Synthesis of DNA conjugatable EtBr derivative was achieved following the synthetic scheme in figure 2.3 and individual steps are detailed below.

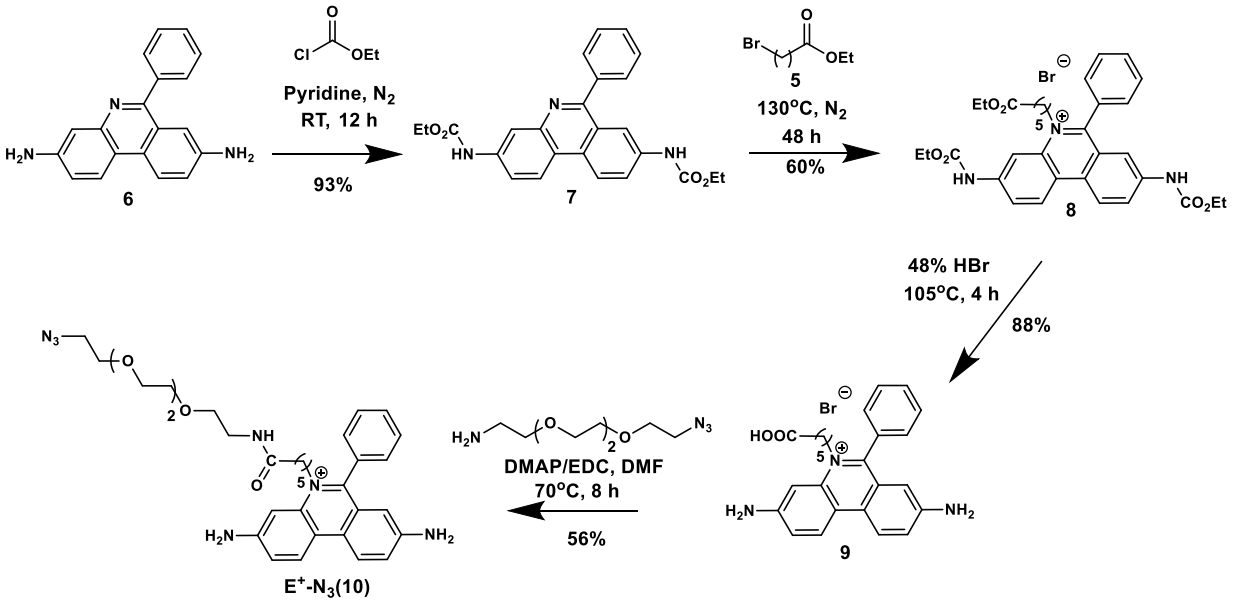

Figure 2.3: Synthesis of E^{+}-N_3(10)

Synthesis of 3, 8- di(ethoxycarbonylamino)-6-phenyl phenanthridine (7): Synthesis of this product was modified from a reported procedure(Rangarajan and Friedman, 2007). To a solution of 3,8-diamino-6-phenyl phenanthridine (6) (5 g, 17.5 mmol) in dry pyridine (40 mL), ethyl chloroformate (4 mL, 42 mmol, 2.5 eq) was added under N_2 at 0°C. The resultant yellow colored solution was stirred at 0°C for 10 minutes and at RT overnight. As the reaction progressed, product formed precipitated and the solution turned to a yellow thick mass. The reaction was quenched by adding 150 mL of water and stirred for 15-20 minutes at RT and yellow product was filtered under vacuum and then dried. The yellowish-brown solid was recrystallized in 200 mL 1:1 water: Methanol and the pale brown solid was collected by vacuum filtration (7 g, 93 % yield). The product was characterized using HRMS and NMR spectra. 1H NMR (400 MHz, DMSO-d_6) δ 10.37 (1H, s), 10.23 (1H,s), 8.93 (1H, d, J=9.6 Hz), 8.85 (1H, d, J=9.6 Hz), 8.59 (1H, s), 8.40

(1H, s), 8.18 (1H, d, J=8.8 H87z), 7.88 (3H, m), 7.75 (3H, m), 4.23 (2H, m), 4.132 (2H, m), 1.304 (3H, t, J=7.6, 6.8 Hz), 1.229 (3H,t, J=7.2, 7.2 Hz). HRMS:

Synthesis of 5-(6-ethoxy-6-oxohexyl)-3,8-bis((ethoxycarbonyl)amino)-6-phenylphenanthridin-5-ium bromide (8): To 3,8-di(ethoxycarbonylamino)-6-phenyl phenanthridine (7) (2 g, 4.7 mmol), ethyl-6-bromohexanoate (20 mL, excess, neat reaction) was added and refluxed at 130^{o}C for 48 hours under N_2. The bright yellow precipitate was filtered under vacuum and purified using column chromatography using methanol/DCM as the mobile phase. Fractions containing pure product were collected together, concentrated and dried to obtain the product as a yellow solid powder (1.8 g, 60 % yield). The product was characterized using HRMS and NMR. ^{1}H NMR (400 MHz, DMSO-d_6) δ (ppm) 10.57 (1H,s), 10.30 (1H, s), 9.07 (1H, dd, J= 4 Hz), 9.02 (1H, dd, J= 6 Hz) , 8.68(1H,s), 8.25 (1H, d, J=12 Hz), 8.13 (1H, d, J=8 Hz), 7.79 (6H, m), 4.52 (2H,m), 4.25 (2H, m), 4.05 (4H, m), 2.19 (2H,t, J_1= 8 Hz, J_2 = Hz), 1.95 (2H, m), 1.4-1.1 (13 H,m).

Synthesis of 3, 8-diamino-5-(5-carboxypentyl)-6-phenylphenanthridin-5-ium bromide (9): To 5-(6-ethoxy-6-oxohexyl)-3,8-bis((ethoxycarbonyl)amino)-6-phenylphenanthridin-5-ium bromide (8) (1 g, 1.5 mmol), about 10 mL of 48% HBr was added. The resulting solution was refluxed at 105^{o}C for 4 hours under a guard tube filled with anhydrous $CaCl_2$. HBr was removed from the reaction mixture under high vacuum at 80-90^{o}C and the reaction mixture was dried. To this, 3-4 mL of DIPEA and 10 mL water was added, and starting material was extracted with diethyl ether (6 mL* 3). The aqueous layer was collected and water was removed under vacuum at 90-100^{o}C. The resultant solid mass was subjected to column chromatography using methanol/DCM to yield the pure product as dark pink solid (634 mg, 88% yield). The product was confirmed by HRMS and ^{1}H

NMR spectroscopy. ^{1}H NMR (400 MHz, DMSO-d_6) δ (ppm) 8.66 (1H, d), 8.59 (1H, d), 7.75-7.69 (5H, m), 7.52 (1H, d), 7.37 (2H, m), 6.54 (2H, s), 6.27 (1H, s), 5.96 (2H, s), 4.24 (2H, m), 2.08 (2H, t, J=), 1.85 (2H, m), 1.30-1.19 (4H, m).

Synthesis of azide functionalised 3, 8-diamino-5-(5-carboxypentyl)-6-phenylphenanthridin-5-ium bromide (10): To 3, 8-diamino-5-(5-carboxypentyl)-6-phenylphenanthridin-5-ium bromide (9) (100 mg, 0.208 mmol), 27 mg of DMAP (0.208 mmol) and 33 mg EDC (0.208 mmol) were added in 1mL of dry DMF, and the mixture was stirred for 30 min at RT under N_2. Then 42 μL (0.208 mml) of bifunctional linker 11-Azido-3,6,9-trioxaundecan-1-amine was added to this mixture and stirred overnight. The resulting mixture was dried and subjected to column chromatography on silica (100-200 mesh) using methanol/DCM solvent gradients to yield the pure product as dark pink solid (80 mg, 56%). The product was confirmed by HRMS and ^{1}H NMR spectroscopy. ^{1}H NMR (400 MHz, DMSO-d_6) δ (ppm) 8.1 (1H, s), 7. 9 (1H, s), 7.7 (3H, s), 7.5-7.3 (2H, d), 7.15-7.25 (3H, m), 6.25 (1H, s), 4.9-4.75 (2H, bs), 4.4-4.25 (2H, bs), 3.7-3.3 (14H, m), 3.4-3.25 (5H, m), 2.1 (2H, m), 1.75 (2H, s), 1.4(2H, s), 1.2(3H, s)

2.B.3.b.ii: Functionalization of D5 with EtBr and assembly of *pcHOClate*

D5-DBCO (0.5 nmol) was added to E^{+}-N_3 (5 nmol) in 50 mM potassium phosphate buffer, pH 7, and stirred for 5h at RT. The product was precipitated with ethanol and characterized by 15% denaturing polyacrylamide gel electrophoresis (PAGE) visualized in EtBr channel with and without EtBr staining (Figure 2.4a).

For *pcHOClate* assembly, fluorophore functionalized D4 and D5 were mixed in equimolar ratios to a final concentration of 10 μM in 20 mM potassium phosphate buffer, pH 7

containing 100 mM KCl. Formation of p*cHOClate* was confirmed by a gel mobility shift assay using 10% native PAGE (Figure 2.4b).

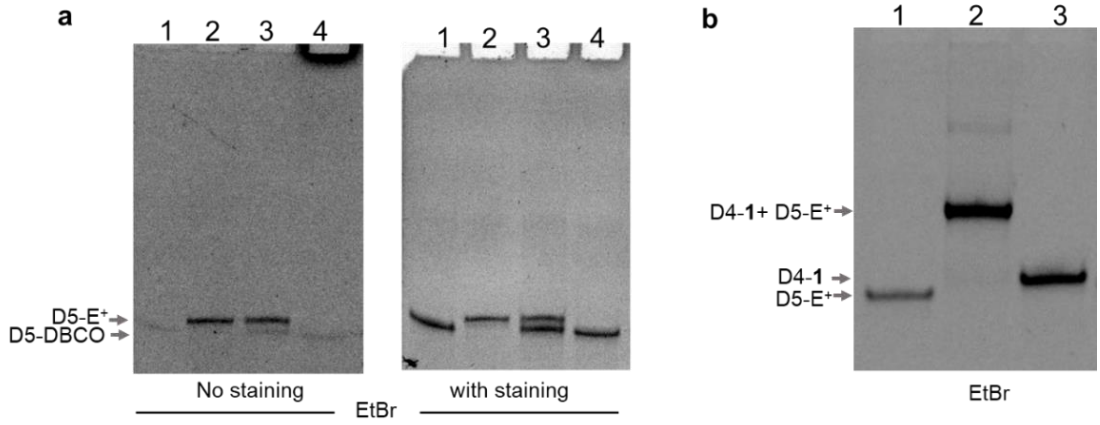

Figure 2.4: Characterization of *pcHOClate*: a) E^+ functionalized D5 using 15% denaturing PAGE with (right) and without (left) EtBr staining (15% Acrylamide, 8M urea, 1X TBE); lane 1: D5-DBCO, lane 2: D5-E^+ reaction mixture, mixture of D5-DBCO and D5-E^+ reaction mixture, lane 4: mixture of D5-DBCO and 9 b) Characterization of *pcHOClate* using 10% native PAGE (10% Acrylamide, 1X TBE), lane 1: D5-E^+, lane 2: annealed mixture of D5-E^+ and D4-1, lane 3: D4-1.

2.B.4: Mass spectrometry

Mass spectrometric characterization was done using LC MS on an Advion Expression-LC mass spectrometer (Ithaca, NY). Samples were run on an analytical C18 column (50*4.6 mm), using a linear H_2O/MeOH gradient (containing 0.1% of formic acid) from 10 to 90% in 10 minutes. Flow rate was 1mL/min.

2.B.5: NMR studies

^1H NMR and ^{13}C NMR spectra of the newly synthesized compounds were recorded on a Bruker AVANCE II+, 500MHz NMR spectrophotometer. TMS is used as an internal

standard. About 2 mg of pure solid product was dissolved 0.6 mL of in the mentioned deuterated solvent for obtaining the spectra.

2.B.6: UV-Vis spectroscopy

All UV experiments and quantification of DNA oligos were done on Shimadzu UV-2700 using an 8-well microcuvette. To test the HOCl reactivity of 1, 1 μM of fluorophore was treated with 0, 100, 200 and 300 μM of HOCl at pH 7 (phosphate buffer, 20 mM) for 20 minutes and UV spectra was recorded for each sample from 400 nm – 750 nm.

2.B.7: *cHOClate* assembly

D1, D2 and D3 (Table 2.1, complimentary regions are color coded) were mixed in equimolar ratios to a final concentration of 20 μM in 20 mM potassium phosphate buffer, pH 7 containing 100 mM KCl. Annealing was performed by heating to 90^{o}C for 5 minutes, cooling to room temperature over 3 h at 5^{o}C/15 min and equilibrating at 4^{o}C overnight. Formation of *cHOClate* was confirmed by a gel mobility shift assay (Figure 2.5b).

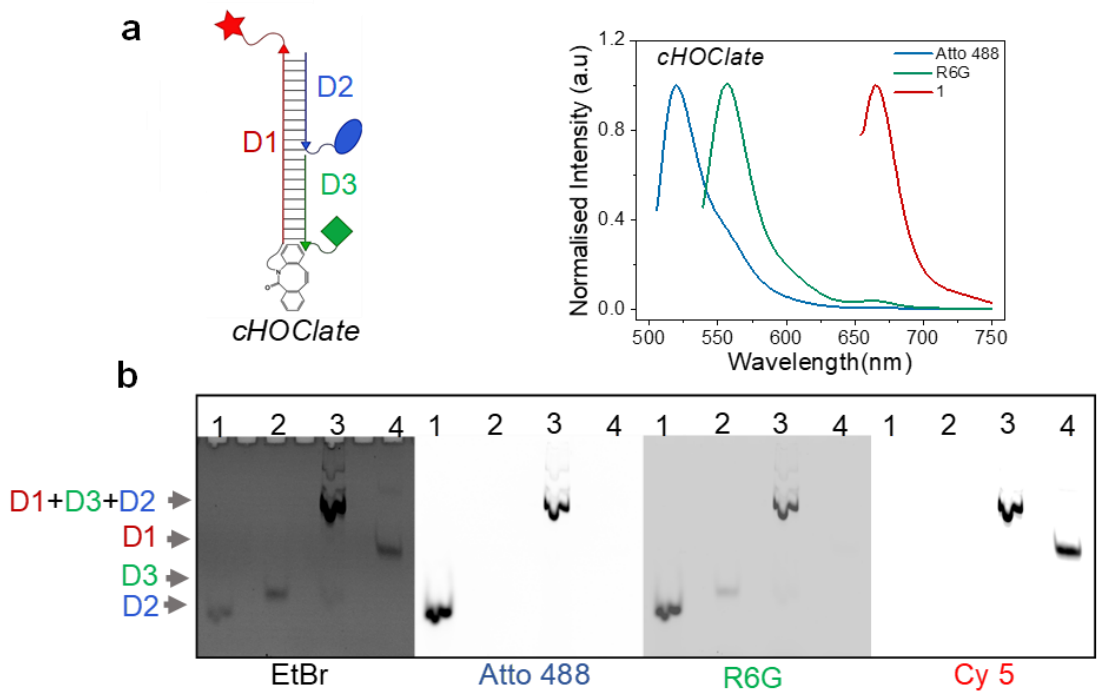

Figure 2.5: Characterization of *cHOClate* assembly. a) *cHOClate* assembly (left) Fluorescence spectra of *cHOClate* in R, G and B channels (right). b) Native PAGE (10 %) in the indicated fluorescent channels showing the successful hybridization of *cHOClate* to a duplex. lane 1: D2, lane 2: D3 and D4-1, lane 3: *cHOClate*, lane 4: D1.

2.B.8: Gel electrophoresis

Fluorophore functionalized D3 and D5 were characterized using denaturing urea PAGE (15-18% Acrylamide, 8M urea, 1X TBE). Formation of *cHOClate* was confirmed by a gel mobility shift assay using 10% native PAGE. 25 pmoles of single strands or duplex were loaded in wells and gel was run at 100 mV in 1x TBE using Bromophenol blue or orange G as the loading dye. The gel was imaged using *BIO-RAD* ChemiDoc MP imaging system for fluorophores in respective channels. The gel was further stained with EtBr solution for

5 minutes and imaged in the EtBr channel. There is a bleed through for Atto-488 in Epi-green filter set, as observed in the gel (Figure 2.5b) due to lack of appropriate filters.

2.B.9: Fluorescence studies

All fluorescence studies were carried out on a Fluoromax-4 (Horiba Scientific, Edison, NJ, USA) spectrophotometer. For fluorescence experiments *cHOClate* was further diluted to 100 nM. Fluorescence from Atto-488 (Blue, λ_{ex} = 488 nm, λ_{em} = 520 nm), R6G (Green, λ_{ex} = 530 nm, λ_{em} = 555 nm) or 1(Red, λ_{ex} = 650 nm, λ_{em} = 665 nm) was recorded with excitation and emission slit widths of 3 nm. All fluorescence experiments were done in 20 mM UB_4 buffer (20mM HEPES, 20mM MES, and 20mM sodium acetate) at 37^{o}C and indicated pH values unless otherwise stated. R/B represents the ratio of emission intensities of 1 to Atto-488 (665 nm/520 nm) and G/B represents the ratio of emission intensities of R6G to Atto-488 (555 nm/520 nm). All spectra were blank corrected and normalized to spectra without ROS/RNS at the respective pH.

2.B.10: HOCl sensitivity

Solutions of 100 nM *cHOClate* in 20 mM UB_4, pH 4.5, were incubated with NaOCl (0 to 100 μM) for 10 minutes at 37^{o}C. Fluorescent emission spectra were recorded in red, green, and blue channels corresponding to 665 nm (R), 555 nm (G) and 520 nm (B) respectively, blank corrected and normalized to no added NaOCl.

For kinetic studies, 100 nM *cHOClate* was added to a cuvette at pH 4.5 and 37^{o}C and initial R/B was measured. To this, 40 μM NaOCl was added and spectra were taken in red and blue channels at 1, 2, 5, 10, 15, 20 minutes. The ratio of R/B at each time point was normalized to initial R/B and plotted against time.

2.B.11: Specificity experiments

Aqueous NaOCl served as a HOCl donor where HOCl concentration was quantified using $\varepsilon = 350\ M^{-1}cm^{-1}$ at 292 nm (Kumar and Margerum, 1987). Aqueous H_2O_2 served as a H_2O_2 donor where H_2O_2 concentration was quantified using $\varepsilon = 43.6\ M^{-1}cm^{-1}$ at 240 nm. Peroxynitrite was prepared *in situ* from $NaNO_2$ and H_2O_2 as reported and quantified using $\varepsilon = 1670\ M^{-1}cm^{-1}$ at 302 nm (Robinson and Beckman, 2005). Xanthine/Xanthine oxidase was used to generate superoxide, which was quantified using Cytochrome C reduction as described (Roubaud et al., 1997). Fenton chemistry using $FeSO_4$ and H_2O_2 was used for the generation of hydroxyl radical ($^{\cdot}OH$) and tert-Butyl peroxide radical ($^{\cdot}TBH$) (Abo et al., 2011). DEA-NONOate was used as a NO donor (Wang et al., 2015).

ROS/RNS generators were added to 100 nM of *cHOClate* in 20 mM UB4, p H 4.5, to a final concentration of 100 μM reactive species, except for HOCl, in which 40 μM NaOCl was added. Samples were incubated for 10 minutes at 37°C and fluorescence spectra were recorded in all channels. Fold change of R/B in each case was normalized to that of *cHOClate* without ROS/RNS.

2.B.12: pH sensitivity

cHOClate was incubated in 20 mM UB_4 buffer, pH 4.5-7.5, for 5 minutes at 37°C and fluorescence spectra were recorded in red (λ_{ex} = 650 nm), blue (λ_{ex} = 488 nm) and green (λ_{ex} = 530 nm) channels as mentioned earlier. Ratios of R/B and G/B were plotted against pH.

2.B.13: Stability of DNA duplex to ROS/RNS

The integrity of the DNA scaffold comprising *cHOClate* was evaluated using p*cHOClate* as a proxy. p*cHOClate* was formed by annealing D4 and D5 as described in 2. B.3b.ii (Figure 2.4). 100 nM p*cHOClate* was incubated with 1-450 μM of NaOCl, or 100 μM of ROS as described in section 2.B.11 for up to 30 minutes, which is the maximum duration of our imaging experiments. Spectra of EtBr and 1 were acquired in respective channels and intensities were plotted as functions of HOCl concentration. Ratio of intensities 1 to EtBr (665 nm /600 nm) for each ROS/RNS was calculated and normalized to that blank sample (where no ROS/RNS added).

2.C: Results and discussions

2.C.1: Mechanism and characterization of HOCl sensing by Cy 5 dyes

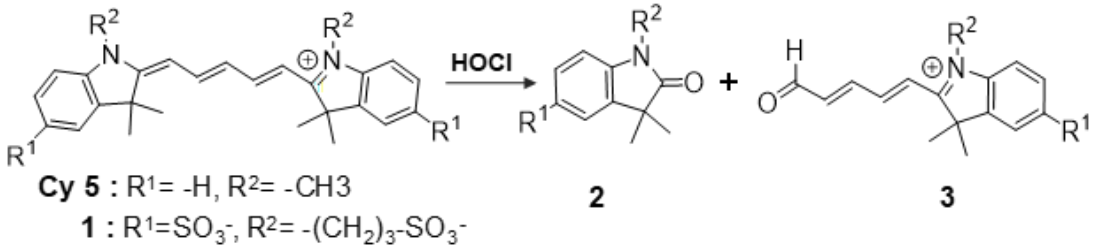

Figure 2.6: Mechanism of HOCl sensing by Cy 5 dyes. The chromophore core of Cy 5 or 1 undergoes oxidative cleavage with HOCl to the corresponding cleaved products.

The first step towards developing an HOCl sensor was to choose an HOCl sensitive fluorophore. We found that the water-soluble and photostable Cy 5 dye 1,1′-bis(3-sulfopropyl)-3,3,3′,3′-tetramethyl-5,5’-disulfo-indodicarbocyanine (1) underwent oxidative cleavage specifically with HOCl, thereby losing its fluorescence (Figure 2.6). Cyanine dye derivatives are prone to cleavage by HOCl, and in comparison with other reporters, 1,1′-bis(3-sulfopropyl)-3,3,3′,3′-tetramethyl-5,5’-disulfo-indodicarbocyanine (1) shows

relatively lower sensitivity which proved advantageous for subsequent applications (Nüsse, 2011). Mass spectrometry revealed that 1 was oxidatively cleaved to 1-(3-sulfopropyl)-3,3-dimethyl-5-sulfo-oxindole (2) and 1-(3-sulfopropyl)-2-(5-oxo-pent-1,3-dienyl)-3,3-dimethyl-5-Sulfo-indole (3) (Fig. 2.7a and b), thus functioning as a turn-off sensor for HOCl in the concentration regime of 5 μM – 1 mM. The oxidative cleavage of the Cy 5 core by HOCl was further confirmed by photophysical experiments. UV-Visible spectra of 1 incubated with HOCl showed a concentration-dependent decrease in absorbance at 650 nm, indicating a degradation of the chromophore core (Figure 2.7c).

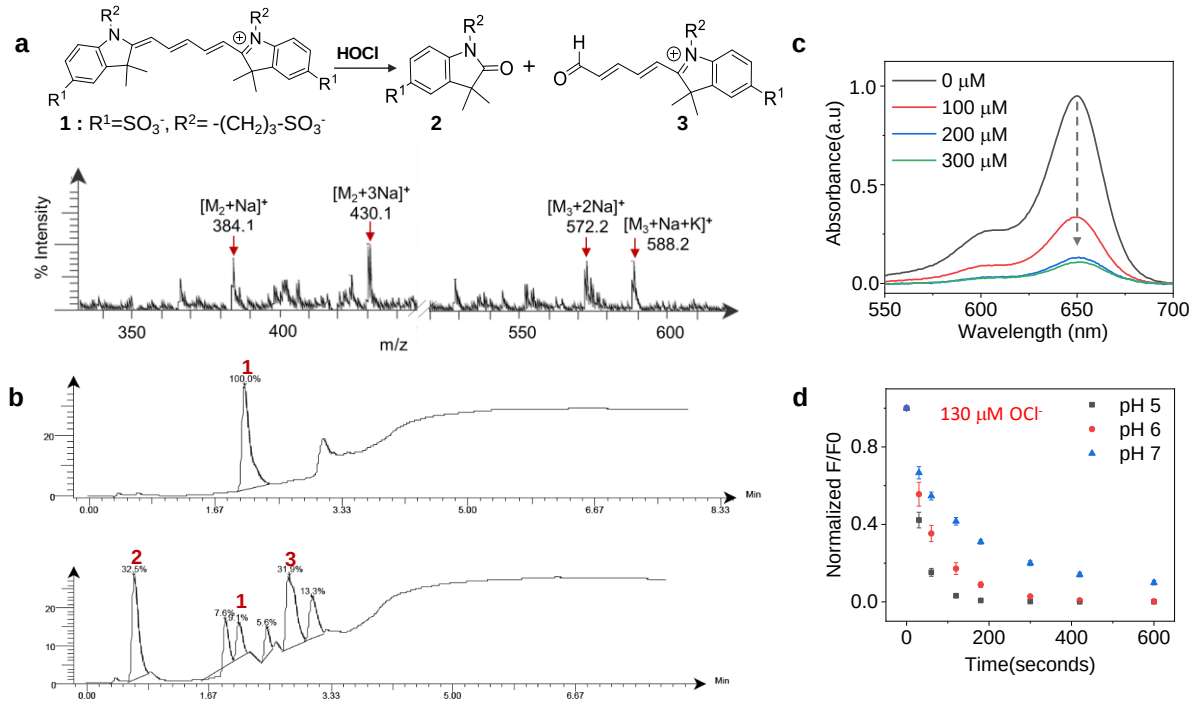

Figure 2.7: Characterization of reaction of 1 with HOCl. a) Scheme of reaction between 1 and HOCl(top), Mass spectra showing products of 1 after reaction with HOCl (bottom). b) LC MS of 1 (top) and 1+HOCl (bottom) shows that 1 undergoes oxidative degradation with HOCl. c). Absorbance spectra of 1 with increasing concentrations of-

HOCl showing degradation of-chromophore core. d) Fluorescence of 1 vs time at pH 5-7 (λ_{em}= 665 nm) after adding 130 μM HOCl, fluorescence intensity of 1 is normalized to the intensity before addition of HOCl.

Added Concentration of NaOCl(μM)	Effective concentration of HOCl (μM)			Initial Rate *10^{-3} (nM/sec)		
	pH 5	pH 6	pH 7	pH 5	pH 6	pH 7
15	14.96	14.57	11.58	2.495±0. 3	1.85±0. 2	1.5±0. 2
30	29.9	29.14	23.2	4.26±0. 8	3.1±0. 5	2.49±0. 2
43	42.7	41.7	33.2	9.4±0. 1	5.02±0. 2	3.53±0.2
86	85.4	83.4	66.2	10.43±0. 7	8.43±0.54	5.63±0. 2
129	128.5	125.4	99.7	13.77±0. 2	10.83±0. 7	7.57±0. 3

Table 2.2: kinetics of HOCl sensing by 1. Initial rate of reaction between 1 and HOCl at different pH's. Effective concentration of HOCl at each pH was calculated using Henderson-Hasslebalch equation.

We then checked the pH dependence of reactivity of 1 to HOCl, using reaction kinetics of 1 with HOCl at various pH values by fluorescence spectroscopy. 1 showed faster kinetics at acidic pH (1.3-fold faster at pH 5 compared to pH 7) suggesting a possible role of H^+ in enhancing the reaction kinetics (Figure 2.7d and Table 2.2). We compared the initial rates of reaction at pH 5, 6 and 7 to the exact concentration of HOCl to see if the increased rate at pH 5 results from a higher ratio of HOCl/OCl^-. The effective concentration of HOCl calculated using Henderson-Hasslebalch equation species shows that reaction kinetics are dependent on the HOCl/OCl^- equilibrium, and independent of pH (Table 2.2). Rate constant calculation revealed that 1 is reacting preferentially with for HOCl over OCl^- (Table. 2.3). Therefore, high photostability, water solubility and pH-independent fast reactivity positions 1 as a suitable HOCl indicator for our sensor.

Reactive species	Concentration of Species			Rate constant (k) from each species, $M^{-1}sec^{-1}$		
	pH 5	pH 6	pH 7	pH 5	pH 6	pH 7
HOCl	14.96 mM	14.57 mM	11.58 mM	1.67±0.12	1.27±0.10	1.29±0.13
OCl^-	44 nM	430 nM	3.42 mM	568±2.11	43±0.21	4.4±0.41
HOCl	29.91 mM	29.14 mM	23.15 mM	1.42±0.20	1.06±0.08	1.07±0.10
OCl^-	88 nM	859 nM	6.85 mM	484±1.61	36.1±1.43	3.64±0.72
HOCl	42.7 mM	41.77 mM	33.2 mM	2.4±0.11	1.2±0.07	1.06±0.06
OCl^-	126 nM	1.23 mM	9.82 mM	828±6.46	40.8±2.65	3.59±0.63

Table 2.3: Selectivity of 1 to HOCl over OCl^-. Rate constants of reaction between 1 and HOCl at various pH values calculated from initial rate using 1st order kinetic equation.

2.C.2: Mechanism of pH sensing by Rhodamine 6G amide

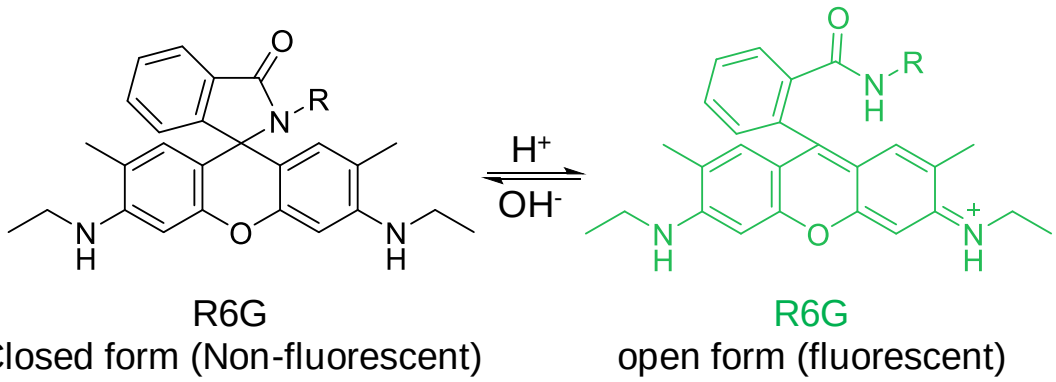

R6G
Closed form (Non-fluorescent)

R6G
open form (fluorescent)

Figure 2.8: Mechanism of pH sensing by R6G. R6G undergoes H^+ mediated ring opening in acidic pH, resulting in a turn on fluorescence and OH^- mediated lactam formation in alkaline pH, resulting loss of fluorescence.

MPO recruitment and activity is reported in various locations intracellularly and extracellularly in biological systems (Chen et al., 2008; Gray et al., 2008; Klebanoff, 2005; Klebanoff et al., 2013; Nurcombe and Edwards, 1989; Odobasic et al., 2016). We wanted to check the HOCl production in the phagosome, which is known for the recruitment of MPO and HOCl production. Phagosomal maturation is characterized by changes in pH depending on the cell type and pathogen in macrophages, while pH remains near neutral in neutrophil phagosomes. Rhodamine6G is known to undergo a reversible fluorescence

change depending on the external pH: at acidic pH it will undergo H^+ assisted lactam ring opening with increase in fluorescence while at basic pH it undergoes ring closure with a decrease in fluorescence (Figure 2.8) (Tian et al., 2012; Yuan et al., 2011).

2.C.3: Design and working principle of DNA based probes for simultaneous sensing of pH and HOCl- *cHOClate*

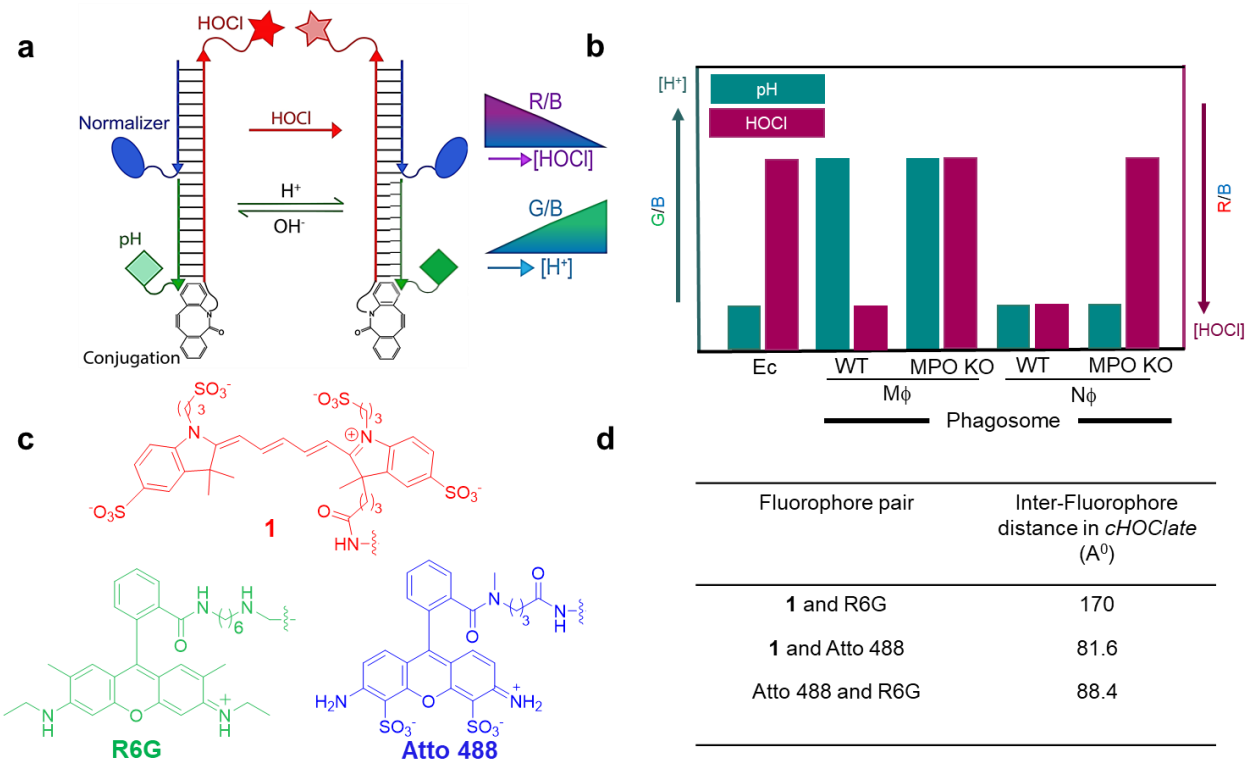

Fluorophore pair	Inter-Fluorophore distance in *cHOClate* (A^0)
1 and R6G	170
1 and Atto 488	81.6
Atto 488 and R6G	88.4

Figure 2.9: Design and working principle of *cHOClate*: a) Structure and working principle of *cHOClate*. *cHOClate* is comprised of: (i) an HOCl sensing module (red strand) containing a HOCl sensitive fluorophore (1, red star(R)), (ii) a pH sensing module (green strand) containing a pH sensitive fluorophore (R6G, green diamond(G)), (iii) a Normalizer (blue strand) containing an HOCl and pH insensitive fluorophore (Atto-488, blue oval(B)), (iv) a conjugation module which is a DBCO group at the 5' end of the HOCl sensing module. Upon reaction with HOCl 1 undergoes a decrease in fluorescence, thereby-

decreasing R/B. At acidic pH R6G undergoes an increase in fluorescence, causing G/B to increase. b). Compared to extracellular media, the phagosomal milieu is more acidic in macrophage (Mϕ) phagosomes and has higher HOCl, resulting in higher- G/B and lower R/B values. The phagosomal milieu is near neutral in neutrophil (Nϕ) phagosomes and has higher HOCl, resulting in lower G/B and lower R/B values. MPO inhibition in phagosomes causes a decrease in HOCl and subsequent increase in R/B values. c) Chemical structure of fluorophores in *cHOClate*; 1, R6G and Atto 488. Wiggly line indicates attachment to DNA. d) Distance between fluorophore pairs in *cHOClate*.

In order to map HOCl in the phagosome as a function of phagosome maturation, we designed *cHOClate* such that it could simultaneously report pH and HOCl. *cHOClate* is a 50-base pair DNA duplex comprising three strands D1, D2 and D3 (refer to Table 2.1 for sequences) and bears four functionalities (Figure 2.9a). The first of these is an HOCl sensing dye 1 (red star, λ_{ex} = 650 nm; λ_{em}=665 nm) at the 3' end of D1 (red strand) which undergoes fluorescence turn off upon reaction with HOCl as described in section 2. C.1. The second is a reference dye Atto-488 (blue oval, λ_{ex} = 488 nm; λ_{em}=520 nm) attached to the 3'end of D2 (blue strand). Atto-488 was used as a reference fluorophore because of its high photostability and insensitivity to pH, ROS and RNS. *cHOClate* incorporates a third functionality, the dye N-(6-Aminohexyl) rhodamine 6G-amide (R6G, λ_{ex} = 530 nm; λ_{em} = 555 nm) at the 3' end of D3 (green strand) which undergoes acid mediated lactam ring opening, sensing pH reversibly as described in section 2. C.2. The fourth functionality is a conjugation module in the form of a Dibenzocyclooctyl group (DBCO) at the 5'-end of D1 in order to conjugate *cHOClate* to a phagocytic cargo using click chemistry. The length

of strands and positioning of each functionalities was chosen in such a way that the FRET between fluorophores are minimum (Figure 2.9d).

In *cHOClate* the ratio of red to blue intensity (R/B) will serve as a quantitative indicator of HOCl while the ratio of green to blue intensity (G/B) will indicate pH changes quantitatively. Since 1 is a turn off fluorophore, the ratio of R/B in *cHOClate* decreases with increasing concentration of HOCl; the ratio of G/B increases with increased acidity (Figure 2.9a).

In phagosomes, where MPO activity produces HOCl, *cHOClate* will show lower R/B than in the extracellular medium. Contrary to that *cHOClate* is expected to show lower G/B values in the extracellular medium since pH is ~7.2. Since phagosomal maturation in macrophage leads to an acidic environment in the lumen of phagosomes there will be a higher G/B compared to extracellular medium; neutrophils phagosome will show similar G/B to that of extracellular medium according to previous reports (Segal et al., 1981). Neutrophil and macrophage phagosomes are expected to show a lower R/B with the recruitment of MPO. This change in R/B can be reverted using specific inhibitors for MPO, or using MPO knockout cells (Figure 2.9b).

The formation and integrity of *cHOClate* was confirmed using gel electrophoresis and fluorescence spectroscopy that indicated >99% yield (Figure.2.5).

2.C.4: In vitro performance of *cHOClate*

The concentration of HOCl in solution is reflected in the R/B ratio of the fluorescence intensities of Atto-488 (B) and (1) (R) (Figure 2.9a) in *cHOClate*. To test this, varying concentrations of NaOCl (0-100 μM) were added to *cHOClate* in UB_4 buffer (20 mM, at

pH 4.5), and fluorescence emission intensities of both Atto-488 and (1) were recorded as a function of time. While the fluorescence of Atto-488 remained unchanged, the fluorescence of (1) reduced with increasing HOCl (Figure 2.10a) over the reported physiological HOCl concentrations (20-400 μM). The response time for 80% signal change was < 2 minutes for 40 μM HOCl, indicating a fast response (Figure. 2.10b) which is advantageous for a fast detection.

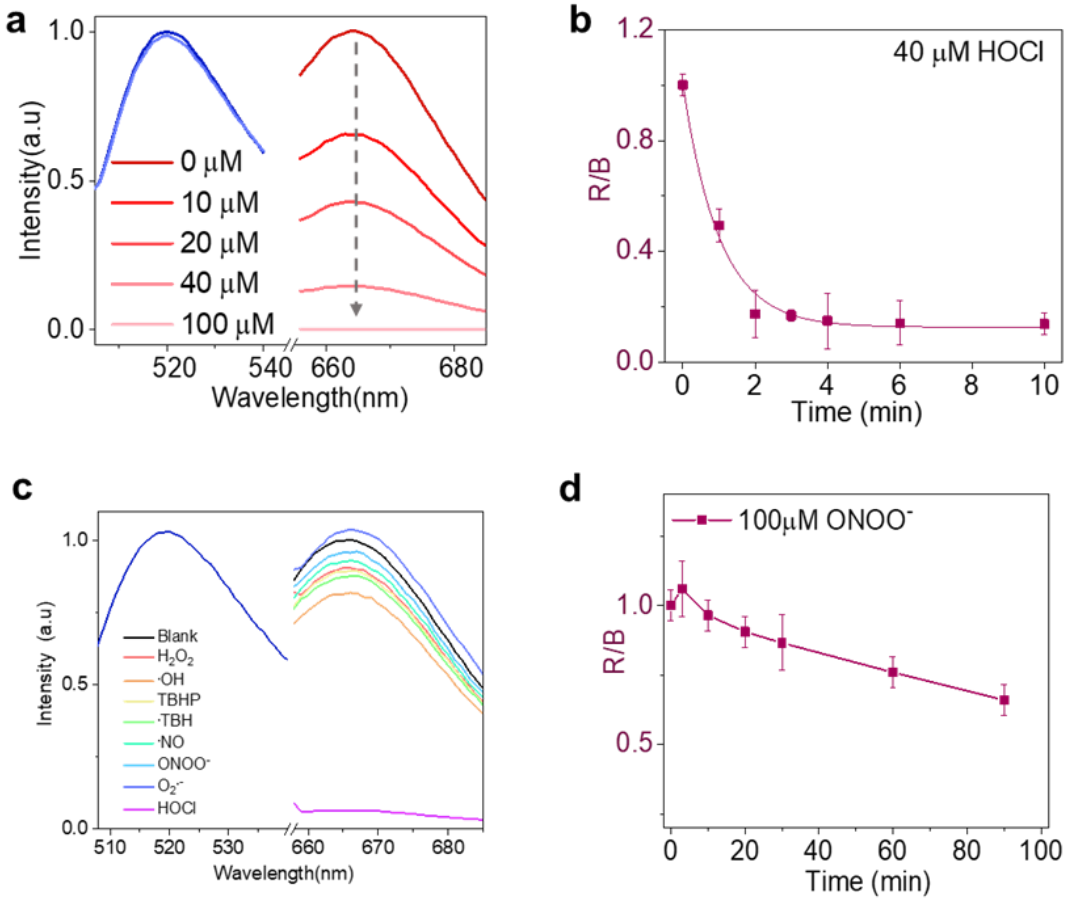

Figure 2.10: Performance of HOCl sensing module in *cHOClate*. a) Normalized fluoresce spectra of *cHOClate* in R (λ_{ex}=650 nm) and B (λ_{ex}=488 nm) channel with various concentrations of HOCl (pH 4.5, 20mM UB_4 buffer). Representative data from three-

independent experiments are shown. b) Kinetics of HOCl sensing by *cHOClate* with 40 μM of HOCl, with data points fitted on Origin using nonlinear curve fit. Representative data from three independent experiments are- shown; error bars, SEM; measure of center, mean. c) Normalized fluorescence spectra of *cHOClate* in R and B channels in presence of 100 μM of the indicated ROS and RNS -Representative data from three independent experiments are shown. d) Kinetics of *cHOClate* reactivity to 100 μM peroxynitrite given by R/B value, showing a gradual decrease in signal beyond 25 min. Representative data from three independent experiments are shown; error bars, SEM; measure of center, mean.

Next, the specificity of *cHOClate* towards various reactive oxygen species (ROS) or reactive nitrogen species (RNS) was tested by incubating it with generators of specific reactive species for 10 minutes and subsequently measuring R/B values. *cHOClate* showed ~20-fold selectivity for HOCl over any other ROS/RNS (Figure 2.10c). Note that on longer timescales i.e., 20 minutes, we observed very modest sensitivity to peroxynitrite ($ONOO^-$) (Figure 2.10d).

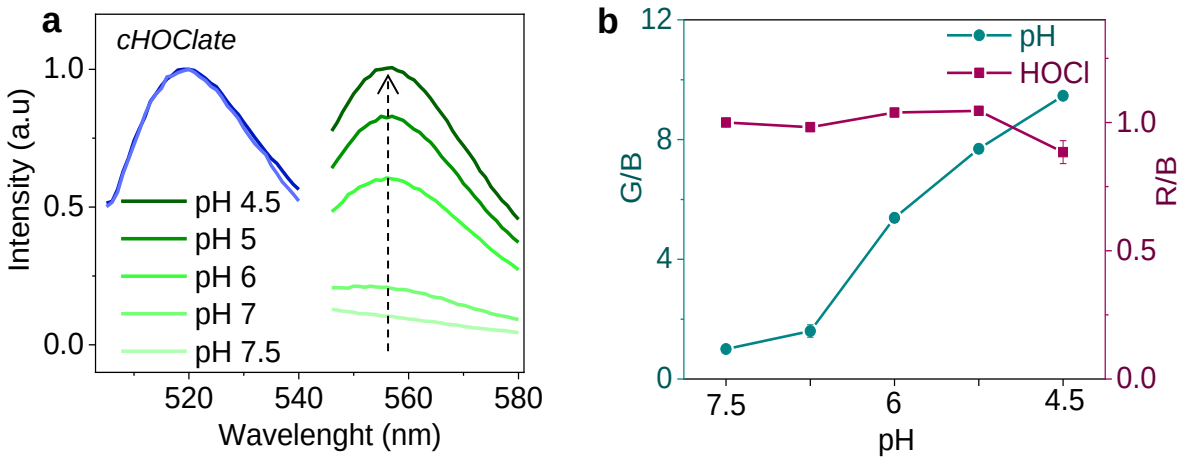

Figure 2.11: Performance of pH sensing module in *cHOClate*. a) Normalized fluorescence spectra of *cHOClate* in B (λ_{ex}=488 nm) and G (λ_{ex}=530 nm) channels with pH. b) Normalized G/B and R/B plotted against pH for *cHOClate*. Representative data from three independent experiments are shown; error bars, SEM; measure of center, mean.

cHOClate functioned well as a ratiometric reporter of solution pH. The ratio of R6G fluorescence (G) to Atto-488 fluorescence (B) in *cHOClate* i.e., G/B ratio, quantitatively reports pH where G/B increases as acidity increases. *cHOClate* showed a 10-fold increase in G/B from pH 7.4 (extracellular pH) to ~pH 5 (lumenal pH in a mature phagosome) (Figure 2.11), indicating that it was also well placed to report on phagosomal pH. The R/B ratio remains unaffected at all investigated pH values (Figure 2.11b), indicating that pH changes does not affect the R/B values.

2.C.5: pH and HOCl modules functions independently in *cHOClate*

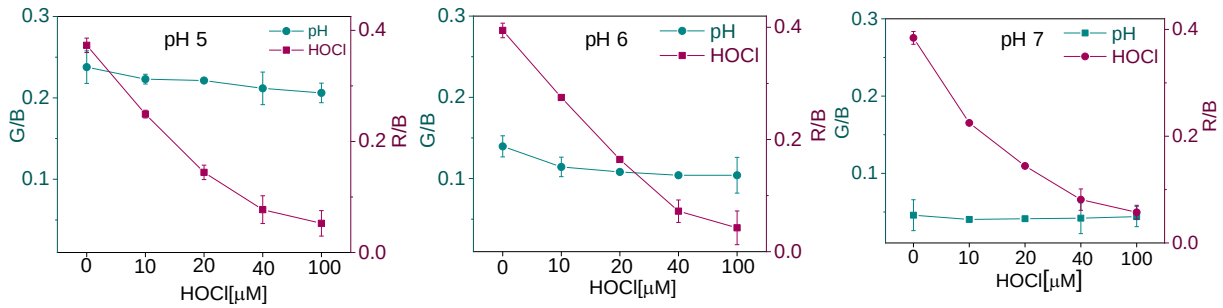

Figure 2.12: pH and HOCl modules function independent of each other. Absolute G/B and R/B values of *cHOClate* at varying concentrations of HOCl in pH 5, 6 and 7. Representative data from three independent experiments are shown; error bars, SEM; measure of center, mean.

Because *cHOClate* is a multianalyte sensor, we needed to check if the HOCl sensitive and pH sensitive modules work independent of each other. For this we checked the HOCl sensitivity of *cHOClate* at various pH values (5 to 7) by adding 0 - 100 μM HOCl, and we and plotted G/B and R/B ratio against effective [HOCl] after 20 minutes. We found that in the physiological pH range and reported concentrations of HOCl, both modules work independently reporting solution phase pH and HOCl (Figure 2.12).

2.C.6: Integrity of DNA nanodevices to ROS/ RNS

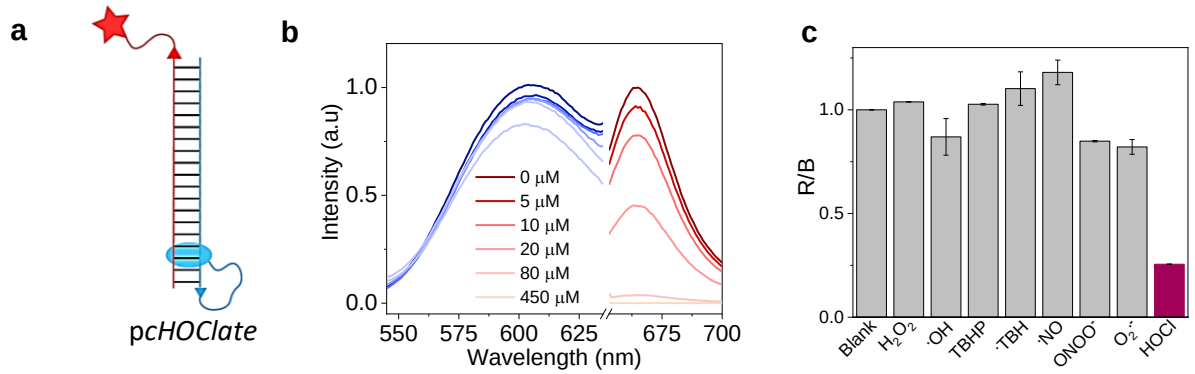

Figure 2.13: **Stability of DNA duplex to ROS/RNS.** a) *pcHOClate* contains 1 at the 5' end D4(red strand) and EtBr at the 5' end of D5(blue strand). EtBr is intercalated into the DNA duplex and hence solvent protected. b) Fluorescence spectra of *pcHOClate* in EtBr and 1 channels with HOCl ranging from 1μM- 450 μM. c) Ratio of 1 to EtBr in p*cHOClate* after incubating with indicated ROS/RNS indicating stability of DNA duplex to ROS/RNS, [HOCl]= 40 μM, all other ROS/RNS = 100 μM.

The integrity of the DNA scaffold comprising *cHOClate* was evaluated using p*cHOClate* as a proxy. Here, EtBr is covalently attached to the 5' end of D5 in p*cHOClate* (Figure 2.13a). EtBr exhibits enhanced fluorescence due to intercalation into the intact duplex DNA of *pcHOClate* (Φ_{free}= 0.03, Φ_{ic} = 0.3). Thus, as long as the duplex is intact, the fluorescence of the intercalated EtBr moiety should not change. Spectra of EtBr and 1 were acquired in respective channels and intensities were plotted as functions of HOCl concentration (Figure 2.13b). Ratio of fluorescence intensities of 1 to EtBr for *pcHOClate* was plotted after incubating with various ROS/RNS (Figure 2.13c). We observe no change in the intensity of EtBr over the entire duration in these harsh *in vitro* conditions,

indicating the high likelihood of preservation of the duplexed state of *cHOClate* within the phagosome for the duration of the experiment.

2.D: Conclusions

Here using DNA based ratiometric sensing we developed a multifunctional sensor called *cHOClate. cHOClate* leverages the modular nature of DNA to integrate ratiometric pH and HOCl sensors such that they function independently to provide information on pH and HOCl levels at the simultaneously in the same location. This involves identification of a photostable derivative of Cy 5 as an HOCl sensitive fluorophore, which can detect HOCl in a dose dependent manner. In vitro experiments proved the specificity and sensitivity *cHOClate* to quantitively sense pH and HOCl independently of each other. In vitro experiments showed that integrity of *cHOClate* was not affected by ROS/ RNS. The i) rapid response and good specificity to HOCl, ii) ability of pH and HOCl sensing modules to perform independently and simultaneously and iii) stability of the DNA scaffold to ROS/RNS positions *cHOClate* very well to quantitatively image phagosomal HOCl over the short timescales of phagosome maturation.

2.E: References

Abo, M., Urano, Y., Hanaoka, K., Terai, T., Komatsu, T., and Nagano, T. (2011). Development of a highly sensitive fluorescence probe for hydrogen peroxide. J. Am. Chem. Soc. *133*, 10629–10637.

Chakraborty, K., Leung, K., and Krishnan, Y. (2017). High lumenal chloride in the lysosome is critical for lysosome function. Elife *6*, e28862.

Chen, J.W., Breckwoldt, M.O., Aikawa, E., Chiang, G., and Weissleder, R. (2008). Myeloperoxidase-targeted imaging of active inflammatory lesions in murine experimental autoimmune encephalomyelitis. Brain *131*, 1123–1133.

Chen, X., Lee, K.-A., Ren, X., Ryu, J.-C., Kim, G., Ryu, J.-H., Lee, W.-J., and Yoon, J. (2016). Synthesis of a highly HOCl-selective fluorescent probe and its use for imaging HOCl in cells and organisms. Nat. Protoc. *11*, 1219–1228.

Corleis, B., Korbel, D., Wilson, R., Bylund, J., Chee, R., and Schaible, U.E. (2012). Escape of Mycobacterium tuberculosis from oxidative killing by neutrophils. Cell Microbiol. *14*, 1109–1121.

Gaut, J.P., Byun, J., Tran, H.D., and Heinecke, J.W. (2002). Artifact-free quantification of free 3-chlorotyrosine, 3-bromotyrosine, and 3-nitrotyrosine in human plasma by electron capture-negative chemical ionization gas chromatography mass spectrometry and liquid chromatography-electrospray ionization tandem mass spectrometry. Anal. Biochem. *300*, 252–259.

Gray, E., Thomas, T.L., Betmouni, S., Scolding, N., and Love, S. (2008). Elevated activity and microglial expression of myeloperoxidase in demyelinated cerebral cortex in multiple sclerosis. Brain Pathol. *18*, 86–95.

Hazell, L.J., Arnold, L., Flowers, D., Waeg, G., Malle, E., and Stocker, R. (1996). Presence of hypochlorite-modified proteins in human atherosclerotic lesions. J. Clin. Invest. *97*, 1535–1544.

Hazen, S.L., and Heinecke, J.W. (1997). 3-Chlorotyrosine, a specific marker of myeloperoxidase-catalyzed oxidation, is markedly elevated in low density lipoprotein isolated from human atherosclerotic intima. J. Clin. Invest. *99*, 2075–2081.

Jiang, X., Wang, L., Carroll, S.L., Chen, J., Wang, M.C., and Wang, J. (2018). Challenges and Opportunities for Small-Molecule Fluorescent Probes in Redox Biology Applications. Antioxid. Redox Signal.

Klebanoff, S.J. (2005). Myeloperoxidase: friend and foe. J. Leukoc. Biol. *77*, 598–625.

Klebanoff, S.J., Kettle, A.J., Rosen, H., Winterbourn, C.C., and Nauseef, W.M. (2013). Myeloperoxidase: a front-line defender against phagocytosed microorganisms. J. Leukoc. Biol. *93*, 185–198.

Kumar, K., and Margerum, D.W. (1987). Kinetics and mechanism of general-acid-assisted oxidation of bromide by hypochlorite and hypochlorous acid. Inorg. Chem. *26*, 2706–2711.

Lou, Z., Li, P., Song, P., and Han, K. (2013). Ratiometric fluorescence imaging of cellular hypochlorous acid based on heptamethine cyanine dyes. Analyst *138*, 6291–6295.

Modi, S., M G, S., Goswami, D., Gupta, G.D., Mayor, S., and Krishnan, Y. (2009). A DNA nanomachine that maps spatial and temporal pH changes inside living cells. Nat. Nanotechnol. *4*, 325–330.

Nurcombe, H.L., and Edwards, S.W. (1989). Role of myeloperoxidase in intracellular and extracellular chemiluminescence of neutrophils. Ann. Rheum. Dis. *48*, 56–62.

Nüsse, O. (2011). Biochemistry of the phagosome: the challenge to study a transient organelle. ScientificWorldJournal *11*, 2364–2381.

Odobasic, D., Kitching, A.R., and Holdsworth, S.R. (2016). Neutrophil-Mediated Regulation of Innate and Adaptive Immunity: The Role of Myeloperoxidase. J. Immunol. Res. *2016*, 2349817.

Pulli, B., Ali, M., Forghani, R., Schob, S., Hsieh, K.L.C., Wojtkiewicz, G., Linnoila, J.J., and Chen, J.W. (2013). Measuring myeloperoxidase activity in biological samples. PLoS One *8*, e67976.

Rangarajan, S., and Friedman, S.H. (2007). Design, synthesis, and evaluation of phenanthridine derivatives targeting the telomerase RNA/DNA heteroduplex. Bioorg. Med. Chem. Lett. *17*, 2267–2273.

Robaszkiewicz, A., Bartosz, G., and Soszynski, M. (2011). Detection of 3-chlorinated tyrosine residues in human cells by flow cytometry. J. Immunol. Methods *369*, 141–145.

Robinson, K.M., and Beckman, J.S. (2005). Synthesis of peroxynitrite from nitrite and hydrogen peroxide.

Roubaud, V., Sankarapandi, S., Kuppusamy, P., Tordo, P., and Zweier, J.L. (1997). Quantitative measurement of superoxide generation using the spin trap 5-(diethoxyphosphoryl)-5-methyl-1-pyrroline-N-oxide. Anal. Biochem. *247*, 404–411.

Saha, S., Prakash, V., Halder, S., Chakraborty, K., and Krishnan, Y. (2015). A pH-independent DNA nanodevice for quantifying chloride transport in organelles of living cells. Nat. Nanotechnol. *10*, 645–651.

Schmitt, F.-J., Renger, G., Friedrich, T., Kreslavski, V.D., Zharmukhamedov, S.K., Los, D.A., Kuznetsov, V.V., and Allakhverdiev, S.I. (2014). Reactive oxygen species: re-evaluation of generation, monitoring and role in stress-signaling in phototrophic organisms. Biochim. Biophys. Acta *1837*, 835–848.

Segal, A.W., Geisow, M., Garcia, R., Harper, A., and Miller, R. (1981). The respiratory burst of phagocytic cells is associated with a rise in vacuolar pH. Nature *290*, 406–409.

Sharma, S., Zaveri, A., Visweswariah, S.S., and Krishnan, Y. (2014). A fluorescent nucleic acid nanodevice quantitatively images elevated cyclic adenosine monophosphate in membrane-bound compartments. Small *10*, 4276–4280.

Shepherd, J., Hilderbrand, S.A., Waterman, P., Heinecke, J.W., Weissleder, R., and Libby, P. (2007). A fluorescent probe for the detection of myeloperoxidase activity in atherosclerosis-associated macrophages. Chem. Biol. *14*, 1221–1231.

Sun, M., Yu, H., Zhu, H., Ma, F., Zhang, S., Huang, D., and Wang, S. (2014). Oxidative cleavage-based near-infrared fluorescent probe for hypochlorous acid detection and myeloperoxidase activity evaluation. Anal. Chem. *86*, 671–677.

Surana, S., Bhat, J.M., Koushika, S.P., and Krishnan, Y. (2011). An autonomous DNA nanomachine maps spatiotemporal pH changes in a multicellular living organism. Nat Commun *2*, 340.

Tian, M., Peng, X., Fan, J., Wang, J., and Sun, S. (2012). A fluorescent sensor for pH based on rhodamine fluorophore. Dyes and Pigments *95*, 112–115.

Wang, J., Zhao, Y., Wang, C., Zhu, Q., Du, Z., Hu, A., and Yang, Y. (2015). Organelle-Specific Nitric Oxide Detection in Living Cells via HaloTag Protein Labeling. PLoS One *10*, e0123986.

Xu, Q., Lee, K.-A., Lee, S., Lee, K.M., Lee, W.-J., and Yoon, J. (2013). A highly specific fluorescent probe for hypochlorous acid and its application in imaging microbe-induced HOCl production. J. Am. Chem. Soc. *135*, 9944–9949.

Yuan, L., Lin, W., and Feng, Y. (2011). A rational approach to tuning the pKa values of rhodamines for living cell fluorescence imaging. Org. Biomol. Chem. *9*, 1723–1726.

Zhang, Y.-R., Chen, X.-P., Jing-Shao, Zhang, J.-Y., Yuan, Q., Miao, J.-Y., and Zhao, B.-X. (2014). A ratiometric fluorescent probe for sensing HOCl based on a coumarin-rhodamine dyad. Chem. Commun. (Camb) *50*, 14241–14244.

Chapter 3

Detection of phagosomal HOCl and pH in live macrophages

3.A: Introduction

Innate immune cells engulf the apoptotic bodies and pathogens and protect the host body from pathology by clearing them (Akira et al., 2006; Mahajan et al., 2016). This compartment formed with the ingested cargo is called phagosome, where the cargo is destroyed by a combined action of hydrolytic enzymes and reactive oxygen species (ROS) (Huynh et al., 2007; Lukacs et al., 1990; Nüsse, 2011; Robinson, 2008). The interplay between chemical composition of phagosome lumen and activity of these hydrolytic enzymes are hence crucial for the proper clearance of these ingested cargo. Phagosomal composition is a function of the ingested cargo and host cell immune machinery (Pauwels et al., 2017).

Defects in phagocytosing and proper degradation of pathogens leads to infectious diseases (Charles A Janeway et al., 2001; Mogensen, 2009). Blocking of phagosome acidification in macrophages or inhibiting the ROS producing enzymes leads to defective pathogen clearance (Hampton et al., 1996; Queval et al., 2017). For e.g., chronic granulomatous disease is an infectious disease caused in patients with mutations in NOX2, a superoxide generation enzyme (Bianchi et al., 2009; Vowells et al., 1995). Moreover, resistant microbes like *Staphylococcus aureus, Mycobacterium tuberculosis* etc. do escape the phagosomal killing by perturbing the chemical environment inside the phagosome and affecting the phagosome maturation (Corleis et al., 2012; Humphreys et al., 1989). Hence, it is important to develop a method by which one can temporally map

interplay between ROS generation and phagosome maturation to reveal possible mechanisms which different pathogen adopts to infect the host cells.

Among ROS generated in the phagosomes peroxynitrite ($ONOO^-$) and hypochlorous acid (HOCl) are considered to be the most powerful ROS which can damage biological molecules (Nüsse, 2011; Spickett et al., 2000; Winterbourn and Kettle, 2013). Having developed *cHOClate* which can sense pH and HOCl simultaneously we sought to use *cHOClate* to unveil the maturation dynamics in the phagosomes of innate immune cells. We chose zymosan as are phagocytic cargo which is well established as a phagocytic cargo in immune cells. The surface functionalization of zymosan and characterization of the phagosome targetable *cHOClate, Z-cHOClate* in cellulo and in vitro is discussed in chapter 3. Using biochemical assay, we show that MPO activity in phagosomes is associated with MPO recruitment to the phagosomes.

3.B: Materials and methods

3.B.1: Surface functionalization of Zymosan with DNA sensors

1 mg of Zymosan (2×10^7 particles) was stirred with 0.34 mg of $NaIO_4$ (2 nmol) in 80 µL of 50 mM sodium acetate buffer, pH 5, at 4°C in the dark for 16 h to oxidize 1,6-glucans on the surface. To quench unreacted $NaIO_4$, 4 µL ethylene glycol was added, stirred for 10 minutes, and centrifuged at 2500 rpm for 15 minutes at 4°C. Supernatant was removed without disturbing the pellet and replaced 100 µM of NH_2-PEG-N_3 in 100 mM borate buffer, pH 10. After stirring for 24h at RT in the dark, the supernatant was removed by centrifugation, and the Schiff base formed was stabilized by $NaBH_4$ (3 nmol) in deionized water. This azide-functionalized Zymosan (Zym-N_3) was incubated with *cHOClate* (10

μM) in 20 mM phosphate buffer, pH 7 with 100 mM KCl, for 4h at RT in the dark. The resulting suspension was centrifuged, washed the pellet with 1x PBS (*3 times) and resuspended in potassium phosphate buffer of pH 7(20mM containing 100 mM KCl). Surface labeling was evaluated by imaging particles at pH 5. As a control for surface labeling, unfunctionalized zymosan particles were treated with *cHOClate* and imaged.

3.B.2: Labeling efficiency of Zymosan with *cHOClate*

Labeling efficiency of zymosan with *cHOClate* was evaluated by fluorescence imaging as well as flow cytometry. Z-*cHOClate* was suspended in pH 5 (20 μL, UB_4 buffer, 20 mM) and the drop mounted on a grass slide using a coverslip, and dried for 5 minutes. The particles were imaged using fluorescence microscopy in DIC, A488, R6G and Cy 5 channels as described in section 3. B.11. Non-functionalized zymosan particles incubated *cHOClate* for the same time and subjected to washings were used as a control. High resolution images were acquired in confocal microscopy to visualized the surface labeling.

For flow cytometry, Z-*cHOClate* and plane zymosan particles (10^8 particles /mL) were suspended in 1X PBS (pH 7.4) and injected $20*10^3$ particles in the flow cytometry, the particles were monitored in Atto-488, R6G and Cy 5 channels. Both forward scattering and side scattering were recorded to check the heterogeneity of labeling. The intensity of the respective channels was collected and compared for 1:1 labeling stoichiometry.

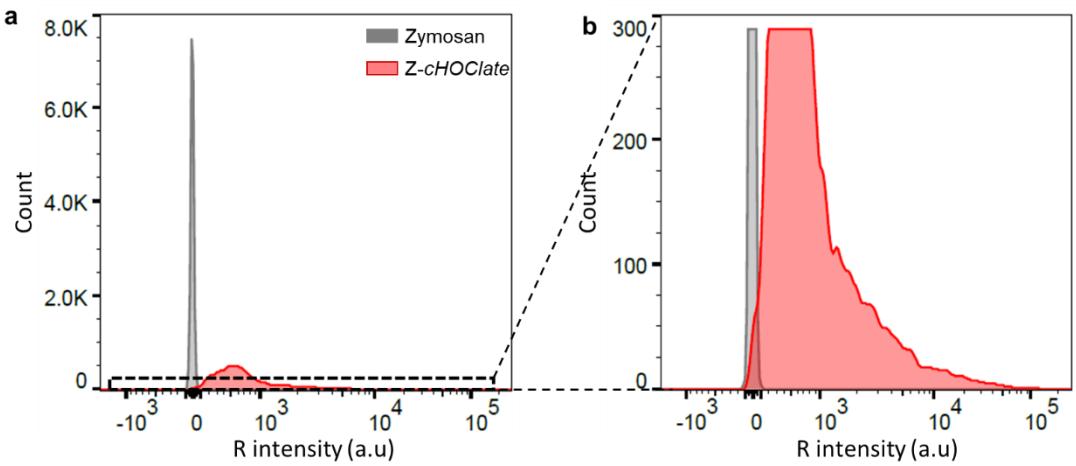

Figure 3.1: Flow cytometric analysis of *Z-cHOClate* labeling efficiency. a) Fluorescence Intensities of ~20000 particles of *Z-cHOClate* (red) and zymosan (grey) in the Cy.5 channel. b) The inset from (a) is enlarged, to represent overlap between Zymosan and Z-*cHOClate*, which corresponds to ~2% of Z-cHOClate. Hence 98% of particles are labeled.

3.B.3: Surface density small molecules and DNA on Zymosan

From theoretical and experimental estimates, we found that on average there are ~10^6*cHOClate* assemblies per zymosan. We used the following methods to estimate the surface density on zymosan.

1. Small molecule cleavage assay

We used an absorbance-based strategy where available azide groups on zymosan was clicked with a chemically cleavable coumarin called BCN-coumarin, and number of azide groups can be estimated through UV-absorbance of the cleaved coumarin (Figure 3.2). BCN-coumarin molecule (8) was synthesised (synthesis and characterization are described below) which was then chemically attached to the azide groups displayed on Zym-N_3 as described in section 3. B.1. This displays hydrolysable 7-hydroxy-4-

trifluoromethylcoumarin groups (λ_{max} = 385 nm, ε = 20573 $M^{-1}cm^{-1}$) on the Zym- N_3 surface to give Zym-(8). Roughly 10^6 Zym-(8) particles were subjected to base hydrolysis of carbonate groups to release trifluoromethyl coumarin into a well-defined solution volume, which was then estimated by UV absorption. This yielded ~27.5×10^7 small molecules per zymosan.

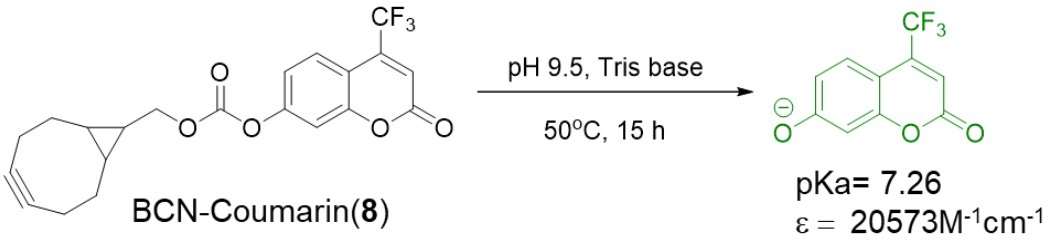

Figure 3.2: Base mediated cleavage of coumarin from BCN-coumarin

Briefly Zym-N_3 (1.7×10^6) was labeled with (8) (20 μM, 1000 pmoles) as described earlier for Z-*cHOClate*. Any free dye was removed by centrifugation and washes with 1x PBS (6 times), 150 mM of Tris base (pH 9.5) was added to ~10^6 Zym-(8) particles and the mixture was stirred for 15 h at 50°C. The resultant suspension was centrifuged at 4000 rpm for 15 minutes, the supernatant was collected. The particles were washed, all the supernatants collected (6×100 μL), combined, concentrated to 100 μL and quantified by UV absorption. Experiments were performed in duplicate (Figure 3.3b).

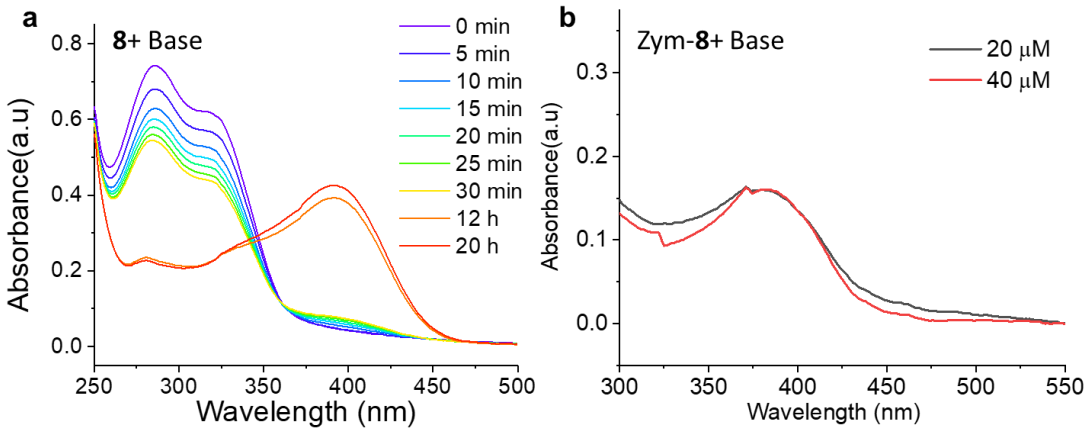

Figure 3.3: Small molecule cleavage assay. a) Kinetics of carbonate bond cleavage of 8 by reaction with tris base at 50°C. b) UV-Absorbance spectra of cleaved coumarin from Zym-8 surface, which was formed from the indicated starting concentrations of 8.

No of moles of cleaved coumarin = 775 ±13 pmoles

No: of moles of azides for attachment / Zymosan = 775 ±13 pmoles /1.7×10^{6} Zymosan

= 456×10^{-18} moles/Zymosan

No: of azide groups / Zymosan = $6.023*10^{23}(456.5 \times10^{-18})$ = 27.5×10^{7}

This corresponds to the maximum number of small molecules that can be displayed on Zym-N3. However, DNA is much larger than (8) and attachment at one site, might preclude accessibility to surrounding azide.

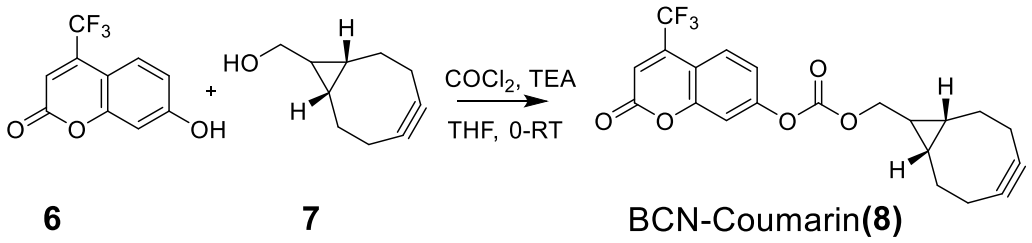

Figure 3.4: synthesis of compound 8

Synthesis of Compound 8: 25 mg (0.1 mmol) compound 6 was taken in a round bottom flask and 0.5 mL anhydrous THF, followed by 0.075 mL (0.5 mmol) triethylamine was added to it under inert atmosphere. Then 0.7 mL (15 wt% in toluene) phosgene solution was added dropwise to the reaction mixture at 0°C and the mixture was stirred for 4 h. THF as well as phosgene was evaporated by purging N_2 through the reaction mixture in a fume hood to obtain corresponding chloroformate. This precipitate was dissolved in dry THF (1 mL) and kept under N_2 atmosphere. In a separate round bottom flask 10 mg of compound 7 (0.067 mmol), dissolved in 0.5 ml anhydrous THF and 0.03 mL (0.33 mmol) triethylamine was mixed and cooled to 0°C. The chloroformate containing THF was then added slowly over a period of 15 min to compound 7 containing reaction mixture and stirred at 0°C - RT overnight. After the completion, THF was evaporated from the reaction mixture under reduced pressure. Compound 8 was purified by silica gel flash column chromatography (20% ethyl-acetate in hexane), Yield = 40%. ^{1}H NMR (500MHz, $CDCl_3$): δ (ppm): 7.96 (s, 1H), 7.53 (s, 1H), 7.27 (s, 1H), 6.79 (s, 1H), 4.42 (m, 2H), 2.31 (m, 4H), 1.57 (m, 4H), 0.88 (m, 3H), ESI-MS: m/z calculated for $[C_{21}H_{17}F_3O_5 + H^+]$ = 407.3, found = 407.2.

2. Theoretical estimate

Assuming Zymosan as a sphere and assuming 50% surface coverage, considering the charge repulsion between DNA duplexes that are radiating outwards from the Zym-N3 surface, we calculated the number of *cHOClate* molecules that can be accommodated on a zymosan particle.

Average diameter of a Zymosan particle = 3.9 μm

Average surface area of a Zymosan = $4\pi r^2$ = 47.78 μm^2

50% surface area covered by DNA = 47.78/2 = 23.89 μm^2

Radius of a DNA duplex ~ 1 nm

Area occupied by a vertically oriented DNA duplex = πr^2 = 3.14 nm^2

Number of DNA molecules at 50% surface coverage = 23890000 nm^2/3.14 nm^2 = 7.60 x 10^6

3. Experimental estimate

Using UV absorbance, we measured the concentration of *cHOClate* in a solution that was used to functionalize ~10^6 Zym-N_3 particles before and after labeling. We were thus able to estimate the change in *cHOClate* concentration post labeling, which was then converted to the number of *cHOClate* molecules that was used up for labeling. Knowing the number of Zym-N_3 particles used for the reaction, the average number of *cHOClate* per Zym-N_3 particle was found to be ~3.87 x 10^6.

Both theoretical and experimental estimates are consistent with each other and are on the order of 10^6 DNA duplexes/ zymosan particle.

3.B.4: Cell culture: J774A.1, SIMA.9 and RAW264.7 cells

J774A.1 cell line was a kind gift from Prof Deborah Nelson, Department of Pharmacological and Physiological Sciences, the University of Chicago. They were cultured in Dulbecco's Modified Eagle's Medium/F-12 (1:1) (DMEM-F12) (Invitrogen Corporation, USA) containing 10% heat inactivated Fetal Bovine Serum (FBS) (Invitrogen Corporation, USA) as per ATCC protocols. RAW 264.7 cell line were a kind gift from Dr. Christine A. Petersen, Department of Epidemiology, College of Public Health, University of Iowa. SIM-A9 (ATCC CRL-3265) cells were purchased from ATCC and cultured according to the ATCC protocol.

3.B.5: pH and HOCl measurements *in vitro*

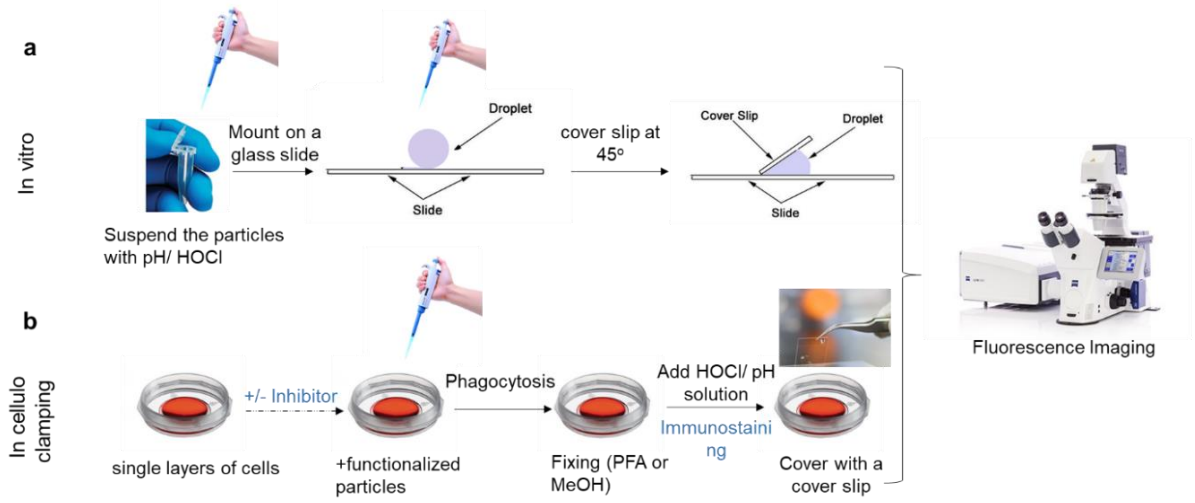

Figure 3.5: Work flow for pH and HOCl measurements using Z-*cHOClate*: a) In vitro pH and HOCl measurements using fluorescence imaging: the particles were incubated required pH or HOCl concentrations in the described buffer, transferred to a glass slide, covered with a 0.17mm cover glass and imaged. b) In cellulo clamping of HOCl/ pH: Macrophages were plated on an imaging dish for overnight, treated with inhibitors and Z-

cHOClate were added and allowed to be phagocytosed, the cells were washed, fixed, added various concentrations of HOCl, covered with a 0.17 mm cover glass and imaged (details in section 3.B.6). For immunostaining the cells which are allowed to phagocyte Z-R6G were used (section 3.B.9).

pH measurements: *Z-cHOClate* (4 μg/μL) was diluted 20-fold in UB_4 buffer, pH 4.5 – 7.5, and incubated for 5 minutes at 37°C. Each solution was pipetted up and down 5 times and immediately transferred to a glass slide. The drop was covered with a 0.17 mm cover glass and incubated for 5 minutes to form a thin film. Glass slides were imaged in respective channels using an IX-83 microscope.

HOCl measurements: *Z-cHOClate* (4 μg/μL) was diluted 20-fold in UB_4 buffer, pH 7 and incubated for 5 minutes with NaOCl (0 -20 μM) at 37°C. Each solution was pipetted up and down 5 times, and immediately transferred to a glass slide. The drop was covered with a 0.17 mM cover glass and incubated for 5 minutes to form a thin film. Glass slides were imaged in respective channels using an IX-83 microscope and R/B and G/B in each case was calculated.

3.B.6: *In cellulo* pH and HOCl clamping

pH clamping: J774A.1 cells were incubated with *Z-cHOClate* for 10-minutes in presence of 100 μM ABAH to allow for phagocytosis and cells were then fixed with 2.5% PFA. The cells were then incubated in pH clamping buffers of a known pH values, e.g. pH 4.5, using UB4 buffer containing ionophores Nigericin (20 μM), Monensin (20 μM), 140 mM NaCl, 10 mM KCl, and 2.5 mM $CaCl_2$ for 30 minutes. Cells containing *Z-cHOClate* particles were imaged as described in section 3.B.11 and the ratio of fluorescence intensities in

green and blue channels (G/B) was obtained and compared with that of un-internalized *Z-cHOClate* particles as a control. The experiment was performed for clamping buffers at different pH values spanning pH 4.5-7.5 and G/B values were plotted as a function of clamping buffer pH to obtain the calibration curve.

HOCl clamping: J774A.1 cells plated on a glass bottom dish was incubated with *Z-cHOClate* for 10 minutes in presence of 100 μM ABAH and were fixed with Methanol at -20^{o}C for 10-15 minutes. This results in permeabilization of plasma membranes as well as phagosomal membranes as indicated by the pH of extracellular and intraphagosomal *Z-cHOClate.* Cells were then washed and incubated in 100 mM UB4 buffer containing 140 mM NaCl, 10 mM KCl, 2.5 mM $CaCl_2$ pH 6. HOCl was added (1 nM - 100 μM) and covered with another coverslip immediately. The cells were imaged in the R, B and G channels at t = 0, 2, 3, 6,10, 15 and 20 minutes and R/B values were plotted against each HOCl concentration. The decrease in R/B signal of internalized *Z-cHOClate* as a function of time quantitatively recapitulates that of extracellular particles upon addition of a known concentration of HOCl to the solution, which also corresponds to the maximum amount of HOCl available in the solution during the experiment i.e, $[HOCl]_{max}$. The initial rate of change of probe signal reflects the rate of HOCl production by MPO and corresponds to a given phagosomal $[HOCl]_{max}$.

3.B.7: Inhibitor studies for in cellulo specificity of *Z-cHOClate*

All inhibitor treatments were performed in DMEM followed by pulsing with *Z-cHOClate* (~10^4 particles) for 10 minutes in DMEM containing 10% FBS and inhibitor of choice, washed, and imaged in fresh DMEM containing inhibitor for every 10 minutes. All steps prior to imaging were done at 37^{o}C, 5% CO_2. To evaluate *in cellulo* specificity, J774A.1

cells were treated with (i) 100 μM ABAH for 3 h for MPO inhibition, (ii) 20 μM DPI for 30 minutes for NOX2 inhibition, (iii) 200 nM 1400W for 1 h for iNOS inhibition and (iv) (20 – 100 μM) of NPPB for 1 h for chloride channel inhibition prior to Z- *cHOClate* pulse (Aiken et al., 2012; Cross, 1987; Garvey et al., 1997; Kettle et al., 1997). Untreated (UT) cells were prepared using the same percentage of DMSO as that of the inhibitor in each case.

3.B.8: Kinetics experiments with Z-*cHOClate* and Z-p*cHOClate*

For kinetics experiments J774A.1 cells pre-treated with or without 100μM ABAH for 3 hours were used. Cells were pulsed with Z-*cHOClate* or Z-p*cHOClate* for 5 minutes and phagocytosis was monitored in real time using fluorescence imaging.

3.B.9: Immunostaining

3.B.9a: Reagents and buffers

Synthesis of Z-R6G and characterization: 1 mg of Zymosan (2×10^7 particles) was stirred with 0.34 mg of $NaIO_4$ (2 nmol) in 80 μL of 50 mM sodium acetate buffer, pH 5, at 4°C in the dark for 16 h to oxidize 1,6-glucans on the surface. To quench unreacted $NaIO_4$, 4 μL ethylene glycol was added, stirred for 10 minutes, and centrifuged at 2500 rpm for 15 minutes at 4°C. Supernatant was removed without disturbing the pellet and replaced with N-(6-Aminohexyl) rhodamine 6G-amide bis(trifluoroacetate)(R6G) (1.3 μmol) in 100 mM borate buffer, pH 10 containing 20% DMSO. After stirring for 24h at RT in the dark, the supernatant was removed by centrifugation, and the Schiff base formed was stabilized by $NaBH_4$ (3 nmol) in deionized water. The R6G-functionalized Zymosan (R6G-Zym) was characterized by fluorescent imaging and used for immunostaining experiments.

Preparation of 4% paraformaldehyde: 10% paraformaldehyde (PFA, Sigma, USA) stock was prepared by dissolving PFA in 1X PBS by heating the solution at 60 °C with vigorous stirring. The solution was then cooled to room temperature, filtered through 0.22 µm filter (Millipore, Germany) and the aliquots were stored at -20°C. Before use, PFA was thawed at 60°C for 10 min and then dilute to 2.5 times using 1X PBS.

1X Phosphate buffered Saline (PBS): 137 mM NaCl, 2.7 mM KCl, 10mM Na_2HPO_4, 2mM KH_2PO_4, pH adjusted to 7.0 using 1N HCl. The buffers were then filter sterilized using 0.22 µm filter.

3% BSA: 3mg of BSA was dissolved in 100 µL of 1X PBS and vortexed for 5-10 minutes.

0.25 % Triton X100: 2.5 µL of Triton X-100 was added to 1mL of 1X PBS and vortexed for 5 minutes.

1º Antibody: Rabbit polyclonal anti-MPO antibody (Abcam Cat # ab 9535) was diluted to 1:200, using blocking buffer (0.3% BSA in PBS).

2º Antibody: Goat anti-rabbit secondary antibody conjugated with Alexa Fluor 647 was diluted to 1:1000, using blocking buffer (0.3% BSA in PBS).

3.B.9b: Immunostaining for MPO

For Immunostaining, J774A.1 Cells were plated on an imaging dish for overnight and pulsed with R6G-Z in DMEM (contains 10% FBS) for 15 minutes at 37ºC, 5% CO_2, washed with PBS, pH 7.4, and pulsed with DMEM (contains 10% FBS). The cells were then washed with PBS, pH 7.4, and fixed using 4% paraformaldehyde at RT for 20 mins. Subsequently, cells were permeabilized using 0.25% Triton X-100 and blocked using 3%

BSA in PBS. Cells were then incubated with rabbit polyclonal anti-MPO antibody (Abcam Cat # ab 9535, 1:200 dilution) in blocking buffer for 1 hour at RT (0.3% BSA in PBS). Cells were then washed for 5 minutes with PBS. Goat anti-rabbit secondary antibody conjugated with Alexa Fluor 647 (1:1000 dilution) was added to the cells and incubated for 1h at RT. Cells were washed again to remove excess secondary antibody using PBS for 5 minutes. DAPI (5 μM) was added 10 minutes prior to imaging to stain nuclear DNA in PBS, pH 6. Cell were then imaged on a Leica SP8 laser scanning confocal microscope (Leica Microsystems, Inc., Buffalo Grove, IL) using excitation wavelengths 405 nm (DAPI), 530 nm (R6G) and 650 nm (AlexaFluor 647). Images were processed using Fiji and maximum intensity projected images of Z-planes were presented. For quantification of MPO intensity, mean MPO intensity from 20 cells with or without Zym-R6G was considered.

3.B.10: Western Blot

3.B.10a: Reagents and buffers

Lysis buffer: RIPA buffer (radioimmunoprecipitation assay buffer) (RIPA buffer was premade and stored at 4^{o}C without protease inhibitor)

150 mM NaCl – 1.0%

1% Nonidet P-40 (NP-40)

0.1% SDS (sodium dodecyl sulphate)

50 mM Tris-HCl, pH 8.0

Protease inhibitors- 5 μL/500 μL- added at the time of experiment.

Loading buffer: 2x Laemmeli buffer (buffer was premade and stored at 4^{o}C)

4% SDS

10% 2-mercaptoethanol

20% glycerol

0.004% bromophenol blue

0.125 M Tris-HCl

Check the pH and adjust to 6.8

Running buffer (Tris-Glycine/SDS)

25 mM Tris base

190 mM glycine

0.1% SDS

Check the pH and adjust to 8.3

Transfer buffer (Make 10x and store in 4^{o}C)

25 mM Tris base

190 mM glycine

20% methanol

0.1% SDS

Check the pH and adjust to 8.3

Tris-buffered saline with Tween 20 (TBST) buffer

20mM Tris, pH 7.5

150 mM NaCl

0.1% Tween 20

Blocking Buffer

2.5 % milk in 1x TBST

1º Antibody: (i) Rabbit polyclonal anti-MPO antibody (Abcam Cat # ab 9535) was diluted to 1:500, using blocking buffer (2.5 % milk in 1x TBST).

(ii) Mouse monoclonal anti-actin antibody (Abcam Cat # ab 14128) was diluted to 1:2000, using blocking buffer (2.5 % milk in 1x TBST)

2º Antibody: HRP conjugated goat anti-rabbit antibody (Invitrogen G-21234) and anti-mouse antibody (Invitrogen G-21040) was diluted to 1:2000, using blocking buffer (2.5 % milk in 1x TBST)

3.B.10b: Western blot for MPO and actin

J774A.1 grown on a 60 mm dish were treated with zymosan particles and allowed to phagocytose for 30 minutes. As control, J774A.1 cells not treated with zymosan were used. Total protein was isolated following standard procedures and quantified using nanodrop. An aliquot (100 µg) of each lysate was subjected to 8% SDS-PAGE and transferred to nitrocellulose using standard protocol (Solutions and Reagents). The nitrocellulose membrane was incubated with a mixture of 1:500 dilution rabbit polyclonal

anti-MPO antibody (Abcam Cat # ab 9535) and 1:2000 dilution of mouse monoclonal anti-actin antibody (Abcam Cat # ab 14128) overnight at 4 °C. The membranes were washed and probed with a mixture of 1: 2000 dilution of HRP conjugated goat anti-rabbit antibody (Invitrogen G-21234) and anti-mouse antibody (Invitrogen G-21040) for 1 h at room temperature. The bands for MPO and actin were visualized by chemiluminescence using super signal II for western blot (Thermo Fisher Cat # 80844-07-1).

3.B.11: Fluorescence microscopy and image analysis

For imaging experiments, J774A.1 and RAW 264.7 cells were scraped and plated in 35 mm glass bottom dishes and kept overnight at 37^{o}C, 5% CO_2. SIM-A9 cells were detached using trypsin-EDTA and plated on 35 mm glass bottom dishes and kept overnight at 37^{o}C, 5% CO_2. Seeded density of cells were 60%.

3.B.11a: Fluorescence microscopy set up

Wide-field images of cell lines and primary cells with *Z-cHOClate* were acquired using IX83 inverted microscope (Olympus Corporation of the Americas, Center Valley, PA, USA) using a 60X, 1.42 NA, phase contrast oil immersion objective (PLAPON, Olympus Corporation of the Americas, Center Valley, PA, USA) and Evolve Delta 512 EMCCD camera (Photometrics, USA). Filter wheel, shutter and CCD camera were controlled by using MetaMorph software (Molecular Devices, PA). Atto-488 channel images (referred to as 'B') were acquired using 480/20 band pass excitation filter, 535/40 band pass emission filter and 86023bs-FITC/Cy5 as dichroic filter. Cy5 channel images (referred to as 'R') were obtained using 640/30 band pass excitation filter, 690/50 band pass emission filter and HQ665lp- long pass dichroic filter. R6G channel images (referred to as 'G') were

obtained using 530/30 band pass excitation filter, 575/40 band pass emission filter and 49014 mKO/mOrange- long pass dichroic filter.

3.B.11b: Image analysis

Image analysis was performed using ImageJ software (NIH). All images were subjected to background subtraction using a rolling ball method with a radius of 12 pixels. For kinetics analysis, only Z-*cHOClate* showing uptake in the DIC channel were considered. For all steady state images, phagosomes of acidic pH ~ 6, i.e., G/B value between 1.5 to 2.5 were considered for HOCl calculations. Data is represented as SEM of three independent replicates.

3.B.12: Statistics

In vitro fluorescence experiments of *cHOClate* for HOCl sensing, pH sensing and specificity were done in 3 independent replicates on three different days and data is presented as mean and error bars represent SEM for indicated conditions. For *in cellulo* imaging of HOCl and pH we considered 50-100 phagosomes from each imaging dish. Three such experiments, performed on three different days for each experimental condition, i.e., inhibitor used, cell type used etc. The mean and the SEM of these three different experiments was then calculated and plotted.

3.C: Results and discussions

3.C.1: Surface functionalization of Zymosan with DNA sensors

In order to target *cHOClate* to the phagosome we sought to conjugate it to zymosan particles that are a well-documented phagocytic cargo (Underhill, 2003). Zymosan is a cell wall preparation of heat-inactivated yeast, *S. Cerevisiae*. Because the surface of

zymosan particles are rich in β-1,3- and β-1,6-glucans, we could functionalize the surface of zymosan with azide groups by periodate oxidation of β-1,6- glucan as described in section 3.B.1 (Ohno et al., 1999). These surface-modified zymosan particles which display azido groups (Zym-N_3), could be subsequently conjugated with *cHOClate* using click chemistry (Figure 3.6). The resultant phagocytic particles were called Z-*cHOClate*, which are phagosome targetable *cHOClate*.

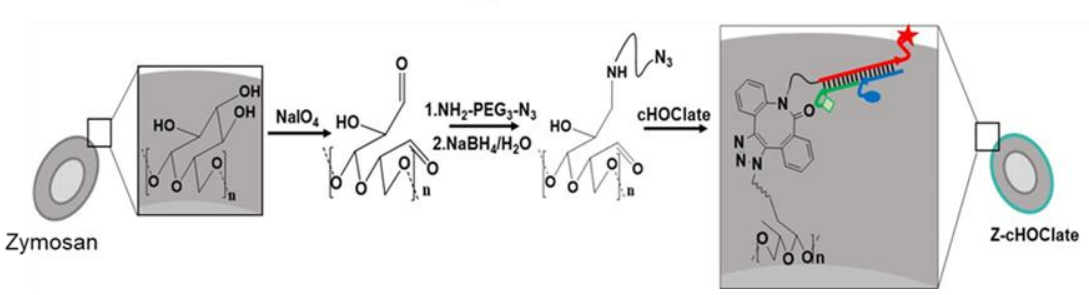

Figure 3.6: Surface functionalization of zymosan with *cHOClate*

Z-*cHOClate* were characterized using fluorescence imaging and flow cytometry. Fluorescence imaging revealed that this procedure resulted in functionalization of zymosan specifically at the surface and no internalization of sensor noticed (Figure 3.7). This procedure yielded surface labeling of ~98% of the particles while maintaining a 1:1 ratio between the fluorophores as observed by Flow cytometry (Figure 3. 1; Figure 3.7a and Figure 3.8b). Further, forward scattering in Blue, green and red channels showed the heterogeneity in size is similarly maintained in all the fluorophores (Figure 3.8a). Using small molecule cleavage assay and knowing the concentrations of recovered *cHOClate* we calculated that average molecules of *cHOClate* on Zymosan is ~10^6 (Section 3.B.3). The FRET between fluorophores on the Z-*cHOClate* was checked by cross excitation and emission in all channels, and we observed negligible FRET between fluorophores (Table 3. 1).

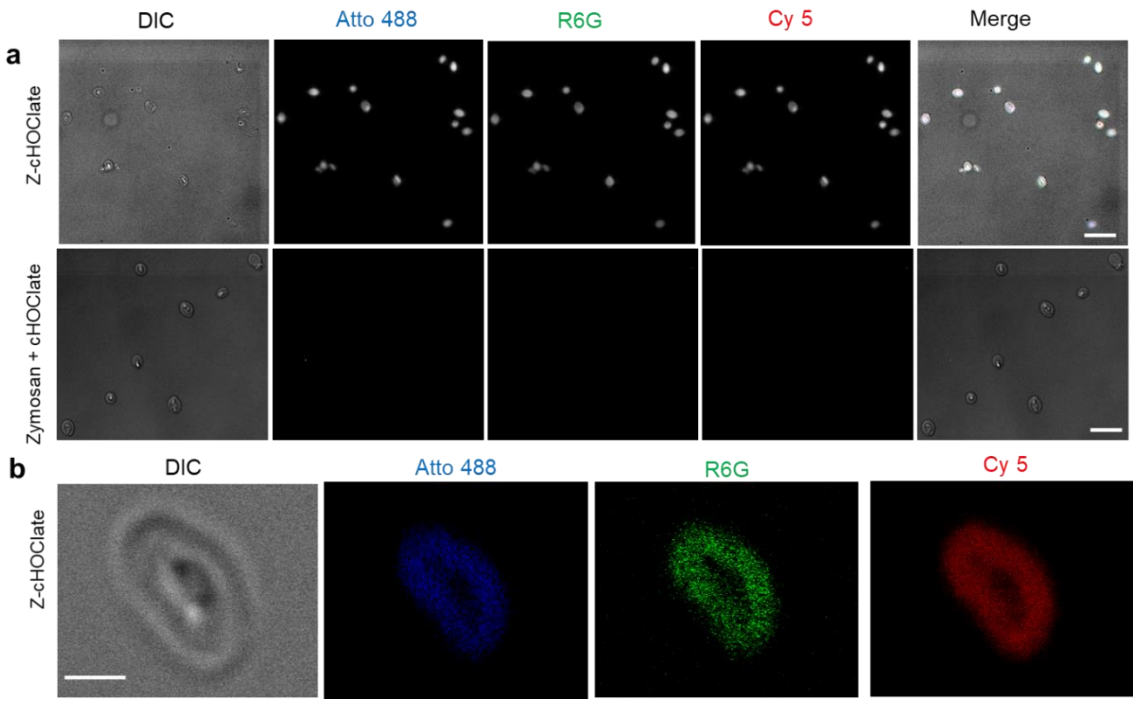

Figure 3. 7: **Surface functionalized of zymosan with *cHOClate, Z-cHOClate.*** a) Low resolution images of *Z-cHOClate* (Zym-N_3 incubated with *cHOClate*) in DIC, blue, green, red and merge with DIC channels showing successful functionalization of zymosan(top), nonfunctionalized zymosan incubated with *cHOClate* under same conditions (bottom) as a control, scale bar= 10 μm. b) High-resolution images of Z-*cHOClate* in respective channels showing that *cHOClate* is indeed at the surface of zymosan in Z-*cHOClate*, scale bar= 2 μm.

λ_{em} / λ_{ex}	Atto 488	R6G	1
Atto 488	3209±355	184±43	10±2
R6G		2790±235	39±4
1	11±0.7	17±1	1661±180

Table 3.1: Fluorescence intensities of *Z-cHOClate* by direct and cross excitation: Absolute fluorescence emission intensities of *Z-cHOClate* particles in each emission channel upon excitation in the indicated excitation channel (n= 50 particles). Blue boxes show direct excitation, yellow boxes show FRET excitation, white boxes show filter bleed through levels, grey box indicates that this excitation-emission is irrelevant (Ex= 530/30X. Em=540/40M), Representative data from three independent experiments are shown; error values, SEM; measure of center, mean.

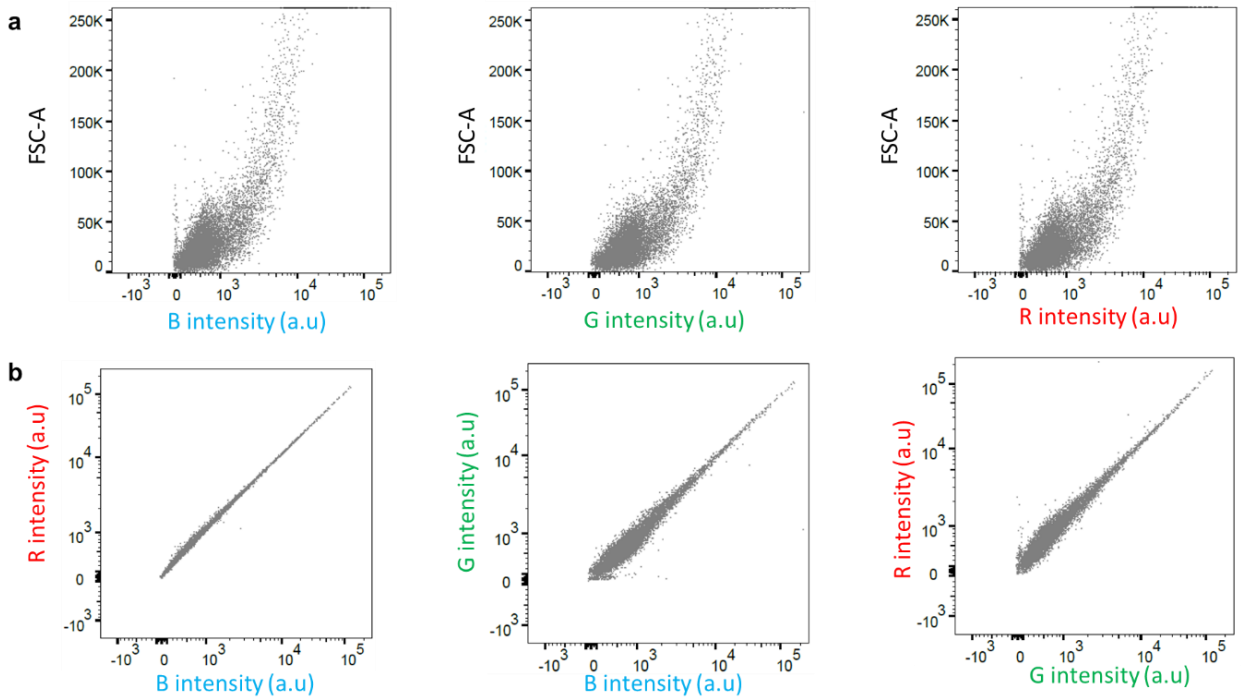

Figure 3.8: Characterization of Z-*cHOClate* using flow cytometry. a) Forward scatter versus intensity in Alexa488 (B), R6G (G) and 1 (R) channels for Z-*cHOClate* showing the heterogeneity in size for Z-*cHOClate*. b) Correlation of intensities between two channels (Red Vs Blue; Green Vs Blue and Red Vs Green) represent 1:1 labeling efficiency in Z-*cHOClate*. n=20000 particles, pH 7, 1x PBS.

3.C.2: Stability of DNA sensors in phagosome

Before using Z-*cHOClate* for investigating HOCl production we checked the stability of DNA sensors in phagosomes. For this we used a similar approach as we used in the in vitro experiments in section 2. C.6, where decrease in EtBr fluorescence intensity will indicate the perturbation in DNA duplex. Z-*pcHOClate* was prepared as described for Z-*cHOClate* using click chemistry (section 3.B.1) (Figure 3.9a-b). Z-*pcHOClate* was pulsed in J774A.1 cells and intensity in the EtBr channels was followed as a function of time for 1 hr. The EtBr intensity of internalized particles was normalized to the intensity of

uninternalized particles in the same images and plotted as a function of time. Values at each time point are normalized to the particle intensity at t = 0, (Figure 3.9c-d). There is no significant change in EtBr intensity in phagocytosed *Z-pcHOClate* which indicates that the reporter integrity is maintained at least for ~1 hour in phagosomes. Thus Z-*cHOClate* is a reliable ratiometric reporter for phagosomal HOCl at least up to ~1 h.

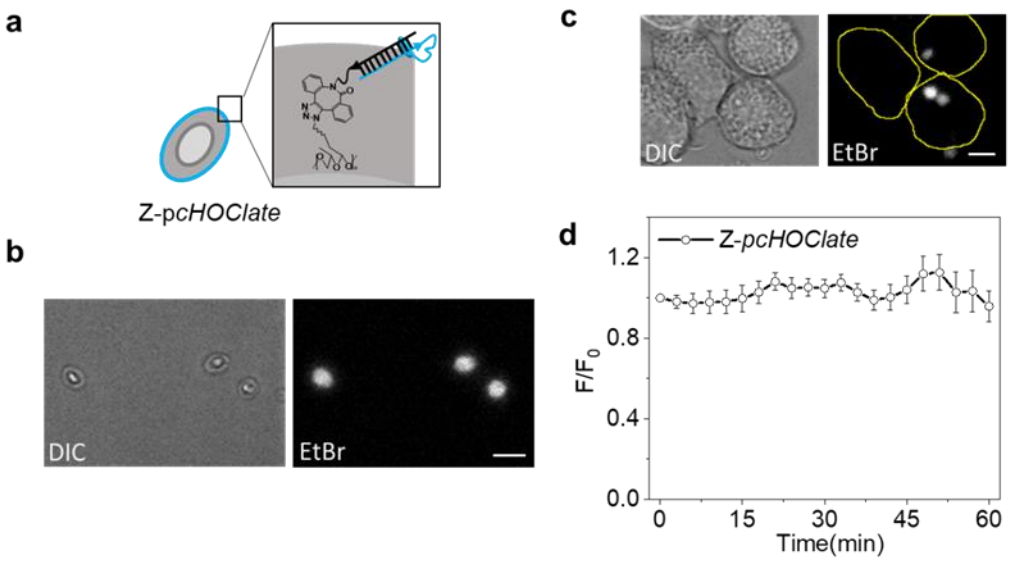

Figure 3.9: In cellulo stability of *cHOClate* in phagosomes. a) Schematic showing Z-p*cHOClate*. b) Images of Z-p*cHOClate* in DIC and EtBr channels, scale bar = 10 μm. c) Representative steady state images of Z-p*cHOClate* in J774A.1 cells. d) Normalized intensity of EtBr(F/F0) of Z-*pcHOClate* which was phagocytosed by J774 cells, n= 50 particles.

3.C.3: Sensing characteristics of Z-*cHOClate*

The response characteristics of Z-*cHOClate* was evaluated *in vitro* and *in cellulo* by fluorescence imaging at various concentrations of HOCl and solution pH. Fluorescence imaging of Z-*cHOClate* with varying pH and HOCl on a glass slide as well as in clamped

phagosome showed that, *cHOClate* in fact maintains its functionality after conjugation to the zymosan surface.

3.C.3a: pH sensing by Z-*cHOClate in vitro* and *in cellulo*

First, the pH response of Z-*cHOClate* was evaluated by incubation in solutions of different pH as described in section 3.B.5, followed by fluorescence imaging in the Alexa488, R6G and 1 channel. The ratio of R/B and G/B the particles as a function of pH revealed 6-fold increase in G/B from extracellular pH (7.4) to mature phagosomal pH (4.5) while R/B remains unaffected (Figure 3.10a-b). This indicate that the pH sensing modules of *cHOClate* is functional after conjugation to the surface of zymosan.

Next, I checked if pH sensing module of Z-*cHOClate* is functioning in the phagosomes. To test this, Z-*cHOClate* were allowed to phagocyte by murine macrophage cell line J774A.1 cells. Cells were fixed and permeabilized, and extracellular pH was changed. The G/B of the particles inside and outside were plotted as a function of pH (Figure 3.10c-d). Z-*cHOClate* respond to the pH changes in the clamped phagosomes similar to its response to solution pH's indicating pH responsive module in Z-*cHOClate* is functional in a phagosome (Figure 3.10d).

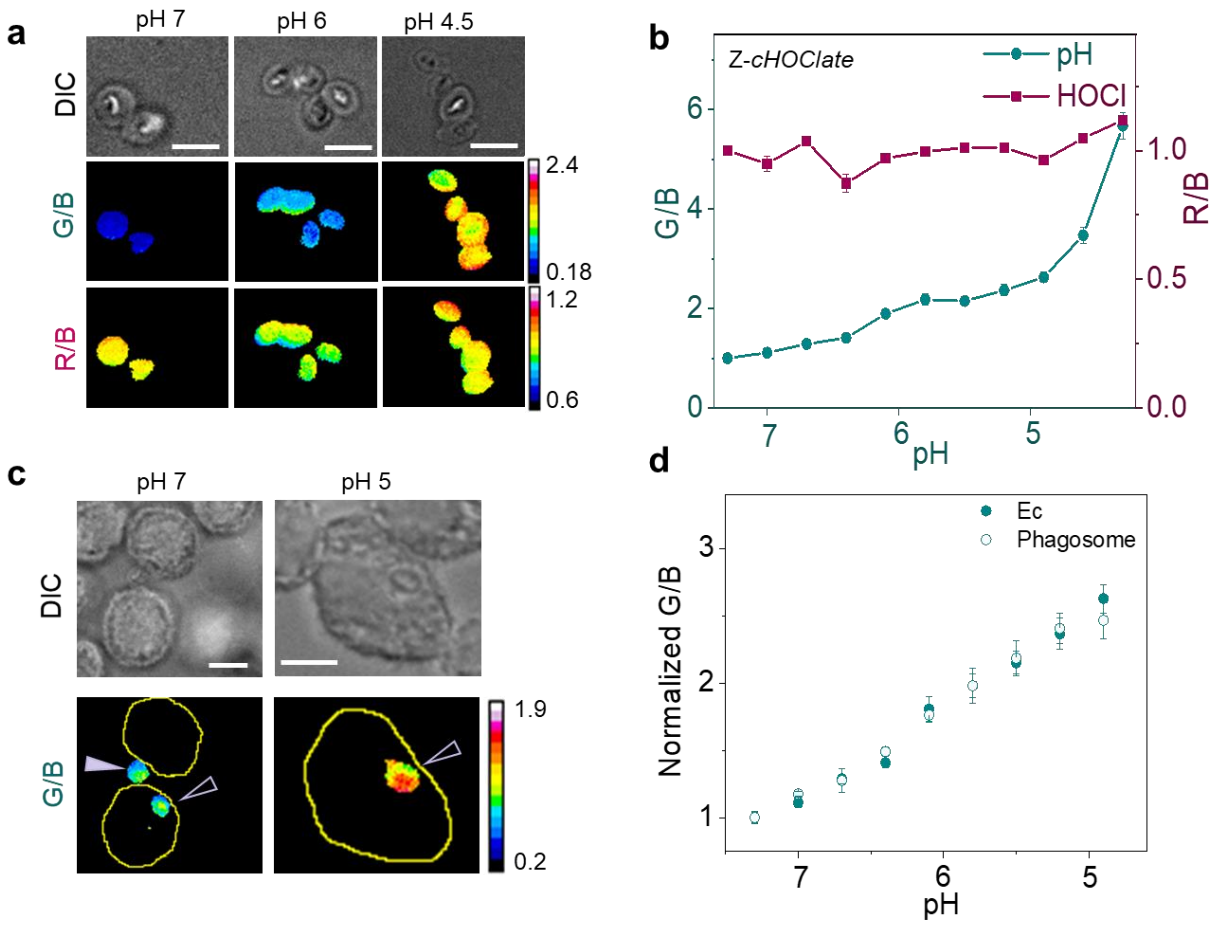

Figure 3.10: pH sensitivity of Z-*cHOClate*. a) Fluorescence imaging of Z-*cHOClate* showing increasing G/B and constant R/B with acidification, scale bar = 10 μm, representative data from three independent experiments are shown. b) Normalized G/B and R/B for Z-*cHOClate* from pH 7.4 to pH 4.3, n ≥ 150 particles. Representative data from three independent experiments are shown. c) Representative steady state images of Z-*cHOClate* clamped at pH 7 and 5 in J774A.1 cells, DIC and heat maps in G/B channel are shown, filled purple arrow indicate extracellular Z-*cHOClate* while open purple arrow indicate phagosomal Z-*cHOClate,* scale bar = 10 μm. d) G/B values of Z-*cHOClate* inside pH-clamped phagosomes (open circles) compared with G/B values of uninternalized Z-

cHOClate particles (filled circles) at the same pH in external pH clamping buffer, under identical microscope settings, n= 68 particles.

3.C.3b: HOCl sensing by Z-*cHOClate in vitro* and *in cellulo*

HOCl sensing characteristics of Z-*cHOClate* in vitro and in phagosomes were evaluated as described for pH. In vitro experiments with increasing concentrations of HOCl from 0-20 μM revealed that R/B ratio underwent a 100-fold decrease, while the G/B ratio was unaffected (Figure 3.11a). Thus Z-*cHOClate* is able to report on pH as well as HOCl such that neither sensing module interferes with the other and each module quantitatively retains its sensing characteristics.

The performance of HOCl sensing module of Z-*cHOClate* in the phagosomes was tested by in cellulo clamping experiments as described in section 3. B.6. J774A.1 were allowed to phagocyte Z-*cHOClate* and were permeabilized using Methanol. This results in permeabilization of plasma membranes as well as phagosomal membranes as indicated by the pH of extracellular and intraphagosomal Z-*cHOClate* (Figure 3.11b). Cells were incubated with various concentration of HOCl and imaged in the R, B and G channels at t = 0, 2, 3, 6, 10, 15 and 20 minutes; R/B values were plotted against time. The decrease in R/B signal of internalized Z-*cHOClate* as a function of time quantitatively recapitulates that of extracellular particles upon addition of a known concentration of HOCl to the solution, which also corresponds to the maximum amount of HOCl available in the solution during the experiment i.e, $[HOCl]_{max}$. This indicate that cellular membranes are effectively permeabilized, as the change in probe signal reveals that the levels of extracellular and phagosomal HOCl were comparable (Figure 3.11c-d). The steady state R/B values plotted against available [HOCl] indicate quantitative sensing by Z-*cHOClate*

in the phagosome in the range of 1-100 μM (Figure 3.11d). This range can be tuned by changing the sensor density on the particle surface.

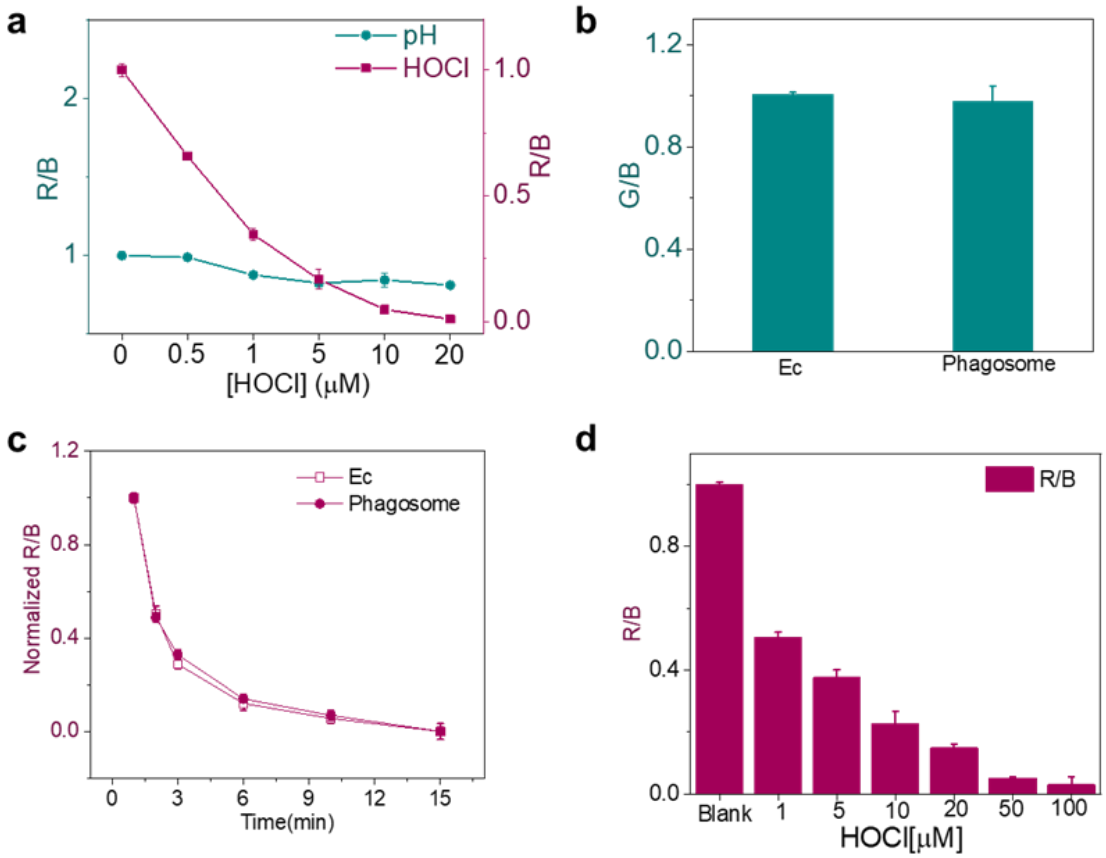

Figure 3.11: HOCl sensitivity of Z-*cHOClate*. a) G/B and R/B ratios of Z-*cHOClate* as a function of indicated concentrations of HOCl G/B, n=50 particles. b) G/B values of extracellular and phagosomal Z-*cHOClate* indicates that phagosomes are clamped at pH 6, n=16 particles or phagosomes. c) Change in Normalized R/B of Z-*cHOClate* in the clamped phagosome with addition of HOCl (50 μM), extracellular Z-*cHOClate* (open square) and phagosomal Z-*cHOClate* (filled circle) shows similar kinetics of HOCl sensing indicating clamping with respect to HOCl, n= 22 particles or phagosomes. d) R/B of Z-*cHOClate* with various added concentrations of HOCl after 20 minutes of incubation at pH 6, UB4 buffer, 100 mM, n=50 phagosomes, representative data from three-

independent experiments are shown in a, b and c and d; error bars, SEM; measure of center, mean.

3.C.4: Z-*cHOClate* senses pH and HOCl specifically in live macrophages

We then measured the HOCl levels given by the R/B ratio of phagocytosed Z-*cHOClate* in mature phagosomes as the latter are easily identified by their G/B value. MPO produces HOCl using both H_2O_2 and Cl^- as substrates. The former is derived due to the activity of NOX2 and the latter is derived from phagosome-resident channels and transporters, or when the chloride-rich lysosome fuses with the phagosome (Di et al., 2006). We chose the murine macrophage cell line J774A.1 due to its well-described propensity to phagocytose a variety of micron-sized particles, especially zymosan (Champion et al., 2008; Nicolete et al., 2011; Underhill, 2003). J774A.1 cells phagocytosed Z-*cHOClate* as efficiently as zymosan indicating that *cHOClate* coating did not significantly perturb phagocytosis. Since previous reports provided evidence for phagosome maturation in macrophages and MPO activity in neutrophils well within 20 minutes post phagocytosis, we limited our investigations to under 30 minutes post phagocytosis (Canton et al., 2014; Kenmoku et al., 2007).

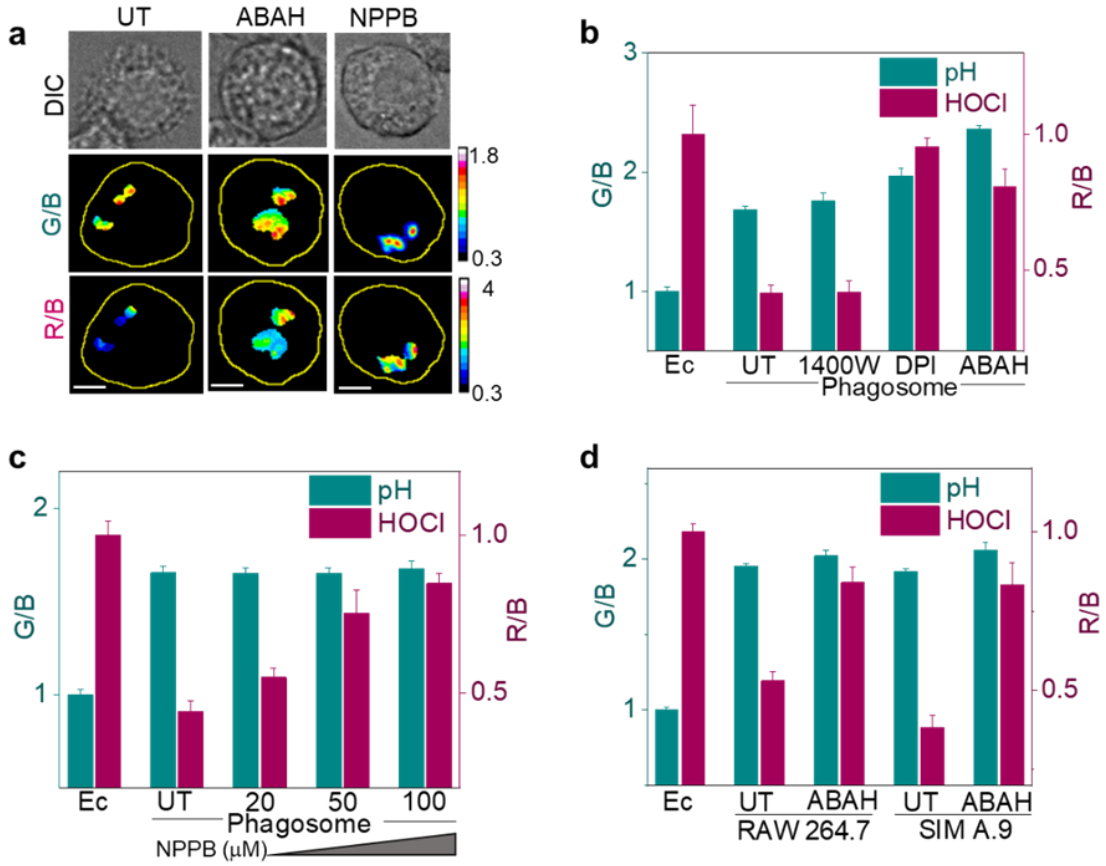

Figure 3.12: Z-*cHOClate* senses pH and HOCl in live macrophages. a) Representative images of Z-*cHOClate* in J774A.1 cells at t = 20 minutes post internalization in presence of the indicated pharmacological inhibitors, scale bar = 10 μm, representative data from three independent experiments are shown. b & c) G/B and R/B ratios from n ≥ 150 phagosomes imaged as in (a) in the presence of the indicated inhibitors. UT= untreated cells Ec = extracellular or uninternalized particles. d) G/B and R/B ratios in RAW264.7 cell lines and SIMA.9 cell lines.

In mature phagosomes of J774A.1 cells treated with a specific inhibitor of iNOS 1400W, we observed that both R/B and G/B values were similar to those of untreated cells (Figure 3.12b). This revealed that reactive nitrogen species such as NO were not responsible for the photophysical changes undergone by Z-*cHOClate* in the phagosome. Upon treatment

with DPI, a NOX2 inhibitor or ABAH, an MPO inhibitor, the G/B value in the phagosome was similar to untreated cells, indicating that the phagosome acidified normally (Figure 3.12a-b). However, the R/B value was comparable to uninternalized Z-*cHOClate* (Figure 3.12b), indicating that the reactive species resulting from NOX2 activity or MPO activity were the entities being sensed by Z-*cHOClate*. In order to confirm that Z-*cHOClate* reports on HOCl as a result of MPO activity, we also treated cells with increasing amounts of NPPB, a pan chloride channel blocker, expected to decrease lumenal Cl^- levels in all endocytic organelles including the phagosome (Aiken et al., 2012). Accordingly, we found that although phagosomal acidification occurred normally as revealed by the G/B ratio, the R/B ratio showed a dose-dependent increase, confirming specific detection of HOCl due to MPO activity within the phagosome (Figure 3.12a and 12c). We could similarly map phagosomal HOCl in other mouse macrophage cell lines like RAW264.7 and SIM-A9 (Figure 3.12d).

3.C.5: Z-*cHOClate* maps pH and HOCl kinetics during phagosome maturation

Next, we sought to map phagosomal HOCl production in concert with phagosomal acidification using Z-*cHOClate* in live cells. Figure 3.13a shows the pseudocolor maps of G/B (middle panel) and R/B (lower panel) values of J774A.1 cells that have just phagocytosed Z-*cHOClate*. The G/B ratio progresses from lower values (blue) to higher values (red) in line with phagosomal acidification. On the other hand, in the same phagosome, the R/B ratio progresses from higher values (red) to lower values (blue) indicating a progressive increase of HOCl within the phagosome (Figure 3.13a-b). The phagosome acidifies rapidly from 5 minutes onwards, reaching maximum acidity at ~12 minutes post internalization (Figure 3.13b). The maximum fold change in G/B observed

for phagocytosed Z-*cHOClate* revealed that the pH of mature phagosomes in J774A.1 cells was pH 6.0 (Figure 3.10d and Figure 3.13b). This is in very good agreement with other studies of phagosomal pH in macrophages.

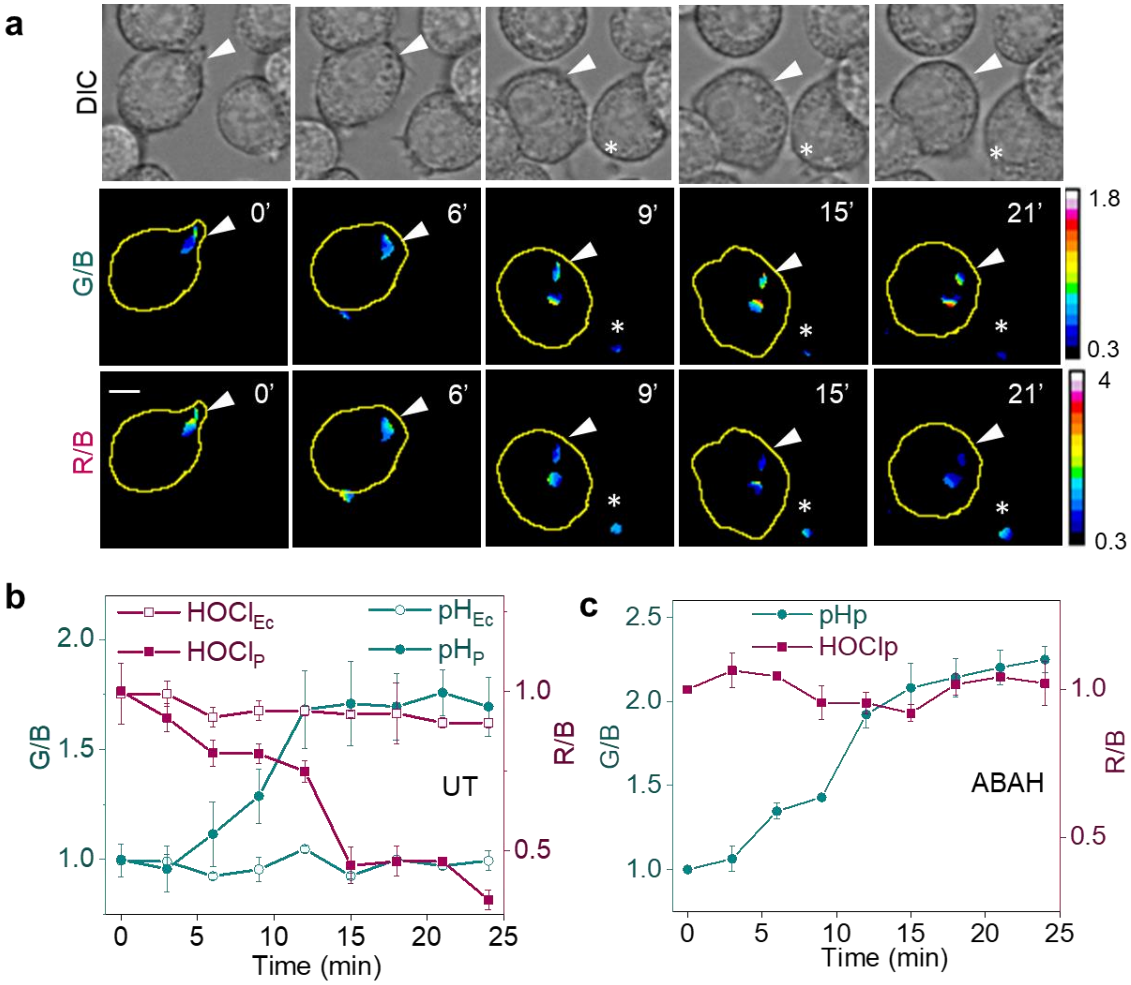

Figure 3.13: Z-*cHOClate* detect maps pH and HOCl during phagosome maturation. a) Representative images of acidification (G/B) in concert with HOCl production (R/B) reported by Z-*cHOClate* within the phagosome (white arrowhead) and extracellularly (white asterisk), scale bar = 10 μm, representative data from three independent experiments are shown. b) G/B and R/B ratios from n= 50 phagosomes as a function of phagosome maturation. Ec=extracellular or uninternalized particles p= phagocytosed-

particles. c) G/B and R/B ratios from n= 50 phagosomes as a function of phagosome maturation in presence of 100 mM ABAH. Representative data from three independent experiments are shown in b and c; error bars, SEM; measure of center, mean.

Phagosomal HOCl, on the other hand, developed very slowly over the first ~8 minutes, reflected in the slow decrease in R/B signal, and, after a critical level of acidification was reached, there was a burst of HOCl reflected by a sharp decay in the R/B ratio that occurred over 3 minutes (t = 12-15 minutes) (Figure 3.13a-b). Cells treated with ABAH showed normal acidification of phagosome and no change in the R/B signal over this duration (Figure 3.13c) reaffirming that Z-*cHOClate* indeed reported on HOCl production. Further, R/B and G/B values of extracellular Z-*cHOClate* particles remain unaffected during the time course of the experiment, revealing that any signal change due to photobleaching is negligible in the time window investigated (Figure 3.13b).

3.C.6: Macrophages upregulates MPO levels upon phagocytosis

Inflammatory diseases such as multiple sclerosis and atherosclerosis are characterized both by high MPO levels as well as an abundance of activated macrophages. To date, MPO in these contexts is considered to be largely derived from neutrophils and the role of macrophage-derived MPO has not yet been addressed. Furthermore, previous studies on mouse macrophages have suggested that HOCl levels have been too low to detect due to poor MPO expression in these cells (Brennan et al., 2001; McMillen et al., 2005). However, given our findings that Z-*cHOClate* could detect MPO activity in mouse macrophage cell lines, we checked the MPO levels in these cells upon phagocytosis.

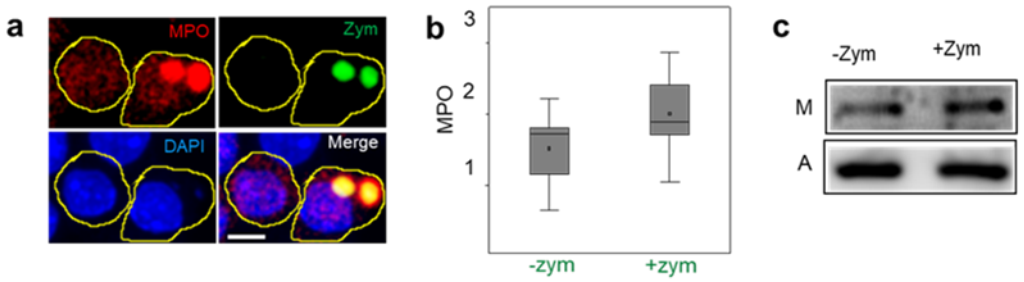

Figure 3.14: Macrophages upregulates MPO levels upon phagocytosis. a) Immunostaining for MPO (red) in J774A.1 cells phagocytosing R6G-zym (green). Nuclei are stained with DAPI, scale bar = 10 μm, representative data from three independent experiments are shown. b) Quantification of mean fluorescence intensity in MPO channel from a; -zym indicates cells which did not phagocytose any particle, while +zym indicates cells which phagocytosed zymosan particles, n= 35 cells. c) Western blot showing levels of MPO (M) from untreated and zymosan-treated J774.1 cells, with actin (A) as the loading control.

Using immunofluorescence, we found that J774A.1 upregulate of MPO levels upon phagocytosis and MPO was recruited to phagosomes (Figure 3.14a-b). These upregulation of MPO protein levels was further confirmed by western blot (Figure 3.14c). Together, this revealed that phagocytosis of zymosan by murine macrophage cell lines upregulates intracellular MPO, which roughly doubles the production of HOCl in the phagosome.

3.D: Conclusions

In summary, we have developed a phagosomal targetable sensor, *Z-cHOClate* for simultaneous mapping of pH and HOCl. *Z-cHOClate* was characterized for its surface labeling, surface density of sensor and its sensing properties. *Z-cHOClate* senses HOCl

and pH specifically in the phagosomes of live macrophages. Our studies reveal that in addition to acidifying the phagosome as well as delivering MPO, lysosome fusion likely elevates phagosomal chloride to the levels needed to efficiently produce HOCl. NPPB treatment reveals no alteration either in uptake or acidification within phagosomes. Recent studies support this conclusion where, defective pathogen clearance was observed in mouse macrophages lacking CLCN7, a CLC channel that mediates lysosomal chloride accumulation without affecting lysosomal pH (Wong et al., 2017). Taken together this suggests a role for lysosomal chloride in innate immunity, where it drives phagosomal MPO activity for pathogen degradation.

Z-cHOClate is generalized to sense pH and HOCl levels in variety of murine macrophage cell lines such as J774A.1, SIM A.9 and RAW264.7. Furthermore, there is an upregulation of MPO levels in the macrophages upon phagocytosis of zymosan which is resulted in its activity, as HOCl production. Thus, our studies have identified macrophages as a potential additional cellular source of MPO that could be involved in pathophysiology.

3.E: References

Aiken, M.L., Painter, R.G., Zhou, Y., and Wang, G. (2012). Chloride transport in functionally active phagosomes isolated from Human neutrophils. Free Radic. Biol. Med. *53*, 2308–2317.

Akira, S., Uematsu, S., and Takeuchi, O. (2006). Pathogen recognition and innate immunity. Cell *124*, 783–801.

Bianchi, M., Hakkim, A., Brinkmann, V., Siler, U., Seger, R.A., Zychlinsky, A., and Reichenbach, J. (2009). Restoration of NET formation by gene therapy in CGD controls aspergillosis. Blood *114*, 2619–2622.

Brennan, M.L., Anderson, M.M., Shih, D.M., Qu, X.D., Wang, X., Mehta, A.C., Lim, L.L., Shi, W., Hazen, S.L., Jacob, J.S., et al. (2001). Increased atherosclerosis in myeloperoxidase-deficient mice. J. Clin. Invest. *107*, 419–430.

Canton, J., Khezri, R., Glogauer, M., and Grinstein, S. (2014). Contrasting phagosome pH regulation and maturation in human M1 and M2 macrophages. Mol. Biol. Cell *25*, 3330–3341.

Champion, J.A., Walker, A., and Mitragotri, S. (2008). Role of particle size in phagocytosis of polymeric microspheres. Pharm. Res. *25*, 1815–1821.

Charles A Janeway, J., Travers, P., Walport, M., and Shlomchik, M.J. (2001). Pathogens have evolved various means of evading or subverting normal host defenses.

Corleis, B., Korbel, D., Wilson, R., Bylund, J., Chee, R., and Schaible, U.E. (2012). Escape of Mycobacterium tuberculosis from oxidative killing by neutrophils. Cell Microbiol. *14*, 1109–1121.

Cross, A.R. (1987). The inhibitory effects of some iodonium compounds on the superoxide generating system of neutrophils and their failure to inhibit diaphorase activity. Biochem. Pharmacol. *36*, 489–493.

Di, A., Brown, M.E., Deriy, L.V., Li, C., Szeto, F.L., Chen, Y., Huang, P., Tong, J., Naren, A.P., Bindokas, V., et al. (2006). CFTR regulates phagosome acidification in macrophages and alters bactericidal activity. Nat. Cell Biol. *8*, 933–944.

Garvey, E.P., Oplinger, J.A., Furfine, E.S., Kiff, R.J., Laszlo, F., Whittle, B.J., and Knowles, R.G. (1997). 1400W is a slow, tight binding, and highly selective inhibitor of inducible nitric-oxide synthase in vitro and in vivo. J. Biol. Chem. *272*, 4959–4963.

Hampton, M.B., Kettle, A.J., and Winterbourn, C.C. (1996). Involvement of superoxide and myeloperoxidase in oxygen-dependent killing of Staphylococcus aureus by neutrophils. Infect. Immun. *64*, 3512–3517.

Humphreys, J.M., Davies, B., Hart, C.A., and Edwards, S.W. (1989). Role of myeloperoxidase in the killing of Staphylococcus aureus by human neutrophils: studies with the myeloperoxidase inhibitor salicylhydroxamic acid. J. Gen. Microbiol. *135*, 1187–1193.

Huynh, K.K., Eskelinen, E.-L., Scott, C.C., Malevanets, A., Saftig, P., and Grinstein, S. (2007). LAMP proteins are required for fusion of lysosomes with phagosomes. EMBO J. *26*, 313–324.

Kenmoku, S., Urano, Y., Kojima, H., and Nagano, T. (2007). Development of a highly specific rhodamine-based fluorescence probe for hypochlorous acid and its application to real-time imaging of phagocytosis. J. Am. Chem. Soc. *129*, 7313–7318.

Kettle, A.J., Gedye, C.A., and Winterbourn, C.C. (1997). Mechanism of inactivation of myeloperoxidase by 4-aminobenzoic acid hydrazide. Biochem. J. *321 (Pt 2)*, 503–508.

Lukacs, G.L., Rotstein, O.D., and Grinstein, S. (1990). Phagosomal acidification is mediated by a vacuolar-type H(+)-ATPase in murine macrophages. J. Biol. Chem. *265*, 21099–21107.

Mahajan, A., Herrmann, M., and Muñoz, L.E. (2016). Clearance deficiency and cell death pathways: A model for the pathogenesis of SLE. Front. Immunol. *7*, 35.

McMillen, T.S., Heinecke, J.W., and LeBoeuf, R.C. (2005). Expression of human myeloperoxidase by macrophages promotes atherosclerosis in mice. Circulation *111*, 2798–2804.

Mogensen, T.H. (2009). Pathogen recognition and inflammatory signaling in innate immune defenses. Clin. Microbiol. Rev. *22*, 240–73, Table of Contents.

Nicolete, R., dos Santos, D.F., and Faccioli, L.H. (2011). The uptake of PLGA micro or nanoparticles by macrophages provokes distinct in vitro inflammatory response. Int. Immunopharmacol. *11*, 1557–1563.

Nüsse, O. (2011). Biochemistry of the phagosome: the challenge to study a transient organelle. ScientificWorldJournal *11*, 2364–2381.

Ohno, N., Miura, T., Miura, N.N., Chiba, N., Uchiyama, M., Adachi, Y., and Yadomae, T. (1999). Inflammatory and immunopharmacological activities of meta-periodate oxidized zymosan. Zentralbl. Bakteriol. *289*, 63–77.

Pauwels, A.-M., Trost, M., Beyaert, R., and Hoffmann, E. (2017). Patterns, receptors, and signals: regulation of phagosome maturation. Trends Immunol. *38*, 407–422.

Queval, C.J., Song, O.-R., Carralot, J.-P., Saliou, J.-M., Bongiovanni, A., Deloison, G., Deboosère, N., Jouny, S., Iantomasi, R., Delorme, V., et al. (2017). Mycobacterium tuberculosis Controls Phagosomal Acidification by Targeting CISH-Mediated Signaling. Cell Rep. *20*, 3188–3198.

Robinson, J.M. (2008). Reactive oxygen species in phagocytic leukocytes. Histochem. Cell Biol. *130*, 281–297.

Solutions, K., and Reagents General Protocol for Western Blotting.

Spickett, C.M., Jerlich, A., Panasenko, O.M., Arnhold, J., Pitt, A.R., Stelmaszyńska, T., and Schaur, R.J. (2000). The reactions of hypochlorous acid, the reactive oxygen species produced by myeloperoxidase, with lipids. Acta Biochim. Pol. *47*, 889–899.

Underhill, D.M. (2003). Macrophage recognition of zymosan particles. J Endotoxin Res *9*, 176–180.

Vowells, S.J., Sekhsaria, S., Malech, H.L., Shalit, M., and Fleisher, T.A. (1995). Flow cytometric analysis of the granulocyte respiratory burst: a comparison study of fluorescent probes. J. Immunol. Methods *178*, 89–97.

Winterbourn, C.C., and Kettle, A.J. (2013). Redox reactions and microbial killing in the neutrophil phagosome. Antioxid. Redox Signal. *18*, 642–660.

Wong, C.-O., Gregory, S., Hu, H., Chao, Y., Sepúlveda, V.E., He, Y., Li-Kroeger, D., Goldman, W.E., Bellen, H.J., and Venkatachalam, K. (2017). Lysosomal degradation is

required for sustained phagocytosis of bacteria by macrophages. Cell Host Microbe *21*, 719–730.e6.

Chapter 4

Z-cHOClate detects differential MPO levels in innate immune cells

4.A: Introduction

MPO derived products are detected in inflammatory diseases like atherosclerosis, renal ischemia reperfusion and multiple sclerosis etc (Aratani, 2018; Lau and Baldus, 2006). In most of these conditions MPO is thought to be derived from neutrophils because MPO expression in neutrophils are 5% of their protein dry weight. The source of active MPO in these diseases has to be reconsidered since inflammatory diseases are characterized by high level of macrophage recruitment and plaque formation (Moore et al., 2013). The role of macrophages derived MPO is under looked in inflammatory disease. Live imaging on the early stages of this MPO derived chlorinated species or HOCl with time will clarify the exact source of MPO in various inflammatory diseases.

There is a differential expression of redox enzymes in innate immune cells which are responsible for the ROS production. MPO expression levels in innate immune cells follows the order Neutrophils> monocytes> macrophages (Klebanoff, 2005). The differentiation process of monocytes to macrophages are reported to get rid of MPO expression and there is no or very little MPO in the tissue resident macrophages. Further the sensitivity of the reporting systems should be high enough to sense macrophage MPO activity. Also, there is no investigations on the macrophage derived MPO activity in inflammatory diseases using mouse models due to the long-standing notion that mouse macrophages in the atherosclerotic plaques MPO activity. For these reasons transgenic

mice with human MPO (hMPO) macrophages were used to study atherosclerosis (Shepherd et al., 2007).

Detection of MPO activity in macrophages cell lines has led us to check the activity of MPO in various innate immune cells. We used *Z-cHOClate* to detect the differential MPO activity in human innate immune cells. Further, we checked if we could access the differentially expressed MPO levels in human as well as mice derived macrophages. Chapter 4 describes these results from primary human and mouse innate immune cells using *Z-cHOClate*.

4.B: Materials and methods

4.B.1: Isolation of human monocytes and neutrophils

Human peripheral blood was obtained from healthy volunteers following obtaining a written consent in compliances with ethical regulations approved by the University of Chicago Institutional Review Board (IRB16-0321). Blood was collected in EDTA coated blood collection tubes, and Ficoll Paque Plus was used differential centrifugation.

15ml of human blood was mixed with 15ml of HBSS without Ca^{2+} and Mg^{2+} (HyClone), and add on the top of the leuocosep centrifuge tubes (VWR), which contains 15ml of Ficoll Paque Plus (GE Healthcare) on the bottom. Centrifuge at 800g at RT for 15 mins without the break. Mononuclear cells were contained in the buffy coat layer and Neutrophils were contained in the bottom layer.

4.B.1a: Isolation of Human Peripheral Blood Monocytes: For monocyte isolation, upper plasma layer was removed and the buffy coat was collected in a 15 mL tube. Monocytes were enriched using anti-CD14 antibody treatment and repeated washes.

Cells were subjected to flow cytometry to check the purity of preparation. The purity of isolation was analyzed using flow cytometry. Trypan blue staining was used to detect the population of live single cells. Flow cytometry using CD14 antibody was used to analyse the percentage of CD14 monocytes in the prep after magnetic bead mediated enrichment.

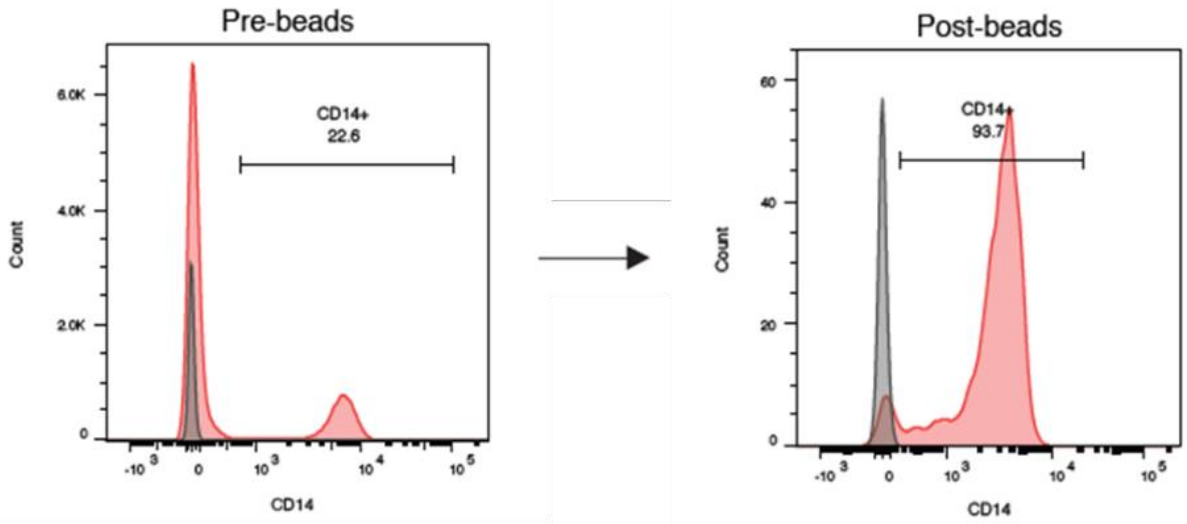

Figure 4.1: Purity of monocytes isolation. Flow cytometry traces showing purity of monocyte preparation using antibody enrichment method. The trace son left shows monocyte population in the prep using CD14 antibody (<25%) while after antibody enrichment the prep contains >90% monocytes.

4.B.1b: Isolation of Human Peripheral Blood Neutrophils: The bottom granulocytes and RBC layer in each tube was separated into three new 50ml tubes (Fisher). 40ml of room temperature 1XRBC lysis buffer was added to each tube and incubate for 10mins. Centrifuge at 500g for 5mins with break, and repeat the RBC lysis buffer step until there were no visual red blood cells. Washed cells twice with DMEM phenol red free serum free media containing sodium pyruvate (HyClone) before plating. After counting cells, plated

the cells in imaging dishes at 1 million cells/600ul density in DMEM phenol red free serum free media containing sodium pyruvate (HyClone) and waited for 30 minutes before experiments.

The purity of neutrophil isolation was analysed by flow cytometry using CD14 and CD16 antibodies and presented in figure 4.2a.

4.B.2: Differentiation of human monocytes to macrophages (HMDMs)

Monocytes was plated on imaging dishes in DMEM containing no FBS and treated with human M-CSF (125 ng/mL) for 7 days in culture. DMEM containing human M-CSF was changed every alternative day. On the 7^{th} day media was replaced with fresh DMEM and used for experiments. For LPS activation, cells were treated with 20 ng/mL of LPS for the last 24 hours.

4.B.3: Isolation and differentiation of mouse monocytes (BMDMs)

Male C57BL/6J with $MPO^{+/+}$and $MPO^{-/-}$(#000664 and #004265) were purchased from Jackson laboratories (Brennan et al., 2001). All animal studies are in compliances with ethical regulations approved by the University of Chicago Institutional Animal Care and Use Committee (ACUP 72209).

To prepare Bone Marrow Derived Macrophages (BMDMs), myeloid cells were isolated from femurs and tibia of WT and MPO KO mice as described (Becker et al., 2012). Cells were differentiated to macrophages using murine L-cell conditioned media 6 days. For LPS activation, cells were treated with 5 ng/mL LPS for 24 hours. Prior to pulse/chase experiments media was replaced with fresh RPMI.

4.B.4: Isolation of mouse primary macrophages

4.B.4a: Adipose tissue macrophages

Mouse adipose tissue macrophages (ATM) were isolated from mammary tissue of WT mice as described (Kratz et al., 2014). Cells were counted using a hemocytometer, plated on glass bottom imaging dishes, and allowed to adhere for 2-3 hours prior to pulse/chase experiments.

4.B.4b: Peritoneal macrophages

To isolate peritoneal macrophages (PM), WT mice were injected with thioglycollate and cells were harvested from the peritoneal cavity 5 days after injection (Zhang et al., 2008). The cells were washed with phosphate-buffered saline (PBS), plated, and allowed to adhere to glass bottom imaging dishes at 37^{o}C for 2 h in serum-free DMEM. Cells were then washed with PBS to remove non-adherent cells and used for pulse/chase experiments with Z-*cHOClate*.

4.B.5: Opsonization of Z-*cHOClate*

Opsonization of Z-*cHOClate* was done using human IgG. Approximately 1* 10^{6} particles of Z-*cHOClate* were incubated with 6 mM of IgG for 1 hour at 37^{o}C on a shaker incubator and 16 hours at 4^{o}C. The resultant particles were spin down at 5000 rpm at 4^{o}C, removed the supernatant and resuspended in DMEM containing no FBS.

4.B.6: pH and HOCl measurements

For kinetics experiments Neutrophils were plated for 30 minutes in the imaging dishes. Cells were pulsed with Z-*cHOClate* for 5 minutes and real time phagocytosis was monitored via fluorescence imaging.

Inhibitor treatments were performed in DMEM followed by pulsing with Z-*cHOClate* (~10^4 particles) for 10 minutes in DMEM containing 10% FBS and inhibitor of choice, washed, and imaged in fresh DMEM containing inhibitor for every 10 minutes. All steps prior to imaging were done at 37ºC, 5%CO_2. Cells were pre-treated with100 μM ABAH for 3 h for MPO inhibition. Untreated (UT) cells were prepared using the same percentage of DMSO.

4.B.7: Fluorescence microscopy and image analysis

For imaging experiments, Neutrophils and monocytes were plated in 35 mm glass bottom dishes and kept 30 minutes at 37ºC, 5% CO_2. Macrophages, differentiated for 7 days in the imaging dishes as described in 4.B.2 were used for the experiments. Opsonized Z-*cHOClate* was used for neutrophil kinetics experiments and for comparison of MPO activity between monocytes, macrophages and neutrophils. For checking activity LPS stimulated macrophages non-opsonized Z-*cHOClate* was used.

4.B.7a: Fluorescence microscopy set up

Wide-field images of primary cells with Z-*cHOClate* were acquired using IX83 inverted microscope (Olympus Corporation of the Americas, Center Valley, PA, USA) using a 60X, 1.42 NA, phase contrast oil immersion objective (PLAPON, Olympus Corporation of the Americas, Center Valley, PA, USA) and Evolve Delta 512 EMCCD camera (Photometrics, USA). Filter wheel, shutter and CCD camera were controlled by using MetaMorph software (Molecular Devices, PA). Atto-488 channel images (referred to as ‘B’) were acquired using 480/20 band pass excitation filter, 535/40 band pass emission filter and 86023bs-FITC/Cy5 as dichroic filter. Cy5 channel images (referred to as ‘R’) were

obtained using 640/30 band pass excitation filter, 690/50 band pass emission filter and HQ665lp- long pass dichroic filter. R6G channel images (referred to as 'G') were obtained using 530/30 band pass excitation filter, 575/40 band pass emission filter and 49014 mKO/mOrange- long pass dichroic filter.

4.B.7b: Image analysis

Image analysis was performed using ImageJ software (NIH). All images were subjected to background subtraction using a rolling ball method with a radius of 12 pixels. For kinetics analysis, only Z-*cHOClate* showing uptake in the DIC channel were considered. For all steady state images in the case of LPS activation experiments, phagosomes of acidic pH ~ 6, i.e., G/B value between 1.5 to 2.5 were considered for HOCl calculations. For all steady state images in the case of comparison between monocytes, neutrophils and monocyte derived macrophages there was no pH cut off considered. Data is represented as SEM of three independent replicates.

4.B.8: Immunostaining of Myeloperoxidase (MPO)

Immunostaining was done as described in section Chapter 3., Section 3. B.9b. LPS stimulated or non-stimulated BMDMs or HMDMs were used for immunostaining experiments. Cell were imaged on a Leica SP8 laser scanning confocal microscope (Leica Microsystems, Inc., Buffalo Grove, IL) using excitation wavelengths 405 nm (DAPI), 530 nm (R6G) and 650 nm (AlexaFluor 647). Images were processed using Fiji and maximum intensity projected images of Z-planes were presented. For quantification of MPO intensity, mean MPO intensity from 20 cells with or without Zym-R6G was considered.

4.C: Results and discussions

4.C.1: Z-*cHOClate* maps HOCl production in neutrophils

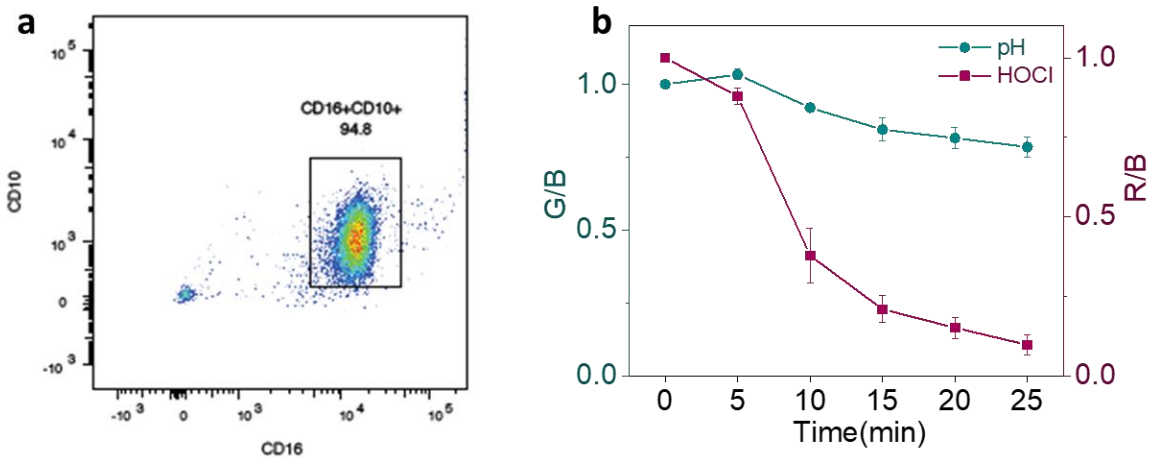

Figure 4.2: Z-*cHOClate* maps HOCl production in neutrophils. a) Flow cytometry characterization of neutrophils isolation purity sing CD10 and CD16 antibodies, the sample contains >90% pure neutrophils. b) G/B and R/B values from phagosomes of neutrophils as a function of time. Number of phagosomes considered = 25 phagosomes.

Myeloperoxidase comprises nearly 5% of total protein in neutrophils. We used Z-*cHOClate* to map phagosomal pH and HOCl kinetics in human neutrophils as a function of phagocytosis. Neutrophils were isolated using density gradient method and the purity of isolation was determined using flow cytometry (Figure 4.2a). In order to enhance phagocytosis in neutrophils, we opsonized Z-*cHOClate* using human IgG as described in section 4. B.5. While phagosomal pH in neutrophils remained near neutral, we observed a burst of HOCl 5-10 minutes post phagocytosis (Figure 4.2b). In comparison with kinetics of HOCl production in macrophages neutrophils exhibit a sharp HOCl production between 5-15 minutes of phagocytosis (Figure 4.2b). Also, *cHOClate* being sensitive to HOCl and

not OCl^-, suggests that even at the neutral pH of neutrophil phagosomes there is copious amount of available HOCl in neutrophil phagosomes.

4.C.2: Z-*cHOClate* detects differential MPO levels in human Neutrophils, monocytes and macrophages

We used Z-cHOClate to compare the activity of MPO as HOCl production in neutrophils, monocytes and monocyte derived macrophages (HMDMs). Since HOCl and pH signals comes to a saturation in macrophages as well as neutrophils at 20 minutes post phagocytosis we checked the G/B and R/B levels at this time points. We found that neutrophils have the highest level of myeloperoxidase (MPO) activity in the phagosome, next monocytes and finally, macrophages (Figure 4.3). This correlates well with MPO levels found in neutrophils, monocytes and macrophages estimated by us and others (Klebanoff, 2005).

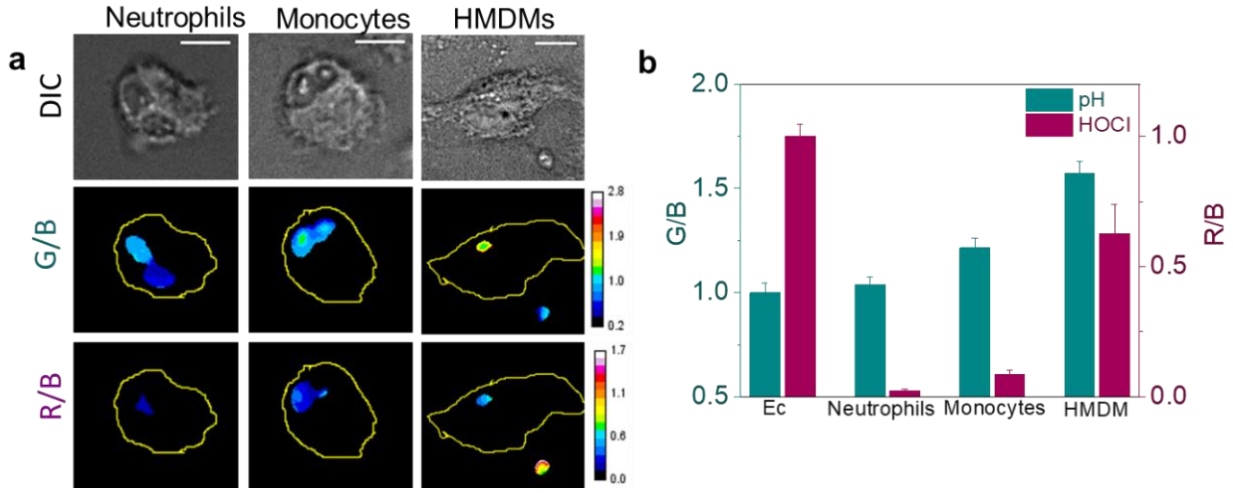

Figure 4.3: Z-*cHOClate* detects differential MPO expression in innate immune cells.

a) Representative images of *Z-cHOClate* phagocytosed by human neutrophils, monocytes and macrophages at t=20 minutes post-phagocytosis in DIC (top), -

G/B(middle) and R/B(bottom) channels, scale bar = 10 mm, representative data from three independent experiments are shown. b) Quantification of G/B and R/B from a, n= 85 phagosomes, representative data from two- independent experiments from a single blood draw are shown; Ec: extracellular, error bars, SEM; measure of center, mean.

4.C.3: Immunostimulated macrophages upregulate MPO expression and activity

Human macrophages produce HOCl upon immunostimulation. However, because of the diffusible nature of both HOCl and its existing reporters it remains unclear whether this HOCl is produced by secreted or phagosomal MPO (Kenmoku et al., 2007; Xu et al., 2013). We investigated this using two approaches. First, we pulsed control and activated human monocyte derived macrophages (HMDMs) with *Z-cHOCate* and measured phagosomal MPO activity (Figure 4.4a). We found that phagosomal HOCl levels increased, following LPS stimulation (Fig.4 4a) and this increase could be abolished by ABAH inhibition of MPO. Second, control and LPS-activated HMDMs were pulsed with R6G-Zym and immunostained for MPO (Figure 4.4b). Interestingly HMDMs showed only a marginal increase in MPO levels when treated with LPS compared to untreated cells (Figure 4.4b). However, within 30 minutes post-phagocytosis, activated HMDMs substantially upregulated MPO and immunostaining revealed that most of it was phagosomal (Figure 4.4b-c).

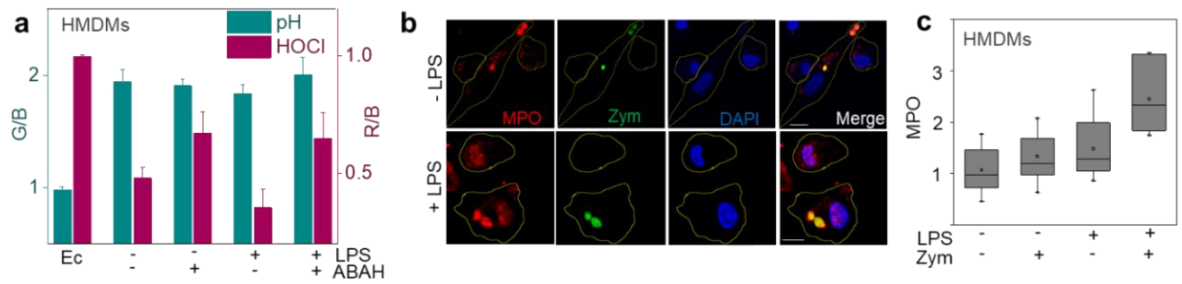

Figure 4.4: Immunostimulation upregulates MPO in human macrophages. a) Phagosomal pH (G/B) and HOCl (R/B) in human monocytes derived macrophages (HMDMs) with or without LPS having phagocytosed Z-*cHOClate*, n ≥ 150 phagosomes. b) Immunofluorescence images of MPO (red) in HMDMs with or without LPS treatment and having phagocytosed R_6G-labeled Zymosan (green), scale bar = 10 μm, representative data from three independent experiments are shown. c) Mean MPO intensities from (b), n = 50 cells.

4.C.4: Presence of functional MPO in mouse macrophages

Previous studies on mouse macrophages have suggested that HOCl levels have been too low to detect due to poor MPO expression in these cells(Brennan et al., 2001; van Leeuwen et al., 2008). However, given our findings that both activation and phagocytosis could cause MPO upregulation, we performed a similar experiment with mouse bone marrow derived macrophages (BMDMs). First, BMDMs derived from wild type mice ($MPO^{+/+}$) showed a large decrease (60%) in R/B signal, while those derived from $MPO^{-/-}$ showed negligible decrease (<5%) in R/B signal compared to uninternalized particles indicating that Z-*cHOClate* is a highly sensitive and specific reporter of phagosomal HOCl (Figure.4. 5a-b).

Given the ability of Z-*cHOClate* to sensitively map phagosomal HOCl, we then explored the capacity of primary murine macrophages from different tissue sources to produce phagosomal HOCl. Mouse macrophages have long been considered insignificant producers of HOCl based largely on measurements of extracellular HOCl. However, this direct observation of endogenous, intracellular HOCl in primary mouse tissue macrophages reveals that they are in fact effective at producing phagosomal HOCl. Phagosomes in primary tissue macrophages derived from mouse adipose (ATM) and peritoneum (PM) labeled with Z-*cHOClate* showed a 4-fold and 2-fold change respectively in the R/B ratio (Figure 4. 5b). This proves presence of active MPO in mice tissue macrophages and suggest a possible use of mouse models for MPO mediated inflammatory diseases and organ damage.

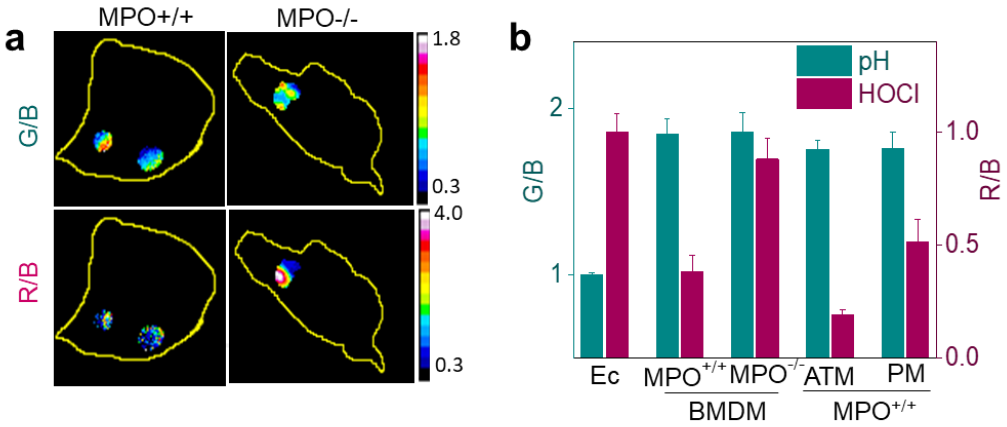

Figure 4.5: Z-*cHOClate* maps HOCl production in primary mouse macrophages. a) Representative images of Z-*cHOClate* phagocytosed by mouse bone marrow derived macrophages from $MPO^{+/+}$ and $MPO^{-/-}$ mice at t=20 minutes post-phagocytosis in G/B (top) and R/B(bottom) channels, scale bar = 10 μm, representative data from three independent experiments are shown. b) Phagosomal pH (G/B) and HOCl (R/B) reported-

by phagocytosed Z-*cHOClate* in BMDMs derived from $MPO^{+/+}$ and $MPO^{-/-}$ mice, adipose tissue macrophages (ATM) and peritoneal macrophages (PM), n ≥ 150 phagosomes.

By immunofluorescence, we found that activated BMDMs showed increased levels of MPO within the phagosome (Figure 4.6a-b). This difference in MPO levels was reflected in the HOCl levels, as detected using Z-*cHOClate* (Figure 4.6c). Together, this revealed that phagocytosis of zymosan by immunostimulated macrophages upregulates intracellular MPO, which roughly doubles the production of HOCl in the phagosome.

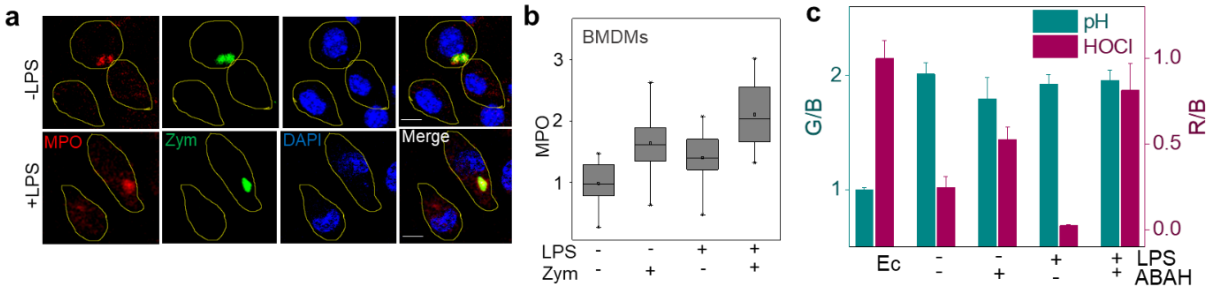

Figure 4.6: Immunostimulation upregulates MPO in primary mouse macrophages. a) Immunofluorescence images of MPO (red) in mouse bone marrow derived macrophages (BMDMs) with or without LPS treatment and having phagocytosed R_6G-labeled Zymosan (green), scale bar = 10 μm, representative data from three independent experiments are shown. b) Mean MPO intensities from (a), n ≥ 50 cells. c) Phagosomal pH (G/B) and HOCl (R/B) in mouse monocytes derived macrophages (BMDMs) with or without LPS treatment having phagocytosed Z-*cHOClate*, n ≥ 150 phagosomes.

4.D: Conclusions

We could use Z-*cHOClate* to successfully map the HOCl and pH in the maturing phagosomes in neutrophils. We observed that neutrophils have high production of HOCl

compared to macrophages which is in line with its MPO content (Rosen et al., 2002). Further pH in neutrophil phagosomes remain near neutral during phagocytosis as reported (Nordenfelt and Tapper, 2011). Z-*cHOClate* reveals differential MPO levels in innate immune cells like neutrophils, monocytes and monocytes derived macrophages. Though the production of HOCl is in micromolar range in human macrophages, our results indicate this can be upregulated in the presence of innate immune stimuli like LPS. This further leads to the conclusion that inflammatory macrophages may upregulate MPO levels and source of MPO derived products could be macrophages.

The presence of MPO in macrophages was further confirmed in mouse macrophages using gene knockout models. Further we have detected the presence of active MPO levels in mouse tissue macrophages like adipose tissue macrophages and peritoneal macrophages. This challenges the long-standing notion that mouse macrophages do not contain active myeloperoxidase. So, wild type mice can work as a model organism where one studies the role of macrophage derived MPO in inflammatory diseases and organ failure.

4.E: Future outlook

Cardiovascular diseases are characterized by increased activity of MPO in the artery tissues in the form of chlorinated LDLs (Anatoliotakis et al., 2013; Nicholls and Hazen, 2005). The origin of MPO or its activity dysregulation is still a question of debate in this case. Further multiple sclerosis is characterized demyelination arising from MPO activity (Gray et al., 2008). Though the extracellularly secreted MPO is thought to be responsible in these cases precise studies are lacking on the origin and mechanism of MPO dysregulation inflammatory disease (Klebanoff, 2005). In vitro activity of MPO showed a

pH dependence on its chlorinating as well as peroxidation activity (Vlasova et al., 2006). The peroxidation activity of MPO is prevalent at neutral pH while chlorinating activity is prevalent at the acidic pH. The extracellular MPO hence should result in high accumulation of tyrosyl radical derived products in the inflamed tissue, while chlorinated species should be arising from an acidic environment. This controversy on the origin and activity of MPO can be addressed using intracellular and extracellular targeted *cHOClate* since it can sense HOCl along with reporting pH of the location, which will report on the enzymatic nature of MPO.

Mechanisms of immune evading by the resistant pathogens are still under study since pathogens infect the host body despite of having multiple killing mechanisms. Bacterial species like S. aureus and M. tuberculosis infects human body where one of the evading mechanisms is by preventing fusion with MPO containing cytoplasmic granules (Charles A Janeway et al., 2001; Urban et al., 2006). This points the possible role of HOCl in killing these pathogens since these granules are rich in chloride and MPO, while the phagosomes contain necessary ROS H_2O_2 for generation of HOCl. Also, studies following the pH of phagosome in these aspects showed that the pathogens prevent acidifications in these compartments which results in the impaired phagosome maturation and there by infect the host cells and host body (Huynh and Grinstein, 2007; Queval et al., 2017). Since pH is the well accepted the functional ques of phagosome maturation, having a sensor which can map any ROS/ ions along with pH can decouple the exact evading mechanism by specific pathogens. In each case the quantitative multianalyte sensor can be attached to the surface of live pathogens and change in analyte concentration/ production can be monitored as a function of phagocytosis.

Inflammatory bowel disease (IBD) patients are characterized by high amounts of MPO in their stool samples, as well as antibodies against fungal cell wall components as ASCA antibodies (Hansberry et al., 2017; Sokol et al., 2017; Standaert-Vitse et al., 2009). Recent studies about fungal mycobiome suggest a plausible role for fungal species imbalance in IBDs(Sokol et al., 2017). These studies suggest that, MPO dysregulation in the phagocytic cells of lamella propria may be responsible for the mycobiome imbalance in the intestine which results in IBD. Z-*cHOClate* or *cHOClate* modified *Candida albicans* can be used to look at the MPO activity of intestinal phagocytes (monocytes, macrophages and neutrophils) from IBD patients and non-IBD patients, which will probably give insight in to cellular level MPO dysregulation which results in inflammatory bowel disease.

4.F: References

Anatoliotakis, N., Deftereos, S., Bouras, G., Giannopoulos, G., Tsounis, D., Angelidis, C., Kaoukis, A., and Stefanadis, C. (2013). Myeloperoxidase: expressing inflammation and oxidative stress in cardiovascular disease. Curr. Top. Med. Chem. *13*, 115–138.

Aratani, Y. (2018). Myeloperoxidase: Its role for host defense, inflammation, and neutrophil function. Arch. Biochem. Biophys. *640*, 47–52.

Becker, L., Liu, N.-C., Averill, M.M., Yuan, W., Pamir, N., Peng, Y., Irwin, A.D., Fu, X., Bornfeldt, K.E., and Heinecke, J.W. (2012). Unique proteomic signatures distinguish macrophages and dendritic cells. PLoS One *7*, e33297.

Brennan, M.L., Anderson, M.M., Shih, D.M., Qu, X.D., Wang, X., Mehta, A.C., Lim, L.L., Shi, W., Hazen, S.L., Jacob, J.S., et al. (2001). Increased atherosclerosis in myeloperoxidase-deficient mice. J. Clin. Invest. *107*, 419–430.

Charles A Janeway, J., Travers, P., Walport, M., and Shlomchik, M.J. (2001). Pathogens have evolved various means of evading or subverting normal host defenses.

Gray, E., Thomas, T.L., Betmouni, S., Scolding, N., and Love, S. (2008). Elevated activity and microglial expression of myeloperoxidase in demyelinated cerebral cortex in multiple sclerosis. Brain Pathol. *18*, 86–95.

Hansberry, D.R., Shah, K., Agarwal, P., and Agarwal, N. (2017). Fecal myeloperoxidase as a biomarker for inflammatory bowel disease. Cureus *9*, e1004.

Huynh, K.K., and Grinstein, S. (2007). Regulation of vacuolar pH and its modulation by some microbial species. Microbiol. Mol. Biol. Rev. *71*, 452–462.

Kenmoku, S., Urano, Y., Kojima, H., and Nagano, T. (2007). Development of a highly specific rhodamine-based fluorescence probe for hypochlorous acid and its application to real-time imaging of phagocytosis. J. Am. Chem. Soc. *129*, 7313–7318.

Klebanoff, S.J. (2005). Myeloperoxidase: friend and foe. J. Leukoc. Biol. *77*, 598–625.

Kratz, M., Coats, B.R., Hisert, K.B., Hagman, D., Mutskov, V., Peris, E., Schoenfelt, K.Q., Kuzma, J.N., Larson, I., Billing, P.S., et al. (2014). Metabolic dysfunction drives a mechanistically distinct proinflammatory phenotype in adipose tissue macrophages. Cell Metab. *20*, 614–625.

Lau, D., and Baldus, S. (2006). Myeloperoxidase and its contributory role in inflammatory vascular disease. Pharmacol. Ther. *111*, 16–26.

Van Leeuwen, M., Gijbels, M.J.J., Duijvestijn, A., Smook, M., van de Gaar, M.J., Heeringa, P., de Winther, M.P.J., and Tervaert, J.W.C. (2008). Accumulation of myeloperoxidase-positive neutrophils in atherosclerotic lesions in LDLR-/- mice. Arterioscler. Thromb. Vasc. Biol. *28*, 84–89.

Moore, K.J., Sheedy, F.J., and Fisher, E.A. (2013). Macrophages in atherosclerosis: a dynamic balance. Nat. Rev. Immunol. *13*, 709–721.

Nicholls, S.J., and Hazen, S.L. (2005). Myeloperoxidase and cardiovascular disease. Arterioscler. Thromb. Vasc. Biol. *25*, 1102–1111.

Nordenfelt, P., and Tapper, H. (2011). Phagosome dynamics during phagocytosis by neutrophils. J. Leukoc. Biol. *90*, 271–284.

Queval, C.J., Song, O.-R., Carralot, J.-P., Saliou, J.-M., Bongiovanni, A., Deloison, G., Deboosère, N., Jouny, S., Iantomasi, R., Delorme, V., et al. (2017). Mycobacterium tuberculosis Controls Phagosomal Acidification by Targeting CISH-Mediated Signaling. Cell Rep. *20*, 3188–3198.

Rosen, H., Crowley, J.R., and Heinecke, J.W. (2002). Human neutrophils use the myeloperoxidase-hydrogen peroxide-chloride system to chlorinate but not nitrate bacterial proteins during phagocytosis. J. Biol. Chem. *277*, 30463–30468.

Shepherd, J., Hilderbrand, S.A., Waterman, P., Heinecke, J.W., Weissleder, R., and Libby, P. (2007). A fluorescent probe for the detection of myeloperoxidase activity in atherosclerosis-associated macrophages. Chem. Biol. *14*, 1221–1231.

Sokol, H., Leducq, V., Aschard, H., Pham, H.-P., Jegou, S., Landman, C., Cohen, D., Liguori, G., Bourrier, A., Nion-Larmurier, I., et al. (2017). Fungal microbiota dysbiosis in IBD. Gut *66*, 1039–1048.

Standaert-Vitse, A., Sendid, B., Joossens, M., François, N., Vandewalle-El Khoury, P., Branche, J., Van Kruiningen, H., Jouault, T., Rutgeerts, P., Gower-Rousseau, C., et al. (2009). Candida albicans colonization and ASCA in familial Crohn's disease. Am. J. Gastroenterol. *104*, 1745–1753.

Urban, C.F., Lourido, S., and Zychlinsky, A. (2006). How do microbes evade neutrophil killing? Cell Microbiol. *8*, 1687–1696.

Vlasova, I.I., Arnhold, J., Osipov, A.N., and Panasenko, O.M. (2006). pH-dependent regulation of myeloperoxidase activity. Biochemistry Moscow *71*, 667–677.

Xu, Q., Lee, K.-A., Lee, S., Lee, K.M., Lee, W.-J., and Yoon, J. (2013). A highly specific fluorescent probe for hypochlorous acid and its application in imaging microbe-induced HOCl production. J. Am. Chem. Soc. *135*, 9944–9949.

Zhang, X., Goncalves, R., and Mosser, D.M. (2008). The isolation and characterization of murine macrophages. Curr. Protoc. Immunol. *Chapter 14*, Unit 14.1.